UCRL 8756

UNIVERSITY OF CALIFORNIA

Ernest O. Lawrence Radiation Laboratory

TWO-WEEK LOAN COPY

This is a Library Circulating Copy which may be borrowed for two weeks. For a personal retention copy, call Tech. Info. Division, Ext. 5545

BERKELEY, CALIFORNIA

DISCLAIMER

This document was prepared as an account of work sponsored by the United States Government. While this document is believed to contain correct information, neither the United States Government nor any agency thereof, nor the Regents of the University of California, nor any of their employees, makes any warranty, express or implied, or assumes any legal responsibility for the accuracy, completeness, or usefulness of any information, apparatus, product, or process disclosed, or represents that its use would not infringe privately owned rights. Reference herein to any specific commercial product, process, or service by its trade name, trademark, manufacturer, or otherwise, does not necessarily constitute or imply its endorsement, recommendation, or favoring by the United States Government or any agency thereof, or the Regents of the University of California. The views and opinions of authors expressed herein do not necessarily state or reflect those of the United States Government or any agency thereof or the Regents of the University of California.

UCRL-8756
Physics and Mathematics

UNIVERSITY OF CALIFORNIA
Lawrence Radiation Laboratory
Berkeley, California

Contract No. W-7405-eng-48

THE NUCLEAR SPINS AND MAGNETIC MOMENTS OF CERTAIN GOLD AND SILVER ISOTOPES

Wesley Bruce Ewbank

(Thesis)

June 1959

Printed for the U. S. Atomic Energy Commission

Printed in USA. Price $2.75. Available from the
Office of Technical Services
U.S. Department of Commerce
Washington 25, D. C.

THE NUCLEAR SPINS AND MAGNETIC MOMENTS OF CERTAIN GOLD AND SILVER ISOTOPES

Contents

Abstract 4

I. Introduction 6

II. Theory

- A. Intra-Atomic Interactions 8
- B. Addition of an External Field 11
- C. Energy Level Transitions 17
- D. Delta-Nu Calculations 20
- E. Magnetic-Moment Calculations 21

III. Experiment

- A. Theory of the Experiment 32
- B. Apparatus 37
  - 1. Beam Production 37
  - 2. Beam Detection 39
  - 3. The Magnet System 43
- C. Isotopes 45
- D. The Silver Isotopes
  - 1. Rhodium Target 50
  - 2. Palladium Target 59
- E. The Gold Isotopes
  - 1. Iridium Target 63
  - 2. Platinum Target 64

IV. Results

- A. Data Processing
  - 1. Normalization 68
  - 2. Omnibus Program 72
  - 3. Sample Analysis 74
- B. Silver Results
  - 1. Nuclear Spins 77
  - 2. Hyperfine Structure Separation of Ag^{105} 91
  - 3. Calculated Magnetic Moment of Ag^{105} 97

THE NUCLEAR SPINS AND MAGNETIC MOMENTS OF CERTAIN GOLD AND SILVER ISOTOPES

Contents

Abstract 4

I. Introduction 6

II. Theory

- A. Intra-Atomic Interactions 8
- B. Addition of an External Field 11
- C. Energy Level Transitions 17
- D. Delta-Nu Calculations 20
- E. Magnetic-Moment Calculations 21

III. Experiment

- A. Theory of the Experiment 32
- B. Apparatus 37
  - 1. Beam Production 37
  - 2. Beam Detection 39
  - 3. The Magnet System 43
- C. Isotopes 45
- D. The Silver Isotopes
  - 1. Rhodium Target 50
  - 2. Palladium Target 59
- E. The Gold Isotopes
  - 1. Iridium Target 63
  - 2. Platinum Target 64

IV. Results

- A. Data Processing
  - 1. Normalization 68
  - 2. Omnibus Program 72
  - 3. Sample Analysis 74
- B. Silver Results
  - 1. Nuclear Spins 77
  - 2. Hyperfine Structure Separation of Ag^{105} 91
  - 3. Calculated Magnetic Moment of Ag^{105} 97

C. Gold Results

1. Nuclear Spins 100

2. Hyperfine Structure Separations of the Gold Isotopes 107

3. Calculated Magnetic Moments of Gold Isotopes 120

V. Discussion

A. Silver Results 123

B. Gold Results 125

Appendix 127

Acknowledgments 128

References 129

THE NUCLEAR SPINS AND MAGNETIC MOMENTS OF CERTAIN GOLD AND SILVER ISOTOPES

Wesley Bruce Ewbank

Lawrence Radiation Laboratory and Department of Physics
University of California, Berkeley, California

June 1959

ABSTRACT

An atomic-beam magnetic-resonance apparatus operating on the flop-in principle has been used to measure the nuclear spins and hyperfine-structure separations of the $^2S_{1/2}$ electronic ground state for several radioactive isotopes of silver and gold. The results of these experiments, together with calculated values of the nuclear magnetic-dipole moments, are as follows:

Isotope	Half life	Spin	hfs $\Delta\nu$ (Mc)	$\lvert\mu_I\rvert$ (nuclear magneton)
Silver-103	1.1 hr	7/2	---	---
104	27 min	2	---	---
104	1.2 hr	5	---	---
105	40 d	1/2	1529.05(5)	0.101(1)
106	24 min	1	---	---
106	8.3 d	6	---	---
110m	253 d	6	---	---
Gold-191	3.0 hr	3/2	5780(20)	0.118(15)
192	4.8 hr	1	374.30(10)	0.0068(10)
193	17.5 hr	3/2	5890(20)	0.121(15)
194	39 hr	1	3503(10)	0.064(10)
195	180 d	3/2	---	---
196	5.6 d	2	---	---

The spin measurements on 27-min Ag^{104} and 24-min Ag^{106} represent confirmation of results of Reynolds et al using different methods of isotope production and separation. All neutron-deficient isotopes were produced by cyclotron bombardment with alpha-particle, deuteron, or proton beams. Silver-110m was produced by the (n, γ) reaction on stable Ag^{109}. Detection of the isotopes was accomplished by counting their radioactivity in low-background scintillation crystal counters. The magnetic moment of silver-105 was obtained from the Fermi-Segrè formula, using values of $\Delta\nu$ and μ_I previously measured directly for stable silver-107 and -109. The magnetic moments of the gold isotopes have been calculated from the Fermi-Segrè formula, using the measured $\Delta\nu$ of stable gold-197 together with a re-evaluation of the magnetic moment of gold-197. The procedure used in the calculation of a nuclear magnetic-dipole moment from its observed interaction with an s electron is described.

I. INTRODUCTION

The techniques and objectives of experiments with beams of neutral atoms or molecules have changed considerably since Dunoyer[1] showed that energetic sodium atoms travel in straight lines through an evacuated space. From this pioneering beginning, the complexity and subtlety of molecular-beams experiments have increased enormously. By introducing inhomogeneous magnetic fields along the beam and studying their effects on the beam, Stern and his associates[2] were able to make crude measurements of the magnetic moments of free atoms. Further refinements by Stern[3] and by Rabi[4] made possible the determination of nuclear spins and magnetic moments from studies of the deflection of molecular beams. Since 1938, when Rabi[5] introduced the magnetic-resonance method of molecular-beam spectroscopy, most experiments with beams have consisted of applying the resonance methods to various problems in physical measurements. The measurements described herein consist of just such an application to certain radioactive isotopes of silver and gold.

The magnetic-resonance apparatus[6] used in the experiments is of the "flop-in" type.[7] In these experiments, it is necessary to detect small signals corresponding to resonances of radioactive isotopes. It is much easier to detect these resonances as a positive signal against an essentially zero background than to detect them as a small change in a large background of radiation. The latter would be the case if a "flop-out" type of apparatus were used.

In the atomic-beam apparatus, neutral atoms originate from a source oven into a high-vacuum chamber. The mean free path of each atom is longer than any dimension of the chamber, so that the atoms, if unaffected, would travel in straight lines to the walls of the chamber. However, the source oven and a series of slits collimate the atoms into a narrow beam which is directed successively between the pole tips of three electromagnets, A, C, and B. The A and B magnets produce very strong fields and are highly inhomogeneous. If the atom possesses a magnetic-dipole moment, it will be deflected in these inhomogeneous fields. The C magnet, on the other hand, is very uniform and hence

can produce no effect on the neutral atoms other than an alignment of their dipole moments. The C field acts on the beam in the space between the A and B magnets. Superimposed on the uniform C field is a small oscillating magnetic field, the frequency of which is controlled by the experimenter. This oscillating field can induce transitions among the energy levels of an atom as it passes through the C field, provided the oscillator frequency is compatible with the strength of the C field and the atomic and nuclear constants of the atom. If this condition is not satisfied, then none of the atoms will be able to pass through the magnet region. The deflections caused by the A and B fields are cumulative, and an atom will be deflected from the axis of the apparatus ("thrown out") if the magnetic moment of the atom remains the same. (This is the characteristic feature of a "flop-in" apparatus as discussed above. In a "flop-out" apparatus, the atom is focused on the axis if there is no change in its magnetic moment.) If the frequency of the oscillating field satisfies the condition imposed by the strength of the C field and the constants of the atom, then transitions among the atomic energy levels may be induced. In particular, transitions may be induced which cause a change in sign for the magnetic moment of an atom. If this situation occurs, the B field will cause the atom to be "flopped in" to a focal point on the axis of the apparatus. Since the atoms investigated here are radioactive, they can be collected at this focus and detected by means of their radioactivity.[8]

A knowledge of the conditions that must be satisfied in order for the focusing of an atom to occur, together with a measurement of the C field and the frequency at which transitions are induced by the oscillating magnetic field, provides a method for obtaining values of the various nuclear and atomic constants involved in determining the conditions. In the present experiments, measurements are made to provide for the determination of nuclear constants only. The electronic constants are presumed to be known from previous work.

The procedure which is used to obtain the nuclear constants from appropriate measurements is described in detail in Section II. The methods by which the measurements are made are described in Section IV. Section V is devoted to discussion and interpretation of the results in the light of current nuclear models.

II. THEORY

A. Intra-Atomic Interactions

One of the advantages of atomic-beam measurements is that the atomic system is studied unencumbered by complicated interactions with neighboring atoms. The atoms in a beam are so isolated one from another that there is no important interatomic term in the Hamiltonian of the system. In the absence of applied external fields, then, the interactions are purely intra-atomic. The systematic study of these interactions can lead to valuable information about the nuclear and electronic constants of the atomic system.

In the absence of external fields, the situation may be described in two equivalent ways. Either the electrons move in the electromagnetic field of the nucleus, or, conversely, the electrons produce a field with which the nucleus interacts. In either case, the problem can be simplified by a multipole expansion of the interacting fields. The problem may then be described in terms of the action of each of the multipole field components on the corresponding multipole moment of the interacting particle or particles.

Two types of interactions may be considered— those of electrostatic origin and those of magnetic origin. The latter arise from the motion of the charges that are present in the nucleus and in the electron shells. The electrostatic part of the interaction includes only terms of multipole order $2^{2\ell}$ for $\ell = 0, 1, 2, \cdots$, i.e., monopole, quadrupole, etc. From general symmetry arguments,[9] the electric dipole, octupole, etc. moments can be shown to vanish. Similar considerations show that for the magnetic interaction, the opposite is true. The only nonvanishing magnetic interactions are those of multipolarity $2^{2\ell+1}$ for $\ell = 0, 1, 2 \cdots$.

One further fact serves to limit the number of electron-nuclear interaction terms. A particle or group of particles whose total angular momentum is λ cannot possess electric or magnetic moments of multipole order greater than $2^{2\lambda}$. Nor can such a configuration give rise to a field of higher multipole order than $2^{2\lambda}$. Thus in an interaction between a nucleus of angular momentum I and an electron system of total angular momentum J, the multipole interaction of highest order will be the $2^{2\lambda}$-pole, where λ is the smaller of I and J.

The ground-state electronic configurations of both silver and gold are $^2S_{1/2}$. None of the isotopes measured here has nuclear spin I = 0. Thus $\lambda = 1/2$, and the highest allowed order is the dipole interaction. The magnetic dipole is the lowest-order magnetic interaction. It therefore represents the entire magnetic interaction between the electron and nuclear systems. As noted above, the electric dipole interaction must vanish for symmetry reasons. Thus, the only electrostatic term is the monopole interaction, which is just the Coulomb interaction between the electronic and the nuclear charges.

The Coulomb interaction gives rise to the whole spectrum of electronic energy levels. The smaller intraelectronic interactions (e.g spin-orbit forces) remove some of the degeneracies in these energy levels, giving rise to the fine structure of atomic spectra. The magnetic-dipole interaction between the nucleus and the electronic system gives rise to further complexity in the energy levels with the addition of a hyperfine splitting of each of the levels. It is the hyperfine-structure separation that is of greatest interest here, because of its direct connection with the nuclear constants of the isotope under investigation.

The hyperfine interaction for a state of definite I and J can be expressed as

$$\mathcal{H}_{IJ} = - \vec{\mu}_I \cdot \vec{H}_J = a \vec{I} \cdot \vec{J} , \tag{1}$$

where $\vec{\mu}_I$ is the nuclear moment, and $\vec{H}_J$ is the magnetic field at the nucleus due to the electron. Since the states are of definite I, the nuclear magnetic moment is expressed as proportional to the nuclear spin $\vec{I}$. In particular, the proportionality factor is conveniently written

$$\vec{\mu}_I = g_I \mu_0 \vec{I} , \tag{2}$$

where μ_0 is the magnitude of the Bohr magneton (see Appendix) and g_I is the nuclear g factor. Similarly, if the states are of

definite J, the magnetic field H_J of the electrons, evaluated at the nuclear position, can be expressed as proportional to J. The proportionality factor has been calculated by Fermi,[10] giving, for the field at the nucleus, for hydrogenlike atoms,

$$\vec{H}_J = 8\pi/3\ g_J\ \mu_0 \left|\psi(0)\right|^2 \vec{J} \tag{3}$$

where g_J is the electronic Lande g factor, and $\psi(0)$ is the electronic wave function evaluated at the origin, r = 0. Use of the factor $\left|\psi(0)\right|^2$ implies that the electron density is constant over the nuclear volume, or alternately, that the nucleus is considered to be a point charge. Combining these expressions gives the result

$$a = -\ 8\pi/3\ g_I g_J \mu_0^{\ 2} \left|\psi(0)\right|^2 \tag{4}$$

for the hyperfine-interaction constant.

For a state of given $\vec{F}$ (where $\vec{F} = \vec{I} + \vec{J}$) the hyperfine interaction energy can be found by

$$W_{IJ}^F = \left\langle IJ, Fm \middle| \mathcal{H}_{IJ} \middle| IJ, Fm \right\rangle = a \left\langle IJ, Fm \middle| \vec{I}\cdot\vec{J} \middle| IJ, Fm \right\rangle$$
$$= \frac{a}{2}\left[F(F+1) - I(I+1) - J(J+1)\right]. \tag{5}$$

The hyperfine-structure (hfs) separation of the two levels F and (F-1) is given by

$$\Delta W_F = W_{IJ}^F - W_{IJ}^{F-1} = \frac{a}{2}\left[F(F+1) - (F-1)F\right] = a\,F. \tag{6}$$

This equation has great significance. If the hfs separation of two levels of known F is measured, the value of the interaction constant, a, can be determined. Furthermore, since a is a function of g_I, the hfs can be considered to be a measure of the actual nuclear magnetic-dipole moment, $\vec{\mu}_I$.

B. Addition of an External Field

In the atomic beams technique, the hfs of an isotope is determined from a study of the radio-frequency (rf) transitions among the energy levels of the atomic system in a uniform magnetic field. An understanding of this procedure requires an understanding of the behavior of the electron-nuclear system in such a uniform field.

Since there is no electric quadrupole interaction (because $J = 1/2$), the Hamiltonian of the atomic system in a magnetic field $\vec{H}$ may be written

$$\begin{aligned} \mathcal{H} &= a\,\vec{I}\cdot\vec{J} - \vec{\mu}_I\cdot\vec{H} - \vec{\mu}_J\cdot\vec{H} \\ &= a\,I\cdot J - g_I\mu_0\vec{I}\cdot\vec{H} - g_J\mu_0\vec{J}\cdot\vec{H}\ . \end{aligned} \tag{7}$$

The first term describes the interaction between the nuclear and electronic magnetic-dipole moments as discussed above. The latter two terms represent the energy of these dipoles in the external field.

A quantum-mechanical representation in which $\vec{I}\cdot\vec{J}$ is diagonal was used before to calculate the eigenvalues of $\mathcal{H}_{IJ}$. The same representation can be used for this field-dependent Hamiltonian, but the interaction will connect states of different F so that off-diagonal elements will result. The nondiagonal portion of the matrix of $\mathcal{H}$ will be proportional to H, however, so that for small fields, the Hamiltonian is "almost" diagonal in both F and m.

In the Fm representation, the diagonal elements of the interaction are easily found:

$$\begin{aligned} \langle Fm|\mathcal{H}|Fm\rangle = \frac{a}{2}\,&[\,F(F+1) - I(I+1) - J(J+1)\,] \\ &- g_J\,[\,F(F+1) + J(J+1) - I(I+1)]\frac{\mu_0 Hm}{2F(F+1)} \\ &- g_I\,[\,F(F+1) + I(I+1) - J(J+1)]\frac{\mu_0 Hm}{2F(F+1)}\ . \end{aligned} \tag{8}$$

From first-order perturbation theory,[11] this is seen to be the first approximation to the energy of the system in the state IJFm when the external field H is small so that the terms involving H are small compared to the zero-field energy W_{IJ}^{F}. The field dependence is just that to be expected for a single dipole, whose moment is along $\vec{F}$ and whose g factor, g_F, is given by

$$g_F = \left[\frac{F(F+1) + J(J+1) - I(I+1)}{2F(F+1)}\right] g_J + \left[\frac{F(F+1) + I(I+1) - J(J+1)}{2F(F+1)}\right] g_I. \tag{9}$$

In weak fields, $\vec{\mu}_I$ and $\vec{\mu}_J$ are coupled tightly together to form $\vec{\mu}_F = g_F \mu_0 \vec{F}$. This $\vec{\mu}_F$ then precesses about the field direction, and the energy is proportional to the component $g_F \mu_0 m$ of $\vec{\mu}_F$ along the field direction.

The off-diagonal elements of $\mathcal{H}$ in the Fm representation are due entirely to the terms in I_z and J_z (from $\vec{I}\cdot\vec{H}$ and $\vec{J}\cdot\vec{H}$). Since $F_z = I_z + J_z$ is diagonal in F and m, the nondiagonal part of the matrix of I_z will be equal and of opposite sign to the nondiagonal part of the matrix of J_z. The matrix elements connecting states of different F and m can then be simplified:

$$\langle Fm | \mathcal{H} | F'm' \rangle = (-g_J + g_I)\mu_0 H \langle Fm | J_z | F'm' \rangle. \tag{10}$$

But the matrix of J_z is diagonal in m.[12] Furthermore, the operator J_z can connect only states for which F changes by ±1. Thus, the most general off-diagonal element of the matrix of $\mathcal{H}$ can be written

$$\langle Fm | \mathcal{H} | F\pm 1, m \rangle = (-g_J + g_I)\mu_0 H \langle Fm | J_z | F\pm 1, m \rangle, \tag{11}$$

where[13]

$$\langle Fm | J_z | F-1, m \rangle = \langle F-1, m | J_z | Fm \rangle$$

$$= \left\{ \frac{(F+J-I)(F+I-J)(I+J+F+1)(I+J-F+1)\,(F^2-m^2)}{4F^2(2F-1)\,(2F+1)} \right\}^{1/2} \tag{12}$$

(The arbitrary phase factor discussed in Ref. 12 is here chosen differently from that in Ref. 13.)

Because the matrix of the interaction is diagonal in m, the secular equation becomes a product of the determinants of $(2F_{max}+1)$ submatrices. The maximum order of these submatrices is given by the number of different F states. For the special case of $J = 1/2$, there are two F states: $F = I \pm 1/2$. The secular equation for the eigenvalues of the matrix is then quadratic and can be solved exactly. This exact solution is known as the Breit-Rabi equation,[14]

$$W(F,m) = \frac{-h\Delta\nu}{2(2I+1)} - g_I \mu_0 Hm \pm \frac{h\Delta\nu}{2}\left[1 + \frac{4mx}{2I+1} + x^2\right]^{1/2}, \tag{13}$$

where $\Delta\nu$ is the hfs separation defined before, and the parameter x is given by

$$x = (-g_J + g_I)\frac{\mu_0 H}{h\Delta\nu}. \tag{14}$$

The sign of the square root in Eq. (13) is positive for the state $F = I+1/2$ and negative for $F = I-1/2$.

If the energy in units of $h\Delta\nu$ is plotted for all states of the system as a function of x, the resulting graph is called a Breit-Rabi diagram. Such diagrams have been drawn in Fig. 1. for the simple cases $J = 1/2$ and $I = 1/2, 1$, and $3/2$. These drawings have been made assuming $g_I > 0$. For the state $F = I+1/2$, the nuclear moment $\vec{\mu}_I$ and the electronic field $\vec{H}_J$ are antiparallel so that the state is of greater energy than that for which $F = I - 1/2$. For $g_I < 0$, the situation is reversed. The state $F = I + 1/2$ then corresponds to alignment of the moment $\vec{\mu}_I$ in the field $\vec{H}_J$ and therefore has a lower energy than the state $F = I - 1/2$. The Breit-Rabi diagram in its dimensionless form shows the general relation between the state energy and the magnetic field. It is easily particularized to a specific case by filling in the proper nuclear constants.

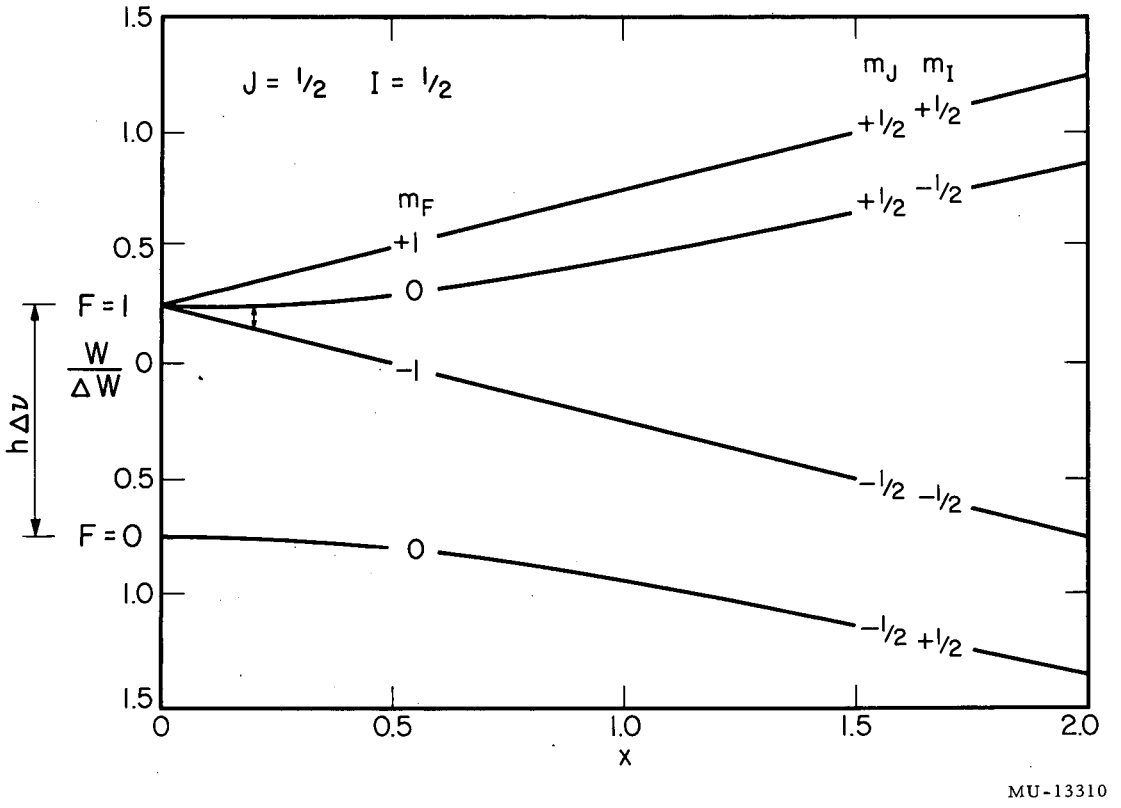

Fig. 1a. Breit-Rabi diagrams for s states.

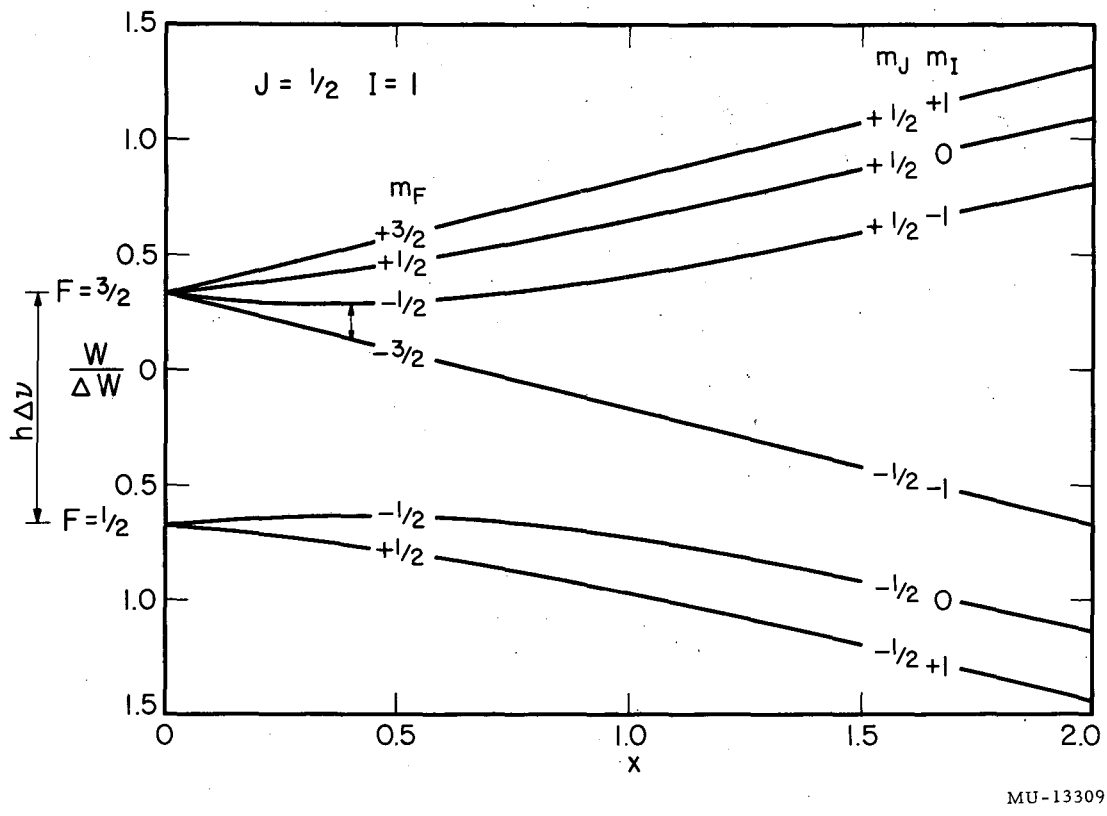
J = 1/2 I = 1
m_J m_I
+1/2 +1
+1/2 0
+1/2 −1
m_F
+3/2
+1/2
−1/2
−3/2
F = 3/2
F = 1/2
$\frac{W}{\Delta W}$
$h\Delta\nu$
−1/2 −1
−1/2 0
−1/2 +1
−1/2
+1/2
1.5
1.0
0.5
0
0.5
1.0
1.5
0
0.5
1.0
1.5
2.0
x
MU-13309

Fig. 1b

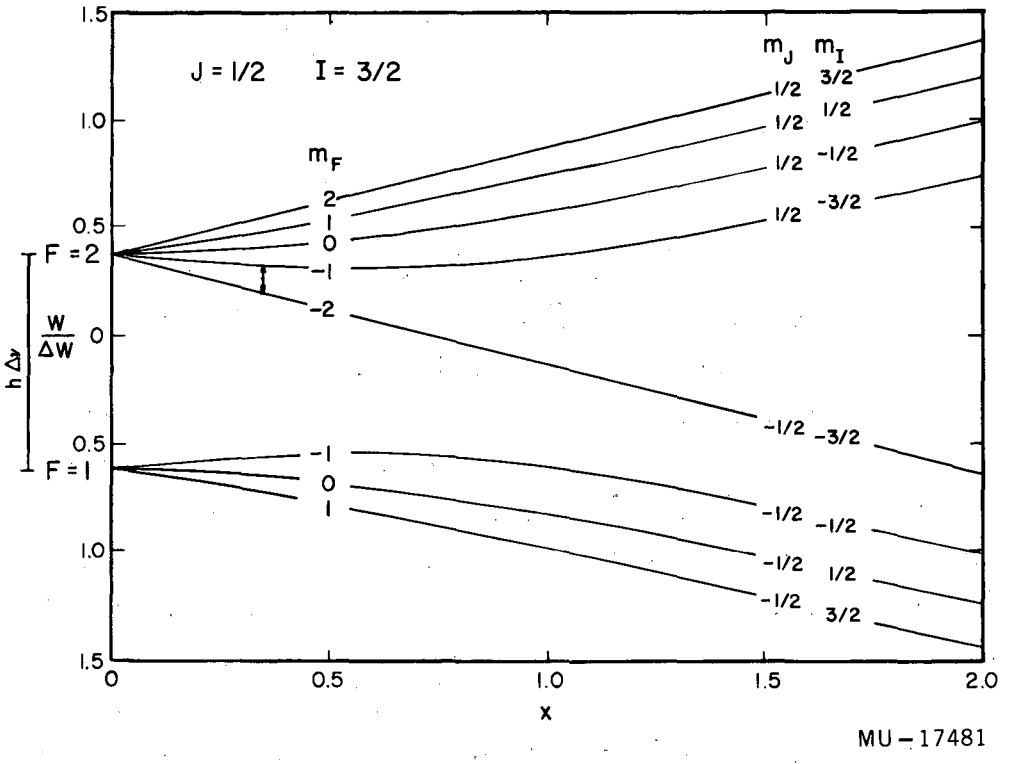

Fig. 1c

In very strong external magnetic fields (such that $x \gg 1$) the approximate form for the energy is

$$W(F,m)_H \xrightarrow[H \to \infty]{} \frac{-h\Delta\nu}{2(2I+1)} - g_I\mu_0 Hm \pm \frac{(g_I - g_J)}{2}\mu_0 H$$

$$= \frac{-h\Delta\nu}{2(2I+1)} \mp \frac{g_J}{2}\mu_0 H - g_I\left(m \mp \frac{1}{2}\right)\mu_0 H$$

$$= -\frac{h\Delta\nu}{2(2I+1)} - g_J\mu_0 H m_J - g_I\mu_0 H m_I , \qquad (15)$$

where m_J and $m_I = m - m_J$ are the respective projections of the angular-momentum vectors $\vec{J}$ and $\vec{I}$ along the field direction. In this extreme case, the energy of each level is given mostly by the interaction with the external field H. Except for the constant involving $\Delta\nu$, the energy is the sum of the individual energies of two magnetic dipoles, $\vec{\mu}_I = g_I\,\mu_0\vec{I}$ and $\vec{\mu}_J = g_J\mu_0\vec{J}$, each precessing independently in the applied field H, and each free to assume the allowed orientations with respect to the field that are indicated by m_I and m_J. Since $g_J \sim M_p/M_e\, g_I \sim 2{,}000\, g_I$, the term in g_J is dominant at large fields. Each of the levels denoted by m_J is $2I+1$ degenerate, this degeneracy being entirely removed by the g_I-dependent interaction with H.

C. Energy-Level Transitions

Since it is actually only the energy differences between levels that can be measured, it is of some interest to write down a few such differences between Breit-Rabi energy levels. By using the subscripts 1 and 2 to denote quantities referring to the different energy levels, and expressing the energy differences as frequencies of radiation of equivalent energy, the transition ν_{12} between the levels denoted by 1 and 2 is easily obtained:

$$\nu_{12} = -\frac{g_I \mu_0 H}{h}(m_1-m_2) + \frac{\Delta\nu}{2}\left\{(\pm)_1\left[1+\frac{4m_1x}{2I+1}+x^2\right]^{1/2} - (\pm)_2\left[1+\frac{4m_2x}{2I+1}+x^2\right]^{1/2}\right\}$$

$$= -\frac{g_I \mu_0 H}{h}(m_1-m_2) + \frac{\Delta\nu}{2}\left\{(\pm)_1\left[1+\frac{2m_1x}{2I+1}+\frac{x^2}{2}-\frac{2m_1^2x^2}{(2I+1)^2}\right]\right.$$

$$\left. -(\pm)_2\left[1+\frac{2m_2x}{2I+1}+\frac{x^2}{2}-\frac{2m_2^2x^2}{(2I+1)^2}\right]\right\} + \mathcal{O}(x^3\Delta\nu) . \tag{16}$$

When the quantity ν_0 is defined as

$$\nu_0 = \frac{x\Delta\nu}{2I+1} = (-g_J+g_I)\ \mu_0 H/h(2I+1) , \tag{17}$$

ν_{12} can be rewritten in terms of ν_0 and $\Delta\nu$:

$$\nu_{12} = -\frac{g_I \mu_0 H}{h}(m_1-m_2) + \frac{\Delta\nu}{2}\left\{(\pm)_1\left[1+\frac{2m_1\nu_0}{\Delta\nu}+\frac{(2I+1)^2\nu_0^2}{2\Delta\nu^2}-\frac{2m_1^2\nu_0^2}{\Delta\nu^2}\right]\right.$$

$$\left. -(\pm)_2\left[1+\frac{2m_2\nu_0}{\Delta\nu}+\frac{(2I+1)^2\nu_0^2}{2\Delta\nu^2}-\frac{2m_2^2\nu_0^2}{\Delta\nu^2}\right]\right\} + \mathcal{O}\left(\frac{\nu_0^3}{\Delta\nu^2}\right)$$

$$= -\frac{g_I \mu_0 H}{h}(m_1-m_2) + (\pm)_1\left[\frac{\Delta\nu}{2}+\frac{(2I+1)^2\nu_0^2}{4\Delta\nu}\right] - (\pm)_2\left[\frac{\Delta\nu}{2}+\frac{(2I+1)^2\nu_0^2}{4\Delta\nu}\right]$$

$$+(\pm)_1\left[m_1\nu_0-\frac{m_1^2\nu_0^2}{\Delta\nu}\right] - (\pm)_2\left[m_2\nu_0-\frac{m_2^2\nu_0^2}{\Delta\nu}\right]$$

$$+\mathcal{O}\left(\frac{\nu_0^3}{\Delta\nu^2}\right) . \tag{18}$$

If both m_1 and m_2 have the same F, then $(\pm)_1 = (\pm)_2$, and

$$\nu_{12}(\Delta F=0) = -\frac{g_I \mu_0 H}{h}(m_1-m_2) \pm \left[(m_1-m_2)\nu_0 - \frac{\nu_0^2}{\Delta\nu}(m_1^2-m_2^2)\right] + \mathcal{O}\left(\frac{\nu_0^3}{\Delta\nu^2}\right), \tag{19}$$

where now the plus sign is taken for transitions among the states with $F = I + 1/2$ and the minus sign for transitions among those with $F = I - 1/2$. If the states 1 and 2 are of different F:

$$\nu_{12}(\Delta F=\pm 1) = -\frac{g_I \mu_0 H}{h}(m_1 - m_2) \pm \left\{ \Delta\nu + (m_1+m_2)\nu_0 + \frac{\nu_0^2}{2\Delta\nu}\left[(2I+1)^2 - 2(m_1^2+m_2^2)\right] \right\} + \mathcal{O}\left(\frac{\nu_0^3}{\Delta\nu^2}\right)$$

$$= \pm\Delta\nu - \frac{g_I \mu_0 H}{h}(m_1 - m_2) \pm \left\{ (m_1+m_2)\nu_0 + \left[(2I+1)^2 - 2(m_1^2+m_2^2)\right] \frac{\nu_0^2}{2\Delta\nu} \right\} + \mathcal{O}\left(\frac{\nu_0^3}{\Delta\nu^2}\right), \qquad (20)$$

where the upper sign is chosen if the state m_1 has $F = I + 1/2$, while the lower sign is chosen if m_1 has $F = I - 1/2$. A negative frequency for the transition $1 \rightarrow 2$ means, of course, that the energy of the state m_2 is greater than that of the state m_1.

General selection rules on the possible transitions among the energy levels limit $\Delta m = m_1 - m_2$ to 0 or ± 1.[15] For $\Delta F = 0$ transitions, clearly the only interesting transitions are those for which $\Delta m = \pm 1$. Of these, only one is used in a detailed study of the hfs of a given isotope. The $\Delta F = 0$ transition which satisfies the detection condition of the apparatus (focusing for flop-in design; defocusing for flop-out design) will be called the "standard" transition. For the standard transition we have: $F=I+1/2$; $m_1=-I+1/2$, and $m_2=-I-1/2$. Its frequency ν_s is given by

$$\nu_s = \nu_0 - \frac{g_I \mu_0 H}{h} + \frac{2I}{\Delta\nu}\nu_0^2 + \frac{2I(2I-1)}{\Delta\nu^2}\nu_0^3 + \mathcal{O}\left(\frac{\nu_0^4}{\Delta\nu^3}\right). \qquad (21)$$

The significance of ν_0 is now clear. Since $g_J >> g_I$, ν_0 is a good approximation to the Zeeman or weak-field splitting of the energy levels of the coupled electron-nuclear system.

Similar approximate formulae may be obtained from the above expression for the direct ($\Delta F = \pm 1$) transitions, but such a procedure is not of such general usefulness as is the standard transition. Many different direct transitions can be used, and it is a simple matter to obtain the result for a particular case from the general formula.

D. Delta-Nu Calculations

All calculations in the preceding section have been made with the assumption that $\Delta\nu$ is known. In an actual experiment, the procedure is just reversed: a transition frequency is measured, and the hfs $\Delta\nu$ must be calculated. The mathematics involved in inverting the equations that have been derived above is involved, but straightforward. Most important of the inversions is for the case of the standard transition. Using the general formula, Eq. (16), particularized to $F = I + 1/2$, $m_1 = -I + 1/2$, $m_2 = -I - 1/2$, gives

$$\Delta\nu = \frac{(\nu_s + g_I \mu_0 H/h)(-\nu_s - g_J \mu_0 H/h)}{\nu_s + g_J \mu_0 H/(2I+1)h + 2I g_I \mu_0 H/(2I+1)h} . \tag{22}$$

In the limit of small fields, this is approximated by

$$\Delta\nu \approx \frac{2I\nu_0^2}{\nu_s - \nu_0 + g_I \mu_0 H/h} , \tag{23}$$

which can be seen from the low-field approximation for ν_s (Eq. (21)).

If the measured frequency corresponds to a direct ($\Delta F = \pm 1$) transition, the appropriate transition expressions can be solved for $\Delta\nu$. This is a difficult procedure in general and is best performed for the particular case at hand. Useful approximate formulas for $\Delta\nu$ can be obtained from the approximations to the direct transition frequencies at low fields which have been given above. (Eq. (20)).

Measurements of direct transition frequencies are usually made at low fields, so that the approximate formulas are of sufficient accuracy. If only the lowest-order terms are included in the formula for the direct transition frequency ν_D, then

$$\Delta\nu \approx \nu_D + \frac{g_I \mu_0 H}{h} (m_1 - m_2) - (m_1 + m_2)\nu_0 , \tag{24}$$

where m_1 is associated with a state for which $F = I + 1/2$, and m_2 with a state for which $F = I - 1/2$. If $m_1 = m_2 = 0$, then higher-order terms must be included:

$$\Delta\nu \approx \nu_D(0-0) - \frac{(2I+1)^2}{2} \frac{\nu_0^2}{\nu_D(0-0)} . \tag{25}$$

E. Magnetic-Moment Calculations

A series of measurements on the transition frequency ν_s at progressively higher fields will give progressively better values for the hfs $\Delta\nu$ of a given isotope. The measurement of a direct transition at low field provides the maximum precision of the apparatus. The hfs $\Delta\nu$ is, however, an interaction. In order to make useful comparison of the results with predictions of any nuclear theory, the nuclear moments must be deduced from the strength of the hfs interaction.

The exact calculation of the hfs interaction between a nucleus and the electron shells has occupied the attention of numerous researchers[16] for many years. In cases in which the nuclear magnetic moment can be measured directly (by some nuclear-resonance method), the precise measurement of the corresponding hfs by atomic beam methods provides a check of any derived relation between μ_I and $\Delta\nu$. As these measurements have become more precise, corrections have been added as necessary to bring the calculated values into agreement with the results of experiment. Considering only the case of a nucleus interacting with a single s-electron, the interaction constant may be expressed as

$$a_s = \frac{2(h\Delta\nu)}{2I+1} = -\frac{8}{3} g_I g_J \mu_0^2 \frac{Z Z_0^2}{a_H^3 n_0^3} \left(1 - \frac{d\sigma}{dn}\right) F_r\left(\frac{1}{2}, Z\right)(1-\delta)(1+\epsilon), \tag{26}$$

where

g_I and g_J are the g factors of the nucleus and electron, respectively;

μ_0 is the Bohr magneton (absolute magnitude);

a_H is the radius of the first Bohr orbit;

z is the atomic number of the atom;

z_0 is the effective atomic charge (in units of electron charge) as seen by the electron when outside all electron shells;

$n_0 = n - \sigma$ is the effective principal quantum number of the electron;

n is the principal quantum number of the electron;

σ is the quantum defect;

F_r is the Racah relativistic correction of electron density at the nucleus;

$1-\delta$ is the Breit-Rosenthal correction for the finite extent of nuclear charge; and

$1+\epsilon$ is the Bohr-Weisskopf correction for the finite extent nuclear magnetism.

This formula is seen to be analogous to Fermi's original expression given above (Eq. (4)):

$$a_s = - \frac{2}{2I+1} \left[\frac{4\pi}{3} (2I+1)\, g_I g_J \mu_0^2 \left|\psi(0)\right|^2 \right] = - \frac{8\pi}{3} g_I g_J \mu_0^2 \left|\psi(0)\right|^2 .$$

The Fermi result is based on the assumption that the nucleus has no finite extent in space. Since the nucleus is considered to be a point dipole, the interaction depends upon the electron density at that point, i.e. $\left|\psi(0)\right|^2$.

A nonrelativistic determination of $\left|\psi(0)\right|^2$ was obtained by Fermi and Segrè,[17] using a semi-empirical approach,

$$\left|\psi(0)\right|^2 = \frac{1}{\pi a_H^3} \frac{\epsilon Z}{2R} \frac{dT}{dn} , \tag{27}$$

where R is the Rydberg constant, and T is the term value for the electron. The standard Rydberg formula for T is

$$T = -\frac{RZ_0^2}{(n-\sigma)^2} , \tag{28}$$

so that

$$\frac{dT}{dn} = \frac{2RZ_0^2}{n_0^3}\frac{dn_0}{dt} = -\frac{2T}{n_0}\left(1-\frac{d\sigma}{dn}\right) , \tag{28a}$$

and

$$\left|\psi(0)\right|^2 = \frac{1}{\pi a_H^3}\frac{ZZ_0^2}{n_0^3}\left(1-\frac{d\sigma}{dn}\right) . \tag{27a}$$

When evaluating the Fermi-Segrè factor $(1-\frac{d\sigma}{dn})$, the usual approach is to express σ by an extended Ritz formula:

$$\sigma = A + BT + CT^2 . \tag{29}$$

Then

$$\frac{d\sigma}{dn} = \frac{d\sigma}{dT}\frac{dT}{dn} . \tag{29a}$$

Substituting from above for dT/dn gives

$$\frac{d\sigma}{dn} = -\frac{d\sigma}{dT}\frac{2T}{n_0}\left(1-\frac{d\sigma}{dn}\right) , \tag{29b}$$

from which

$$\frac{d\sigma}{dn} = \frac{d\sigma/dT}{d\sigma/dT - n_0/2T} . \tag{30}$$

The correction factor itself is seen to be

$$1-\frac{d\sigma}{dn} = \frac{1}{1-\frac{2T}{n_0}\frac{d\sigma}{dT}} . \tag{31}$$

In most cases, the term values T and effective principal quantum numbers n_0 have been obtained from optical spectroscopy. A graph of σ as a function of T will provide the necessary derivative, $d\sigma/dT$.

If the spectroscopic terms T are not perturbed by adjacent energy levels,[18] then σ will be a linear function of T. The derivative $d\sigma/dT$ can then be replaced by a relative difference $\Delta\sigma/\Delta T$, which is easily evaluated from spectroscopic data. Often an assumption such as this will provide as good an approximation to the Fermi-Segrè factor as is needed for the calculation. A more precise determination of $1-\frac{d\sigma}{dn}$ can be obtained by evaluating A, B, and C in the above equation, Eq. (29), for σ. This can be done from optical observations on three spectroscopic terms. Then

$$\frac{d\sigma}{dT} = B + 2CT \,, \tag{32}$$

which now depends on the term value, T.

The evaluation of $|\psi(0)|^2$ by Fermi-Segrè does not include the effects of relativity. For an s-electron, however, the velocity of the electron in the neighborhood of the nucleus may be an appreciable fraction of the velocity of light. In order to include relativistic effects, a correction to $|\psi(0)|^2$ was proposed by Racah.[19] For an electron of total angular momentum j in an atom with atomic number Z, the relativistic correction to $|\psi(0)|^2$ is given by

$$F_r(j,Z_i) = \frac{4j(j+\frac{1}{2})(j+1)}{\rho(4\rho^2-1)} \quad ; \quad \rho^2 = (j+\tfrac{1}{2})^2 + (\alpha Z_i)^2 \,, \tag{33}$$

where α is the fine-structure constant, and Z_i is the effective nuclear charge for the electron inside the electron shells ($Z_i = Z$ for an s electron). For a $^2S_{1/2}$ electronic state, the relativistic correction becomes

$$F_r(\tfrac{1}{2},Z) = \frac{3}{\rho(4\rho^2-1)} \quad ; \quad \rho^2 = 1 + \alpha^2 z^2 \,. \tag{33a}$$

Calculation of this correction is straightforward. A table of $F_r(j,Z)$ is included by Kopfermann[16] for $j \leqslant 5/2$ and $Z \leqslant 92$.

Since the nucleus is not a point charge, the electrostatic potential in the neighborhood of $r = 0$ will deviate from the purely Coulombic potential, $V_c = Ze/r$. The effect of this deviation will be

particularly large for s states, where the electron spends an appreciable fraction of its time near the origin $r = 0$. The interaction between the nuclear and electron magnetic moments is proportional[20] to

$I = \int_0^\infty \phi_1 \phi_2 y^{-2} dy$, where ϕ_1, ϕ_2 are Darwin-Gordon radial functions, and $y = \frac{2Zr}{a_H}$ is a radius parameter. Expressions for ϕ_1 and ϕ_2 can be found for small y, and these can be matched at large y to the corresponding unperturbed functions $\phi_1^{(0)}$ and $\phi_2^{(0)}$ which are appropriate to a purely Coulombic potential. If the integrands $\phi_1 \phi_2 y^{-2}$ and $\phi_1^{(0)} \phi_2^{(0)} y^{-2}$ are plotted as a function of y, the total area under the perturbed curve is equal to the area under the unperturbed curve between some y_1 and infinity, i.e.,

$$I = \int_0^\infty \phi_1 \phi_2 y^{-2} dy \cong \int_{y_1}^\infty \phi_1^{(0)} \phi_2^{(0)} y^{-2} dy . \tag{34}$$

Then

$$I \cong \int_{y_1}^\infty \phi_1^{(0)} \phi_2^{(0)} y^{-2} dy = \int_0^\infty \phi_1^{(0)} \phi_2^{(0)} y^{-2} dy - \int_0^{y_1} \phi_1^{(0)} \phi_2^{(0)} y^{-2} dy$$

$$= I^{(0)} - \int_0^{y_1} \phi_1^{(0)} \phi_2^{(0)} y^{-2} dy . \tag{34a}$$

The integration involves only unperturbed radial functions:

$$\int_0^{y_1} \phi_1^{(0)} \phi_2^{(0)} y^{-2} dy = \frac{2(k-\rho)\rho(2\rho+1)}{(2k-1)[\Gamma(2\rho+1)]^2} (y_1)^{2\rho-1} I^{(0)}, \tag{35}$$

where

$$k = -\ell - 1 , \quad \text{for} \quad j = \ell + \frac{1}{2}$$

$$= +\ell , \quad \text{for} \quad j = \ell - \frac{1}{2} .$$

The correction to the interaction constant can then be written as $1 - \delta$, where

$$\delta = \frac{2\rho(k-\rho)\,(2\rho+1)}{(2\rho-1)\,[\Gamma(2\rho+1)]^2}\,(y_1)^{2\rho-1} . \tag{36}$$

For an s electron, $k = -1$, so that

$$\delta_s = \frac{2\rho(\rho+1)(2\rho+1)}{3[\Gamma(2\rho+1)]^2}(y_1)^{2\rho-1} . \tag{36a}$$

Assuming the nuclear charge to be on the surface, Rosenthal and Breit[20] found $y_1 \cong 2y_0$ for large Z (y_0 is the value of y corresponding to $r = R_0$, the nuclear radius). More recently, Crawford and Schawlow[21] have repeated these calculations, assuming a uniform nuclear-charge distribution. They find, for this case, $y_1 \cong y_0$.

The previous calculations have considered the magnetism of the nucleus to be concentrated in a point dipole at $r = 0$. If one considers the origin of nuclear magnetism, however, it must be admitted that such an assumption may produce at best only an approximation to the actual situation. The nucleus is made up of a distribution of particles, each of which has an intrinsic magnetic moment. If these particles move in orbits, as predicted by the shell model,[22] then one would expect a further contribution from such motion. Collective motion of the nuclear particles[23] could produce further deviations from the simple point-dipole interaction between the nucleus and the electrons.

A correction to the hfs interaction energy has been calculated by Bohr and Weisskopf[24] to include the effects of the distribution of nuclear magnetism. They consider two kinds of magnetism, spin magnetism and "orbital" magnetism. The first is, of course, caused by the distribution throughout the nucleus of particles, each of which

possesses an intrinsic spin and magnetic moment. The orbital contribution is due to circulating currents caused by the movement of charged particles within the nucleus. The latter type of magnetism will have a smaller effect on the correction to the hfs, because the effective dipole distribution for a nuclear current loop has a maximum at the center of the loop, thus more nearly approximating the point-dipole nucleus. As was true of the Breit-Rosenthal correction, the Bohr-Weisskopf correction is most important for s states. It is of little importance for $p_{1/2}$ states and virtually insignificant for states of higher J. If an electron orbit does not penetrate into the nuclear volume, then the assumption of a point charge and a point-dipole moment becomes more valid.

If α_s and α_ℓ are the respective fractions of the nuclear magnetism that are due to spin and orbital angular momentum in the nucleus, then the Bohr-Weisskopf correction is given by $(1+\epsilon)$, where

$$\epsilon = -(\alpha_s \overline{K}_s + \alpha_\ell \overline{K}_\ell) . \tag{37}$$

The quantities $\overline{K}_s$ and $\overline{K}_\ell$ represent averages of K_s and K_ℓ over the nuclear coordinate, R, where

$$K_s = \int_0^R [1+\zeta(\frac{r}{R})^3]\, FG\,dr \Big/ \int_0^\infty FG\,dr \tag{38a}$$

$$K_\ell = \int_0^R [1-(\frac{r}{R})^3]\, FG\,dr \Big/ \int_0^\infty FG\,dr . \tag{38b}$$

The factor ζ is the nuclear average of an operator which includes the effects of asymmetry of the distribution of spin magnetism. It depends on the particular nuclear model and has been calculated by Bohr[25] for several different coupling assumptions. For the single particle model, Bohr obtains

$$\zeta = \frac{2I-1}{4(I+1)} \qquad \text{for } I = \ell + \frac{1}{2}$$

$$= \frac{2I+3}{4I} \qquad \text{for } I = \ell - 1/2 \,. \tag{39}$$

The integrals in the expressions for K_s and K_ℓ can be evaluated[24] by writing the radial functions F and G in two parts. Inside the nucleus, the wave equations are solved for a uniformly charged sphere of radius R_0, with F and G being expressed as a power series in (r/R_0). These functions are matched at $r = R_0$ with the standard solutions for an unscreened Coulomb potential.[19, 20] The evaluation of the numerators of K_s and K_ℓ will consist in integration of a series of terms of progressively higher order in (r/R_0). After this integration, the quantities K_s and K_ℓ will contain a series of terms of increasing order in (R/R_0). (These must still be averaged over all values of $R<R_0$, using some assumed distribution function $w(R)$.) In their original paper, Bohr and Weisskopf included only second-order terms, approximating the contribution of $(R/R_0)^4$ and higher orders by multiples of $(R/R_0)^2$. The results of these calculations (including the correction of Bohr) are

$$\overline{K}_s = (1 + 0.38\zeta)\, b\, \overline{(R/R_0)^2} \tag{40a}$$

$$\overline{K}_\ell = 0.62\, b\, \overline{(R/R_0)^2} \,, \tag{40b}$$

from which

$$\epsilon = -\left\{(1 + 0.38\,\zeta)\, a_s + 0.62\, a_\ell\right\} b\, \overline{(R/R_0)^2} \,. \tag{41}$$

The factor b is a function only of Z and R_0, and is tabulated in Ref. 24. (It should be noted that in calculating b, Bohr and Weisskopf used $R_0 = A^{1/3} r_0$ with $r_0 = 1.5\times10^{-13}$cm, rather than the more recent value[26] of 1.2×10^{-13}cm.)

In a recent review article, Eisinger and Jaccarino[27] have extended the Bohr-Weisskopf calculation to include terms of order $(R/R_0)^4$.

The error introduced in K_s and K_ℓ by neglecting higher powers of (R/R_0) is stated by them to be less than 2%. Their expressions for $\overline{K_s}$ and $\overline{K_\ell}$ are more elaborate, involving six constants rather than the single one of the original work:

$$\overline{K_s} = (b_{s2} + \zeta\, b'_{s2})\, \overline{(R/R_0)^2} - (b_{s4} + \zeta\, b'_{s4})\overline{(R/R_0)^4}\,, \tag{42a}$$

$$\overline{K_\ell} = b_{\ell 2}\, \overline{(R/R_0)^2} - b_{\ell 4}\, \overline{(R/R_0)^4}\,. \tag{42b}$$

The constants are tabulated in the paper[27] for $10 \leqslant Z \leqslant 90$ in steps of 5.

In order to evaluate the averages involving the nuclear coordinates, R, it is necessary to make some assumptions regarding the distribution of particles in the nucleus. Bohr and Weisskopf assumed $(R/R_0)^2 \approx 0.8$ for their comparisons of calculated hfs anomalies with experimental results. This value is a compromise between 3/5 for a uniform distribution and 1 for a surface distribution, the thought being that an unpaired particle might tend to stay nearer the nuclear surface. To calculate the averages $(R/R_0)^2$ and $(R/R_0)^4$, Eisinger and Jaccarino assume a single-particle model, in which the odd nucleon moves in a spherically symmetric square potential well. Their calculations are summarized by means of graphs which are easily used to find the desired averages to within a few percent. For $A \geqslant 100$, the calculated averages are fairly insensitive to changes in A, but depend significantly on the principal quantum number and on the orbital angular momentum of the single-particle state.

Even after calculation of the nuclear averages $\overline{K_s}$ and $\overline{K_\ell}$, there remains a certain amount of ambiguity about the size of the correction, because the two fractional contributions α_s and α_ℓ of the spin and the orbital magnetic moment to the nuclear moment are not known. The factors α_s and α_ℓ can be calculated if a particular model of nuclear structure is assumed. The agreement between the measured moment and that calculated from the measured hfs $\Delta\nu$ then becomes a test of the particular nuclear model that was used to evaluate ϵ.

If α_s and α_ℓ are expressed in terms of the nuclear g-factors, then

$$\alpha_s = \frac{g_s}{g_I} \frac{g_I - g_\ell}{g_s - g_\ell} , \tag{43a}$$

$$\alpha_\ell = \frac{g_\ell}{g_I} \frac{g_I - g_s}{g_s - g_\ell} . \tag{43b}$$

The g factors are defined by $g_I \vec{I} = g_s \vec{s} + g_\ell \vec{\ell}$, quite independent of the chosen nuclear model, if only the respective spin and orbital angular momenta can be described by the vectors $\vec{s}$ and $\vec{\ell}$. It is usually desired to calculate g_I or $\mu_I = g_I \mu_0 I$ from measurements of the hfs. If Eq. (26) is inverted, the expression for μ_I is

$$\mu_I = -3/4 \; \frac{h\Delta\nu}{2I+1} \; \frac{I}{g_J \mu_0} \; \frac{a_H^3 n_0^3}{Z Z_0^2} \; \frac{1}{1-\frac{d\sigma}{dn}} \; \frac{1}{F_r(1/2,Z)} \; \frac{1}{1-\delta} \; \frac{1}{1+\epsilon} . \tag{44}$$

If μ_I is expressed, as usual, in nuclear magnetons

$\mu_N = (m_e/M_p)\mu_0$, and $\Delta\nu$ in Mc/sec, then

$$\mu_I(n,m) = \frac{\mu_I}{\mu_N} = -1.5722 \times 10^{-2} \; \frac{n_0^3}{g_J Z Z_0^2} \; \frac{1}{1-\frac{d\sigma}{dn}} \; \frac{1}{F_r(\frac{1}{2},Z)} \; \frac{1}{1-\delta} \; \frac{1}{1+\epsilon} \; \frac{I}{2I+1} \; \Delta\nu . \tag{45}$$

(All constants used in these calculations are listed in the Appendix).

This expression must be considered to be only approximately correct because of uncertainties in the various corrections it includes. A procedure that partially avoids these uncertainties is often used to obtain nuclear moments from hfs measurements. The assumption is made that the various corrections are very nearly the same for all isotopes of a given element. Consequently, a comparison of the hfs of two isotopes of the same element can lead to a similar comparison of the magnetic moments of the two isotopes, i.e.,

$$\frac{\mu_1}{\mu_2} = \frac{\Delta\nu_1}{\Delta\nu_2} \frac{I_1}{I_2} \frac{2I_2+1}{2I_1+1} \quad . \tag{46}$$

This relation is called the Fermi-Segrè formula and has been found to hold with an accuracy of better than 1%. Slight deviations from the Fermi-Segrè formula (< 1%) are discussed as "hfs anomalies" and have been attributed principally to variations in the distribution of nuclear magnetism. The Bohr-Weisskopf theory discussed above has had considerable success in accounting for the observed hfs anomalies. However, the success of the theory in predicting nuclear moments from observed hfs $\Delta\nu$ is considerably less, which fact will be demonstrated for the nuclei under investigation here. It should be noted too that experimental results are available for only a relatively small number of isotopes (for a summary in April 1958, see Ref. 27). As more data become available, the suitability of the Bohr-Weisskopf description of anomalies will be under close examination.

III. EXPERIMENT

A. Theory of the Experiment

The effect of a homogeneous magnetic field on a magnetic dipole is to align the dipole with the field. If the field is inhomogeneous, there will also be a net force on the dipole, directing it toward a region of lower field. The coupled spin system of an atom behaves like a magnetic dipole. Its effective moment is field-dependent, being given for any state of the system by

$$\mu_{eff} = - \frac{\partial W}{\partial H} ,$$

where W is the energy of the state. Thus, for an atomic system which is describable by a Breit-Rabi diagram, the effective magnetic-dipole moment of each state is given by the negative slope of the curve that corresponds to that state.

In an atomic-beam magnetic-resonance apparatus, the beam of atoms is directed through two successive inhomogeneous strong magnetic fields, where the field gradient is perpendicular to the beam. The beam is thus deflected by these fields, much like an electron beam passing between charged plates. The effective moment of an atom in the beam is given (for large H) by

$$\left| \mu_{eff} \right|_{H \to \infty} = g_J \mu_0 m_J + g_I \mu_0 m_I .$$

Since $g_J \sim 2000\, g_I$, the effective moment in the inhomogeneous fields is determined almost entirely by the electronic substate m_J. This is illustrated in Fig. 1 by the fact that for large x, the lines of each diagram form two groups of essentially parallel lines, the slopes of which correspond to the two values $m_J = \pm 1/2$ in the above expression.

If the fields and gradients of the two inhomogeneous fields (A and B fields) are oriented as shown in Fig. 2, the apparatus is said to operate on the flop-in principle.[7] Unless there is a change in the strong-field effective moment of an atom after the atom leaves the

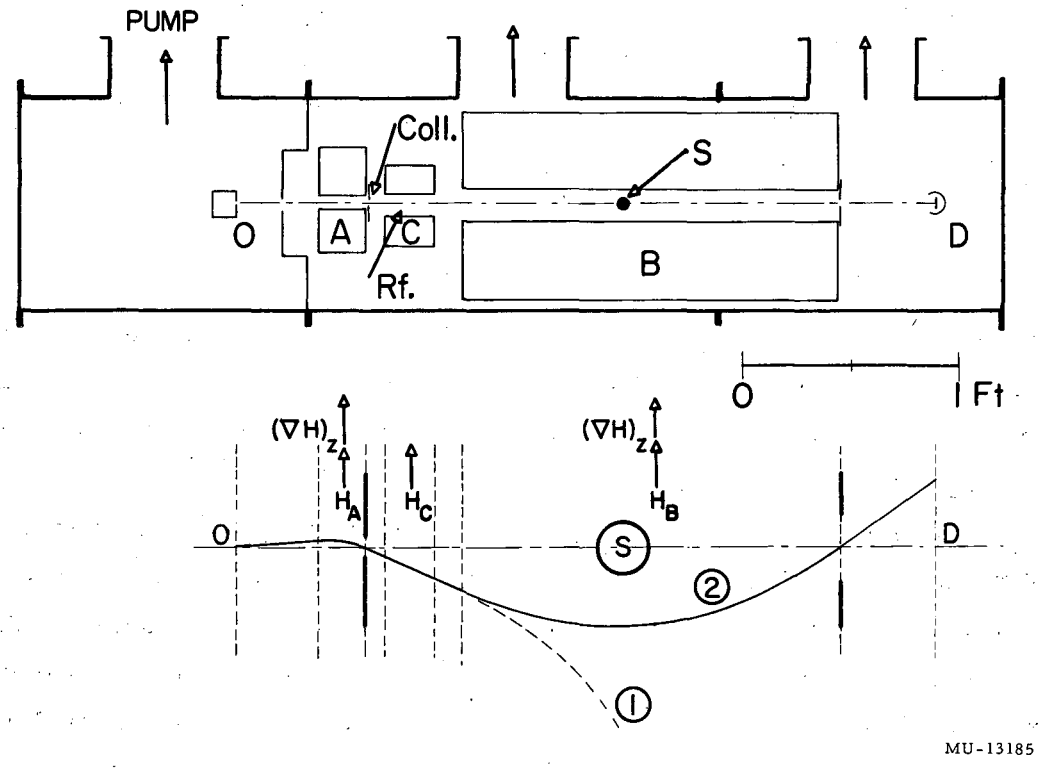

Fig. 2. Schematic diagram of the atomic-beam magnetic-resonance apparatus, showing arrangement of fields for flop-in operation. (Deflections shown for typical trajectories are much exaggerated.)

A field, the deflection in the B field will be in the same direction (path 1) and the atom will be "thrown out" away from the detector. If a change in the strong field μ_{eff} of the atom does occur or is induced between the deflecting fields, then the deflection in the B field will be in the opposite sense to that in the A field. The result (path 2) is a focusing or "flop in" to the detector of only those atoms for which such a change of effective moment has occurred.

From the Breit-Rabi diagram (Fig. 1), it can be seen that most of those transitions for which $\Delta m_J = \pm 1$ involve an energy difference of about $h\Delta\nu$ at most fields. There is one exception, however. The transition energy between the levels $(I+1/2, -I-1/2)$ and $(I+1/2, -I+1/2)$ actually approaches zero as the applied external field decreases to zero. The field dependence of this "standard" transition has been found to be (Eq. (21)):

$$\nu_s = \nu_0 - g_I \mu_0 H/h + \frac{2I}{\Delta\nu} \nu_0^2 + \frac{2I(2I-1)}{\Delta\nu^2} \nu_0^3 + \mathcal{O}\left(\frac{\nu_0^4}{\Delta\nu}\right) ,$$

with

$$\nu_0 = (-g_J + g_I) \mu_0 H/h(2I+1) .$$

An experimental procedure now suggests itself. A homogeneous magnetic field of variable intensity is applied along the beam path in the region between the homogeneous A and B fields. The strength of this "C field" serves to determine the separation of energy levels for--but does not alter the trajectories of--the atoms passing through it. If a weak magnetic field, oscillating at an rf frequency ν, is superimposed on the homogeneous C field, then transitions may be induced[28] between any two energy levels whose energy difference is $h\nu$. In particular, if the frequency of the applied rf field is nearly the same as ν_s for the particular C field, transitions will be induced between the levels $(I+1/2, -H/2)$ and $(I+1/2, -I+1/2)$. The fraction of the atoms in the beam that do undergo such transitions is a maximum at $\nu = \nu_s$; since this transition satisfies the focusing condition of the apparatus (change in sign of μ_{eff}), the number of atoms reaching the detector

will be a maximum at $\nu = \nu_s$. The fraction of atoms that make focusing transitions in the C field will be proportional to the number of states participating in the transitions. If only a single transition is induced, then the number of states involved is two. There are a total of 2(2I+1) distinct energy levels. Therefore the fraction of the beam that undergoes the transition, i.e. the intensity of a resonance signal, is proportional to $\frac{1}{2I+1}$. If the same number of focusing transitions can be induced for two different isotopes, which form equal parts of a beam, then the resonance heights for the two isotopes will be in the ratio of $2I_1+1/2I_2+1$, with the larger resonance associated with the smaller spin.

At very low C fields, ν_s is given (neglecting terms in g_I) by

$$\nu_s \approx - g_J \mu_0 H/h(2I+1) \approx \nu_0 .$$

If g_J is known from previous work on stable isotopes, a knowledge of H coupled with the measurement of ν_s provides a straightforward determination of the nuclear spin, I. The magnetic field strength is not known a priori, but is easily measured by using some calibration isotope with a known spin and hfs. In the same C field, the frequency of the standard transition for such a calibration isotope is given by

$$\nu_{cal} \approx -g_J^{cal} \mu_0 H/h(2I_{cal}+1) .$$

A simple substitution yields

$$\nu_s = \frac{g_J}{(g_J)_{cal}} \frac{2I_{cal}+1}{2I+1} \nu_{cal}$$

at low fields.

If both the unknown and the calibration isotope have $^2S_{1/2}$ electronic ground states, their g factors will both be nearly equal to two, and the ratio of frequencies determines the spin of the one from a knowledge of the spin of the other. A search for the nuclear spin of an isotope

consists of applying successively, into the uniform C-field region, discrete radiofrequencies given for various possible spins by the above equation. If one of the spins is that of the isotope under observation, then an increase will be observed in the number of atoms that reach the detector. This simple picture is valid only for low fields, when $\nu_s \approx \nu_0$.

As the transition field strength is increased, higher order terms become important in the expression for ν_s (Eq. (21)). These terms involve the hfs separation $\Delta\nu$ as well as the nuclear spin. Repeated resonances at higher and higher fields provide measurements of $\Delta\nu$ with increasing precision. When the $\Delta\nu$ of an isotope is known to within a few megacycles per second by such techniques, it is practical to attempt to induce one of the direct ($\Delta F=\pm 1$) transitions at low fields. Observations of direct transitions with the C field near zero produce the most accurate values of the hfs $\Delta\nu$.

B. Apparatus

The design and construction of the atomic beam apparatus used in these experiments (Fig. 3) have been described by Sunderland.[29] Some modifications were made by Shugart,[30] whose thesis also includes a short history of atomic beams work at the University of California. The description included here will be limited to those parts of the apparatus which are directly involved in producing, deflecting, and detecting the atomic beams.

1. Beam Production

The beam of radioactive atoms originates from a tantalum oven (Fig. 4). A cavity is drilled into the top of the oven to receive the radioactive substance, and the hole can be closed with a press-fitted oven cap. The atoms escape from the oven through a small hole in the front, which may be closed off by a pair of adjustable jaws. Ordinarily the jaws are separated slightly, producing a slit source about 0.1 inch high and a few thousandths of an inch wide. Relatively high temperatures ($\sim 2000^{\circ}$C) were often used in these experiments, and electron bombardment provided the only practical way of achieving them. Bombardment currents of as much as 500 ma at 600 v have been obtained from a hot thoriated tungsten filament which is mounted near the front of the oven. High-voltage contact to the oven with minimum heat loss is provided by three pins, which project from a solid oven platform. The pins also aid in alignment of the oven. The entire oven assembly is mounted on an "oven loader" with which the oven may be removed from or loaded into the apparatus without disturbing the high vacuum inside. Behind the "radioactive" oven is a second oven which is used to calibrate the

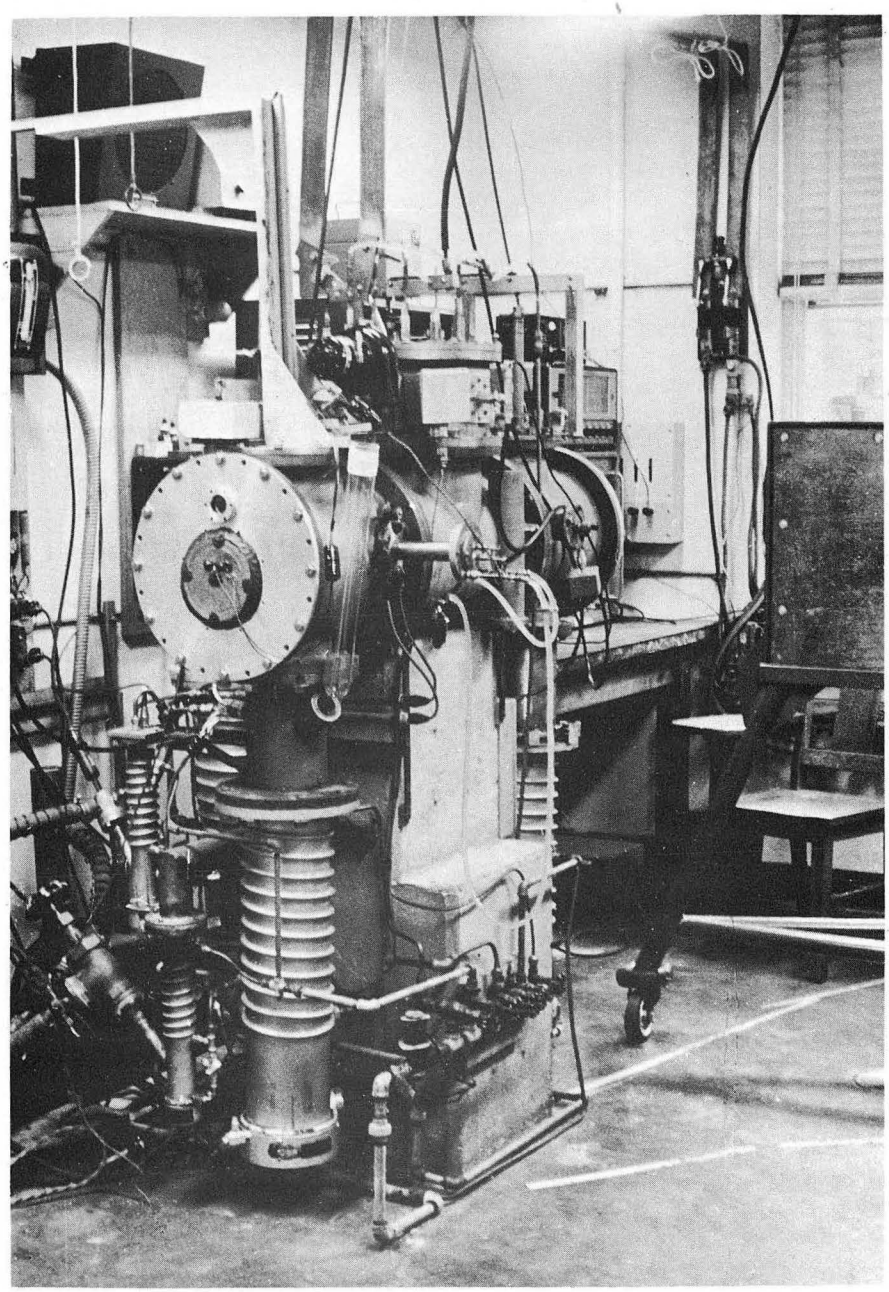

ZN-1723

Fig. 3. The atomic beam apparatus as viewed from the source end.

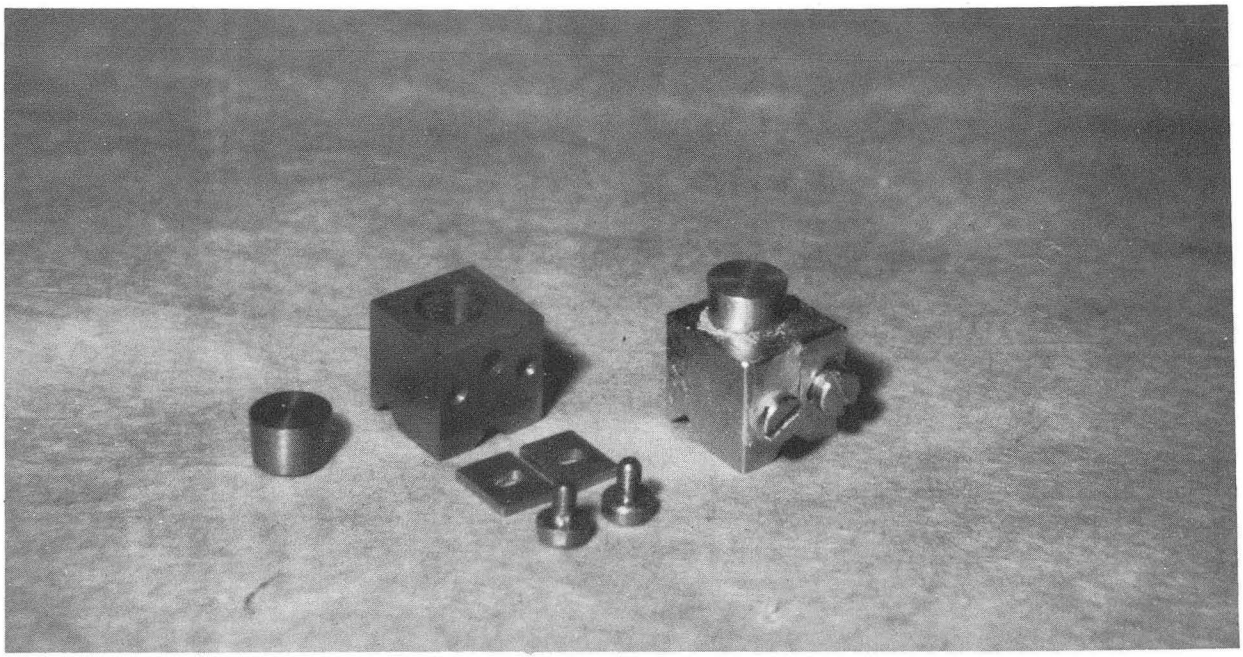

ZN-2195

Fig. 4. Tantalum atomic-beam-source ovens, showing the adjustable-slit assembly.

transition field of the apparatus. When it is desired to calibrate the field, the "radioactive" oven must be moved to one side, so that the beam of the calibration oven can enter the magnet system. This movement is provided from outside the apparatus by a movement of the entire oven loader.

In order to calibrate the value of the field in which the rf transitions take place, a beam of alkali atoms is used. The atomic and nuclear constants of the stable alkali atoms are known well enough that the field may be precisely calculated from the frequency at which a resonance is observed to occur. Of course, the simplest way to produce a beam of alkali atoms is to heat some of the metal in an oven. However, the alkali metals are very reactive and deteriorate rapidly in the atmosphere. A standard method of producing a source of alkali atoms is to heat together an alkali halide and freshly cut filings of calcium metal. The reaction is a simple one, the calcium exchanging with the alkali at a moderate temperature. In these experiments, this reaction proceeded in an iron oven set on pins and heated by conduction from an insulated tantalum coil filament. The calibration oven was mounted inside the apparatus, and since it could not be removed and refilled so conveniently it was designed with a larger capacity than the "radioactive" oven. Most of the time the calibration beam is obstructed by the other oven, but when it is necessary to calibrate the fields, the tantalum oven is moved aside, and the alkali beam can enter the field regions.

2. Beam Detection

Detection of the alkali beam is not a problem. The surface ionization detector[31] makes use of the low ionization potential of the alkali metals. If the alkali atom strikes a hot tungsten surface (not thoriated), it is quickly "evaporated" off again. Since the work function of the tungsten is somewhat higher than the ionization potential of the alkali atom, the single valence electron is left behind when the atom leaves the tunsten surface. In this particular application, the resulting positive ions are collected on the grid of an electrometer tube, thus unbalancing the electrometer circuit and causing a galvanometer deflection.

Surface-ionization detection is possible, of course, only for those elements which have a very low ionization potential. For silver or gold, which are of interest here, other means must be employed.[32]

Since all the isotopes under investigation here are radioactive, it is convenient to look for and identify them by means of that radioactivity.[8] To this end, provision is made for collecting samples of the beam and for counting the radioactivity of these samples. In order to be able to take samples of the beam, it is necessary to have some surface to which the radioactive atoms will stick after striking. Surfaces of fused sulfur have been found to be satisfactory for a wide range of elements, including gold and silver. The sulfur is melted into a milled slot in a brass holder called a button. Use of this holder provides a convenient means for handling the sample and for reproducible positioning in the apparatus and in the counters. When a sample of the beam is to be taken, a button is introduced into the apparatus by a "button loader" so that the sulfur surface on the button is in such a position as to be hit by the beam. The button loader includes a vacuum lock similar to that on the oven loader, so that buttons may be quickly placed in or removed from the high vacuum without disturbing that vacuum. After a timed exposure to the beam, each button is removed from the apparatus, and the sulfur surface is covered with Scotch tape. This procedure precludes brushing any activity off the button after its exposure, particularly in the x-ray counters, where the sulfur surface must be placed in close proximity to the sodium iodide scintillation crystal.

On the side of each button is a groove which locks the button to a spring-loaded ball bearing in the button loader. This device serves to place the sulfur surface of each button in the same position relative to the beam. The same type of locking device positions the buttons in counters which determine how much radioactivity has been accumulated on each of them.

Since most of the isotopes under investigation decay by electron capture, special x-ray counters have been found to be very useful for counting. These counters use a very thin ($\sim$2 mm)NaI(Tℓ) crystal, which is sufficient to stop radiation of energies up to about 70 kev. The crystal

is slightly larger than the surface on which the radioactivity is collected. It is desirable for the crystal to be as small as possible in order to minimize the cross section it can present to background radiation. The light pulses are sorted by a photomultiplier tube and single-channel pulse-height analyzer. The quality of this counting system is found to be very high for x-rays between about 20 and 80 kev. For lower energies, the background due to electronic noise becomes appreciable, while for higher energies, the resolution is poor. Higher-energy radiation can be counted with these crystals, but with reduced efficiency (see Section III-D). If a quantum of radiation goes completely through the sodium iodide crystal, the amount of energy lost in the crystal (and reradiated as light visible to the phototube) is not a sensitive function of the energy of the quantum. Since the energy lost in the crystal by the quantum determines the apparent energy of that quantum as measured by the pulse-height analyzer, all radiation above $\sim$ 100 kev seems to have about the same energy. Thus, if a nucleus decays by any process that includes some gamma radiation, it can be counted in the x-ray crystal counters, although there is virtually no resolution. The efficiency of counting is also decreased for high-energy radiation. Even if there is only a single gamma transition, to the counter the gamma quanta will <u>appear</u> to be of many different energies, depending on how far they traveled in the crystal, i.e., at what angle they passed through. Since it is desirable to count as narrow a range of energies as possible in order to reduce the background rate, the counter is able to record only a part of the pulses caused by incident gamma quanta of a given energy. Furthermore, since the counter background consists of radiation that does not stop in the crystal, the background can be expected to have a similar behavior to that of high-energy nuclear radiation. Consequently, when the counters are so adjusted as to best count whatever high-energy radiation is emitted by the sample, they are also set to best count the background radiation that can reach the crystal. The counter background is observed to have a maximum at just those counter settings at which nuclear gamma radiation is most efficiently counted.

The sodium iodide crystals in the x-ray counters must be protected from the atmosphere because of their deliquescence. If a crystal takes up enough moisture, its transparency and hence its usefulness is permanently impaired. The crystals of the x-ray counters used here are protected from moisture by immersion in mineral oil. The part of the crystal that is exposed to radiation is protected from the air by a thin (0.001-inch) aluminum-foil window, through which the radiation must pass in order to reach the scintillator. The unavoidable absorption by this window is much larger for beta particles than for electromagnetic radiation.

A second type of radiation counter has been used for some of the more recent experiments on the β^+ - emitting 30-minute isotones of silver. The new type of counter avoids any attenuation of the radiation from the button-mounted sample by effectively using the sulfur surface of the button as part of the ionization chamber of an ordinary gas counter. The buttons are inserted into the counter so that the sulfur surface (not covered with Scotch tape this time) is actually inside the counting chamber. A continuous flow of gas (methane) is maintained to flush out the air that may be admitted whenever the samples are changed.

The gas counters have not yet proved very satisfactory for precision work when it is necessary to differentiate between two isotopes with similar half lives. The counters seem to be subject to sudden changes in counting efficiency. As a result, the decay curves of certain samples have been observed to be somewhat erratic. Although the higher efficiency of the gas counters aided greatly in the search for resonances, the final statement on the composition of a resonance was withheld until a confirmation run could be made and counted in the crystal counters. If no x-ray could be detected in the spectrum of an isotope, then its decay curve was obtained by (inefficient) counting of the higher-energy nuclear gamma rays that followed beta decay.

3. The Magnet System

The "heart" of an atomic beam apparatus consists of two strong inhomogeneous magnetic fields (A and B), a variable homogeneous C field between these deflecting fields, and an rf loop in the C field to induce transitions. The apparatus used in these experiments is asymmetric, i.e., the B magnet is ~9 times as long as the A magnet (21-1/4 in. compared with 2-1/4 in.). To retain the focusing properties, compensation for this asymmetry is obtained by having a larger field gradient in the A field (about five times as large). Both fields are of nearly the same strength. Their windings are connected in series across a 4-v output from banks of submarine batteries. The A- and B-field coils normally draw currents of 500 to 600 amp and produce a field strength of about 5000 gauss.

It is in the C field that transitions are induced among the energy levels of the atomic system. This field is produced by an electromagnet, the pole tips of which must be accurately parallel to provide a high degree of field uniformity. The strength of the transition field is continuously variable from 0 to 640 gauss. The required magnet currents (0 to 125 ma) are supplied by a voltage-divider circuit which is connected across a regulated power supply. Temperature effects in the potential divider are believed to be one factor contributing to the observed drift of the C field. A second contribution to this drift may be magnetic coupling between the C field and the inhomogeneous fields on either side. As the current changes in the deflection-field windings (1 to 3 amp per hour, depending on battery charge), the changing strength of those fields could be expected to "pull" the much weaker C field. Fortunately, the transition field strength is observed to drift only slightly during a given set of exposures, so that the small correction can be neglected in many cases. If a correction is deemed necessary, the assumption of a linear drift with time is sufficient to remove much of the uncertainty in a given measurement.

The radio-frequency magnetic field which actually causes transitions is produced by a conducting loop ("hairpin") carrying an oscillating current. The rf hairpin is oriented in the region of uniform field (C field), so that the beam may pass through the loop. The

oscillating current in the loop is supplied from an rf source, the exact nature of which depends on the desired frequency range. Often an oscillator will not produce sufficient power to establish an rf magnetic field that is strong enough to cause transitions. Then it is necessary to increase the rf power output by suitable amplification. The particular rf equipment that was used in these experiments is listed in Table I.

Table I

Radiofrequency sources

Frequency range (Mc)	Equipment
1 - 20	Tektronix 190 signal generator
15 - 210	Hewlett-Packard HP608A variable oscillator plus wide-band linear amplifiers (HP640 AB or ifi 500 and 510)
200 - 1500	Airborne Instruments Model 124c power oscillator
500 - 1000	Gertsch FM 4A + traveling-wave-tube amplifier (Wave Particle Company No. 505A)

At no time did poor oscillator stability seem to be a problem, although the Airborne 124c had to be well adjusted to prevent its drifting.

The oscillator frequencies were continually monitored by a Hewlett-Packard 524B frequency counter. Plug-in units 525A and 525B extend the monitoring range to ~200 Mc/sec, and a transfer oscillator HP 540A provides harmonics to beat against higher frequencies. The internal 100 kc crystal timing standard of the frequency counter was periodically standardized by comparison with an Atomichron cesium clock.

C. Isotopes

The atomic-beam measurements described here include work on six neutron-deficient isotopes each of silver and gold. In addition, the neutron-excess isotope silver-110m has been studied. All thirteen isotopes are well known (with the possible exception of ~1-hr silver-104) and are included in most compilations of radioactive isotopes.[33] For many resonance samples the isotope assignments were made by a crude measurement of the half life of the sample. Therefore, the accuracy of the isotope assignment is dependent upon previous measurements of isotopic half lives. In Table II are listed all the isotopes for which measurements have been made. In subsequent columns are tabulated the half life and principal mode of decay (if known) of each isotope. In the final column are listed a few primary references for the isotope. These include references for the original identification, the best half life value, decay branching ratios, etc.

Table II

Summary of measured isotopes

Isotope	T 1/2	Decay modes	References
Silver-103	1.1 hr	β^+, EC	34, 35
104	27 min	β^+	36
104	1.2 hr	EC, β^+	37, 38
105	40 d	EC	37, 39
106	24 min	β^+, EC	34, 40, 41, 42
106	8.3 d	EC	42, 43, 44, 45
110m	253 d	β^-	46, 47, 48, 49, 50
Gold-191	3.0 hr	EC	51
192	4.8 hr	EC	52, 53, 54
193	17 hr	EC	52, 53, 54
194	39 hr	EC	52, 55
195	180 d	EC	52, 55, 56
196	5.6 d	EC	52, 55, 57, 58

1. Isotope Production

The only neutron-excess isotope in this series (silver-110m) was produced by the (n, 3γ) reaction on stable silver-109 in the Materials Test Reactor (MTR) at Arco, Idaho. The long half life (253 days) made necessary a very high neutron flux to produce appreciable quantities of the isotope. At the time of the experiment, the MTR was the nearest reactor with a flux large enough ($\sim 10^{14}$ neutrons/cm^2/sec) to produce a sample with high specific activity. [The Knudson condition[59] effectively limits the rate at which the silver may be boiled out of the oven in a usable beam. There must be a certain minimum amount of radioactive silver in this beam, thus establishing a minimum specific activity for an oven charge.] Neutron bombardment of stable silver also produced silver-108, but its 2.3-min. half-life precluded any interference with the measurements on the 253-day isotope, which were conducted several weeks later.

The neutron-deficient isotopes of silver and gold were produced in the Crocker 60-in. cyclotron on the Berkeley campus of the University of California. This cyclotron accelerates protons, deuterons, or alpha particles to energies of about 12 Mev/nucleon. All three types of bombarding particle have been used in various stages of this work and will be discussed in detail in later sections.

2. Cyclotron Targets

Two general types of cyclotron target have been used in these experiments. The internal target, which uses a single foil of the target material, is inserted into the cyclotron tank to intercept the beam at any desired radius (giving some control over the particle energies). The external target, an aluminum assembly for holding solid target materials of any form, is attached to the edge of the cyclotron vacuum tank, and the beam is deflected out from its circular orbit to the target. The beam current that may be directed onto an external target is considerably less than that which may be used on an "internal probe" target. The external target is isolated from the main cyclotron tank by a system of thin aluminum foils, and if too high a beam current is

directed through these foils, they may rupture, thus raising the tank pressure above its operating level. Ion currents of as much as 50μa have been used on external targets for short periods of time with no apparent damage. On the internal probe, a beam current as high as 125 μa has been used for bombardments of several hours' duration.

Target material for the internal probe must be in the form of a single piece of foil 1-3/4×1-1/2 in. The material must be soft enough so that the foil can be rolled into a semicylindrical shape without cracking. The necessary thickness of the foil is determined by the range of the bombarding particles and by the length of the bombardment. (Another consideration is the amount of target material it is feasible to dissolve in a time short compared with the half lives of the desired isotopes produced.) If the bombardment is to be long (as when a long-lived isotope is being produced), the foil should be thick enough to stop the incident beam completely. Otherwise, the unstopped beam strikes the water behind the target. The result is a corrosive action on the back of the target, which will cause the target to fail during an extended bombardment. The ranges of 12-Mev protons, 24-Mev deuterons, and 48-Mev alpha particles are roughly in the ratios of 1:2:1 for a given target material.

Owing to the high cost and limited availability of rhodium and iridium foils, no attempt was made to run them on an internal probe. Neither would seem to be very suitable because of the brittleness of the foils. Palladium and platinum were both bombarded on the internal probe with good results. Although the platinum foil could be rolled equally well in either direction, the palladium seemed to have a preferred direction of rolling. If the foil was rolled the wrong way, cracks appeared which caused an early failure of the target. It has not been determined whether this phenomenon is a general characteristic of palladium foils or merely a consequence of the methods used in the production of this particular foil.

For the external target, there is no necessary form for the target material. Large and small pieces of foil of various thicknesses have been used with uniform success. An aluminum cover foil is used to hold small pieces of foil in the target. One advantage of the external target over the internal probe is a greater control by the experimenter over the energy of the particles incident on the target material itself. Any desired thickness of aluminum foils can be placed on top of the target material to degrade the beam energy to a preferred value. This is of particular importance in alpha-particle bombardments, in which it may be desirable to produce one of the (α, kn) reactions with a minimum contamination from the other α-induced reactions.

The photograph of the external target assembly used in these experiments is presented in Fig. 5. The assembly is made of dural to minimize its contamination by a bombardment. Water cooling is used to dissipate the heat produced by the cyclotron beam. The target foil is placed directly on the water-cooled back plate and covered with the desired thickness of aluminum foil to degrade the beam. The grid serves to hold the target in place, and also improves the thermal contact between the target foil and the back plate. The most serious damage to the target that has been observed is the melting of the thin (0.001-inch)aluminum cover foil which was used when the full energy of the beam was needed on the target. Cooling of this cover foil is provided principally by conduction through the target material. When this material consists of foil pieces, there are necessarily gaps between the pieces where there is no cooling of the cover foil at all. Unequal cooling may also warp the cover foil to such an extent that it is separated from the target foil and can be easily melted. A decrease in beam current would prevent such effects. Since the target material is in the form of pieces with appreciable size, there is no danger of contamination if the cover foil ruptures. However, such a rupture might allow the target foil to fall away from the region of high cyclotron beam density, thus decreasing the efficiency of the bombardment.

A principal design feature of this external target assembly is the ease and speed with which the target foil may be removed. After bombardment, the three screws may be loosened. The swivel socket is used to flip one screw out of the way, allowing the cover foil and grid to pivot around one of the two at the other end of the assembly. The target foil is then exposed for suitable disposition.

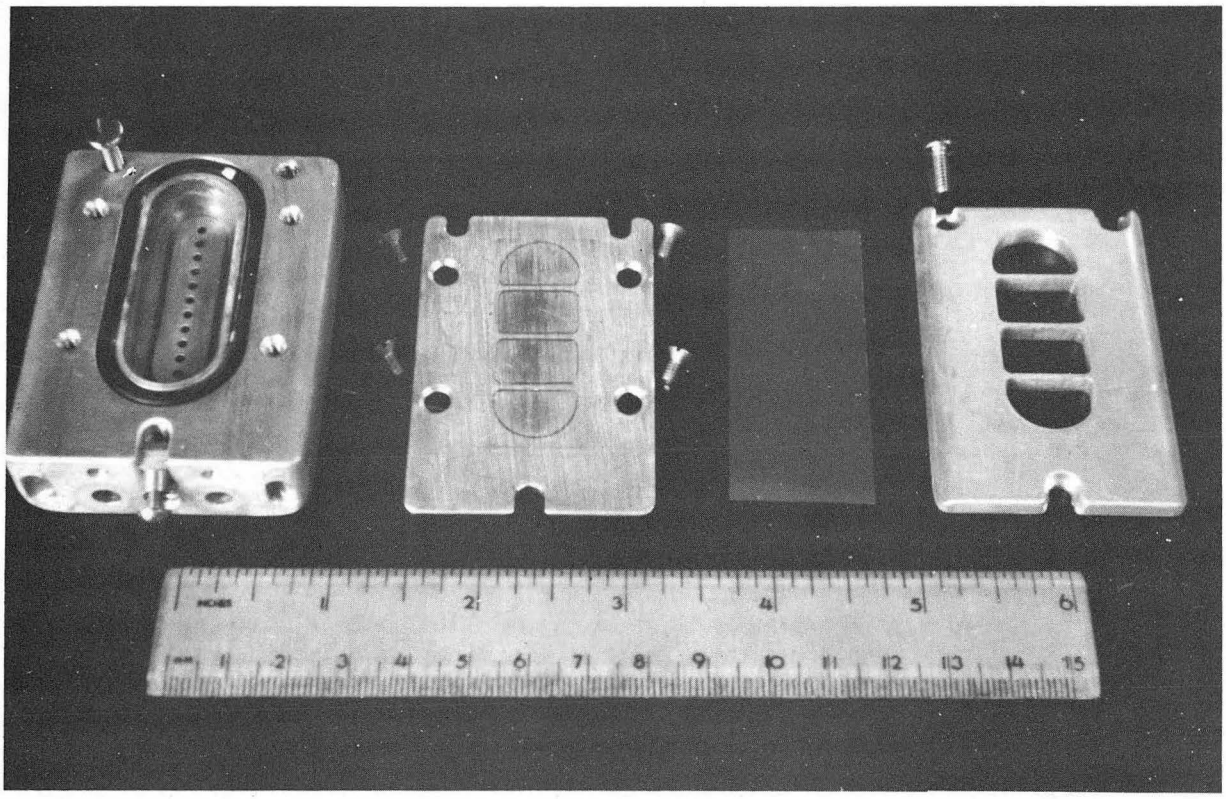

ZN-2193

Fig. 5. External target assembly.

D. The Silver Isotopes

1. Rhodium Target

The only stable isotope of rhodium is Rh^{103}. Since the ~48-Mev alpha particles from the 60-in. cyclotron can be expected to produce (α, kn) reactions with $1 \leqslant k \leqslant 4$, it is possible to produce silver isotopes with mass number A between 103 and 106. The dominant reaction is determined by the actual energy of the alpha beam as it passes through the rhodium target. By degrading the beam energy and using targets of various thicknesses, it is possible to produce whichever of these isotopes is desired.

Since the long-lived Ag^{105}(40-d) and Ag^{106} (8.3-d) are also produced by Pd(p, n) reactions, it is more convenient to make them that way and use the more lengthy chemical separation. The recovery of the silver is nearly 100% for the palladium chemistry, while it appears to be only about 50% for the separation from rhodium. The long half lives and consequent low-level activities make the higher yield desirable. For the short-lived silver isotopes, the yield must be sacrificed in favor of a fast separation.

To determine the foil thickness and alpha-particle energy for each of the short-lived silver isotopes (1.1-hr Ag^{103}, 1.2-hr Ag^{104}, 27-min Ag^{104}, 24-min Ag^{106}) a "stacked foil" experiment was performed. In this experiment, twelve small pieces of 1-mil rhodium foil were stacked in a target holder such that the alpha beam could not enter a given foil without passing through all preceding foils. The assembly was placed in the cyclotron and exposed for one second to a 15-μa beam of ~48-Mev alpha particles. The target was then broken open, and each of the pieces of foil was placed in a standard beam-collecting button. These buttons were rotated through three types of counters for several hours, until the rates leveled out into the long-lived components. The three types of counters were: (a) a standard x-ray crystal counter set to count the silver x-ray; (b) a similar counter set to count (inefficiently) the higher-energy gamma radiation; (c) a continuous-flow gas ionization chamber. The decay curve for each button in each counter was plotted and analyzed into two components, one of 25-min half life, another of

70-min half life. The decay fit was performed on the IBM650 by the OMNIBUS computer program of H. B. Silsbee. The program, which will be discussed later, determines the activity at time $t = 0$ due to each component by performing a least-squares fit to the observed data. (The data obtained were not sufficient to differentiate between 24-min and 27-min or between 66-min and 72-min half lives.) The longer-lived components ($T_{1/2} > 1$ day) were not identified, but were treated as a constant background with essentially infinite half life. The results of this analysis provided crude information about the relative cross section for production of each of the short-lived silver isotopes as a function of the energy of the alpha beam. These results are illustrated for each type of counter in Fig. 6. From these graphs, two important pieces of information are gained (besides the confirmation of existence of the four isotopes). These are: (a) the approximate alpha energy required to produce a maximum amount of each of the isotopes; and (b) the most advantageous method of counting for each of the four isotopes.

Apparently 1.1-hr Ag^{103} and 1.2-h Ag^{104} decay principally by K capture, while 27-min Ag^{104} and 24-min Ag^{106} decay by positron emission or isomeric transitions. The counting can thus be done according to the most efficient method for the isotope that is to be measured.

The combinations of degrading foils and rhodium target foils which were used in the target to produce each of the silver isotopes are summarized in Table III. As can be seen from Fig. 6, Ag^{103} was always produced in the presence of Ag^{104}, since the Rh target was 2 mils thick.

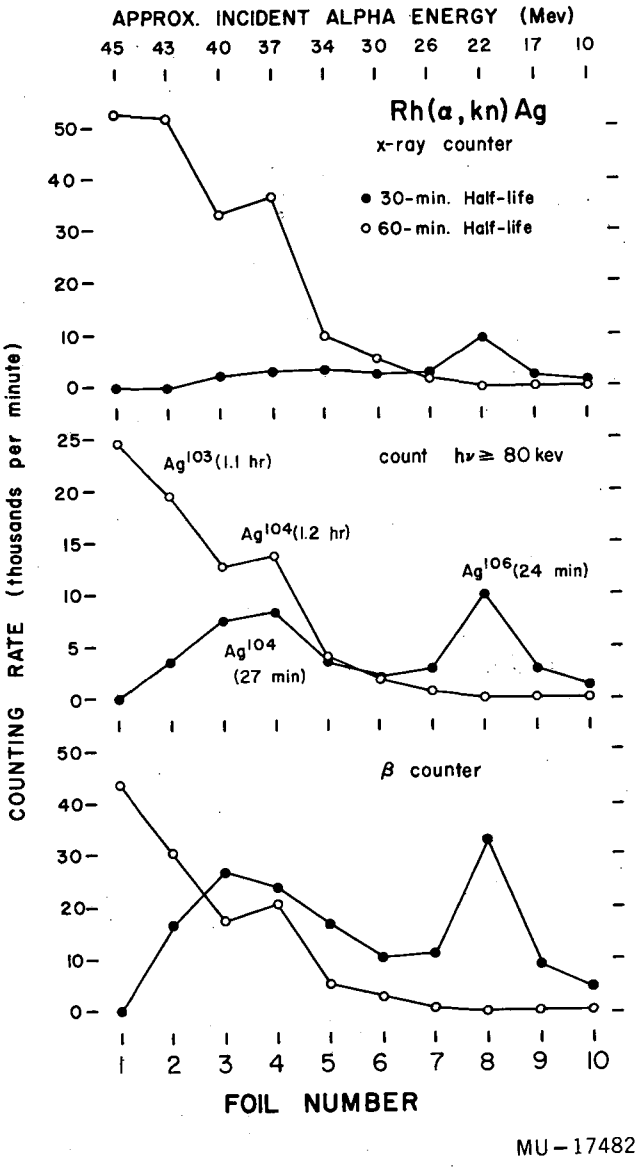

Fig. 6. Results of "stacked-foil" experiment on rhodium.

Table III

Targets for Rh^{103} (α, kn) reactions		
Isotope desired	Thickness of aluminum cover foil (mils)	Thickness of rhodium target (mils)
A = 103	≤ 1	2
104	5-7	4
106	~ 21	2

In most experiments with rhodium-produced activities, the target foil was cut into small pieces before the cyclotron bombardment. After irradiation, these pieces were put into an atomic-beam oven and loaded into the apparatus. If the oven were heated sufficiently, the radioactive silver could be driven out of the rhodium to form a satisfactory beam. If the oven became too hot, however, the rhodium melted, and all the silver was expelled in a very short time.

In many of the early trials of this method of obtaining a beam, the rhodium did melt. As a result, the counting rate was always high for whichever button was being exposed when the rhodium melted. After several of these runs, it was possible to predict at what oven power the rhodium would melt. A more satisfactory procedure for running could then be devised. The oven temperature was raised to a value just below that at which the rhodium would melt. This assured getting as much active silver out of the target as was possible without melting it. The beam intensity decreased rapidly and had to be monitored frequently. It did not, however, decrease to zero, but remained measurable for almost an hour. This was sufficient time to perform a spin-search experiment or to take a single resonance.

The rapid decay of the beam intensity is generally an undesirable feature for a run. Any uncertainty in the monitored beam will produce corresponding uncertainties in the normalized rates of the various samples that are taken. If the beam is changing rapidly, then the uncertainty in any interpolated normalizing factor will be greater than it would be if there were only minor changes in the beam. Furthermore, any small uncertainty in the time at which a given exposure was made is magnified by the rate of beam decay to produce a more appreciable uncertainty in the normalizing factor and hence also in the normalized rate. Thus, while it is possible (and sometimes necessary, e. g. with very short half lives) to obtain a reasonable normalization with a rapidly varying beam, it is preferable to have a beam which varies only slowly with time. This can be provided only by a prior separation of the silver from the rhodium target, so that the atomic-beam oven contains essentially pure metallic silver.

Since rhodium is virtually insoluble in the standard reagents, chemical separation techniques are practically useless. As an alternate procedure, use has been made of the fact that the melting and boiling points of silver are much lower than those of rhodium. It is this fact that causes the sudden loss of all the radioactive silver when the rhodium melts in the atomic-beam oven. If some means were to be devised to catch the radioactive silver as it was freed from the oven, the two metals shouldbe physically separated, since the rhodium should not be evaporated in any quantity.

The evaporator apparatus which was designed to perform this physical separation is shown in Fig. 7. The procedure is to place the irradiated rhodium foil in the cylindrical tantalum "pot," which is then heated by electron bombardment until the rhodium is melted. When the rhodium melts, the silver is released through the collimating snout which is directed into a standard atomic-beam oven. This oven is then removed from the evaporator and loaded into the atomic-beam apparatus, where the experiment is performed. To help stabilize the beam, 25 to 50 mg of stable silver carrier was usually evaporated into the atomic-beam oven before the radioactivity. Since

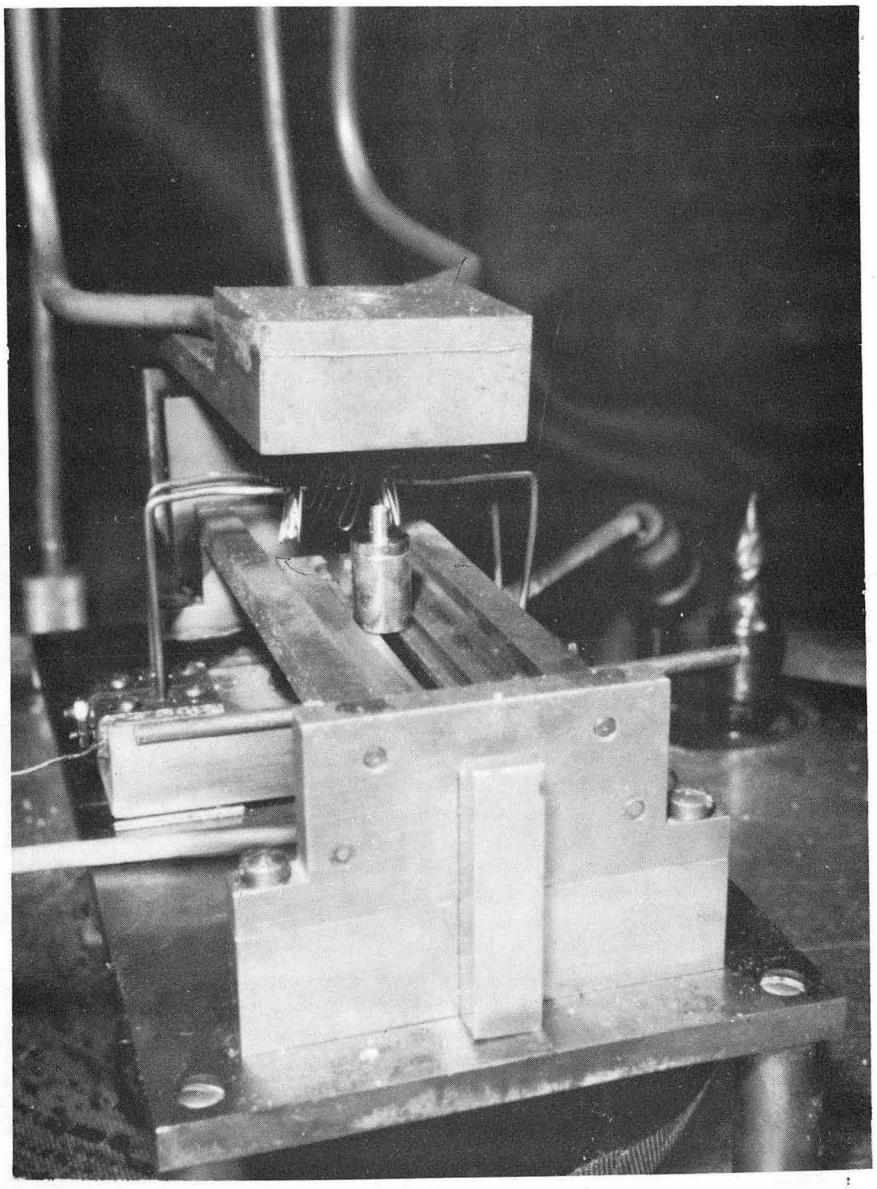

ZN-2194

Fig. 7. Illustrating the use of an evaporator for separation of radioactive silver from a rhodium target.
a. Evaporator pot on rails.
b. Evaporator pot in position.
c. Evaporator collimation.

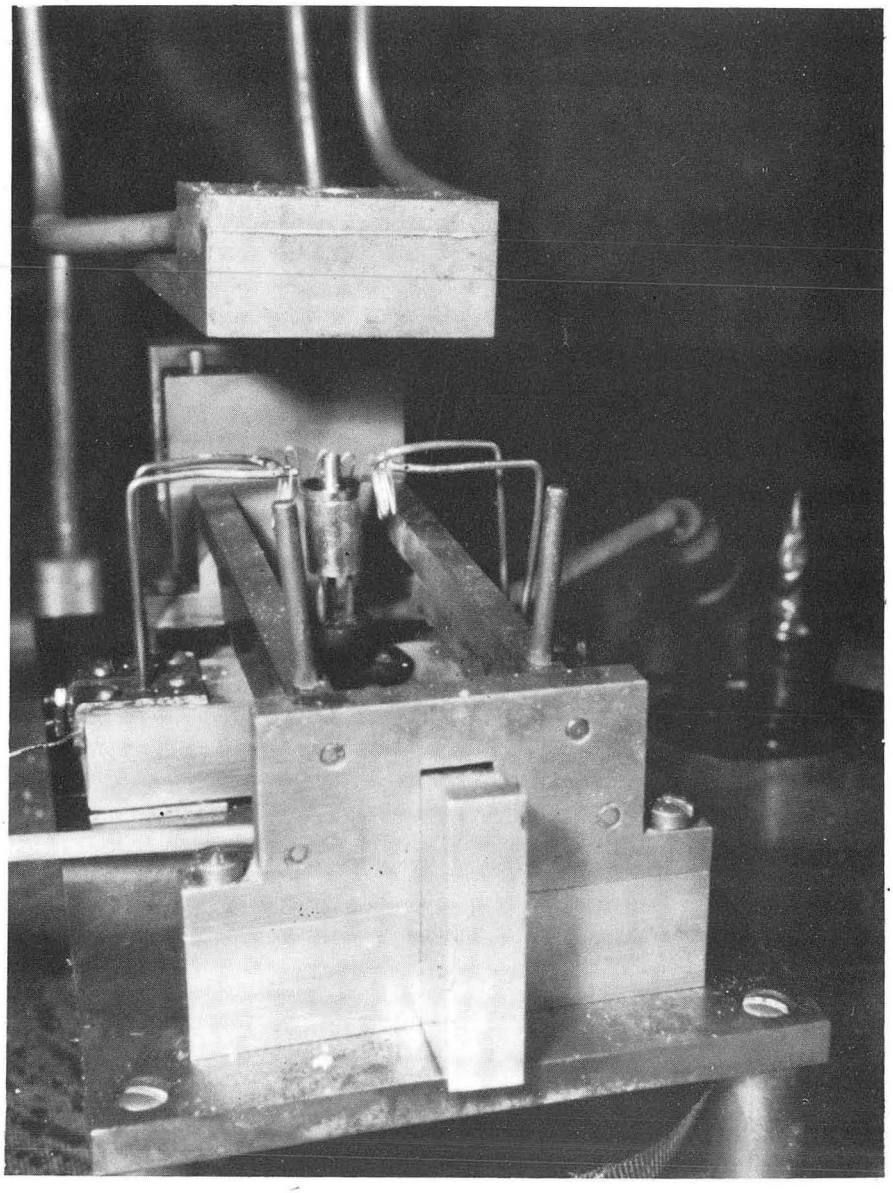

ZN-2196

Fig. 7b

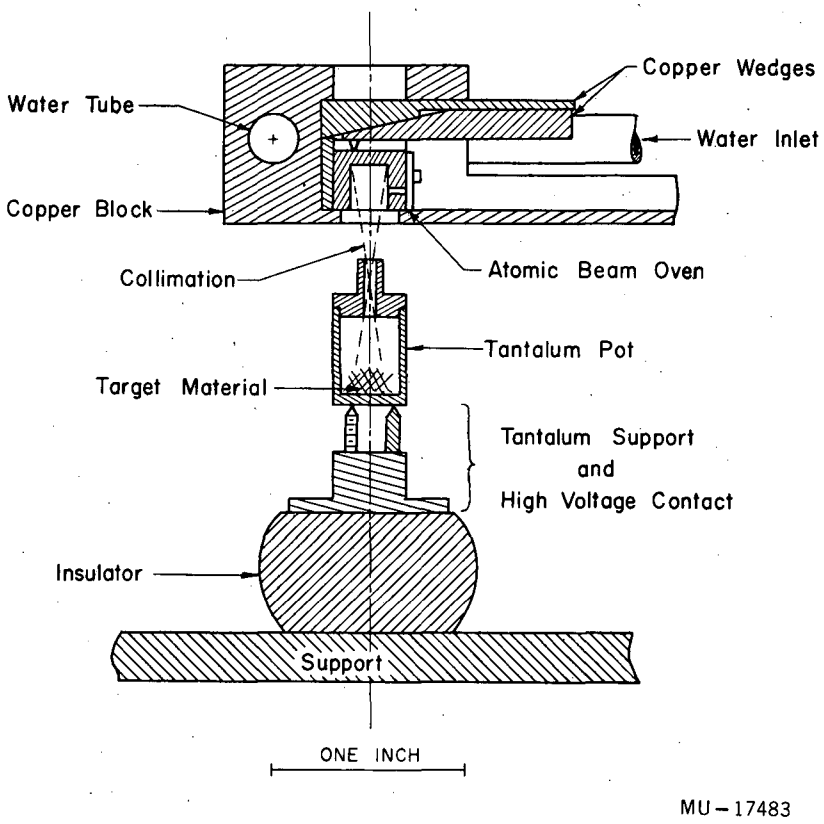
Copper Wedges
Water Tube
Water Inlet
Copper Block
Collimation
Atomic Beam Oven
Tantalum Pot
Target Material
Tantalum Support
and
High Voltage Contact
Insulator
Support
ONE INCH
MU-17483

Fig. 7c

Since the evaporator was designed especially for the separation of the short-lived silver isotope from rhodium, a number of features were included which contribute to the speed of the process. To facilitate loading of the pot into the evaporator head, a pair of rails are used. These provide a track (Fig. 7a) that guides the pot to a position directly in line with the hole of the oven, which is held in a water-cooled copper assembly. The rails are then allowed to fall away, (Fig. 7b) leaving the pot standing on the pins that serve as its high-voltage contact. The high-voltage platform is insulated from the rest of the system by a large solid piece of a high-temperature ceramic.

After the pot has been set on its pins, it is desirable to get a good vacuum very quickly. Provision has been made for this by using a 6-inch oil diffusion pump separated from the chamber by a 6-inch valve. After the chamber has been roughed by a mechanical pump to about 100 microns, the large valve is opened, and an operating vacuum is reached after a few minutes. Further pumping speed can be obtained by a liquid nitrogen trap which extends into the vacuum chamber.

As an electron source for heating the pot, an ac-heated filament of 15-mil thoriated tungsten wire has been looped around three sides of the pot. A bombardment current of $\sim$300 ma at 600v was ordinarily found to be sufficient to melt the rhodium. The evaporation could be monitored by placing a meter on top of the evaporator chamber several inches from the pot. As the activity was transferred from the pot to the atomic-beam oven, the radiation level at that point nearly doubled as a result of the increase in solid angle intercepted by the counting chamber. When the radiation level stopped rising, the evaporation was assumed to be complete. The chamber was isolated from the vacuum system and brought up to air.

The atomic-beam oven is held in close contact with the water-cooled copper by a system of copper wedges. After these are removed, the oven may be easily picked out of the apparatus.

The yield of the evaporator method of separation has been estimated to be of the order of one-half of all the radioactive silver that is in the rhodium. Since only a small part of the lost activity remains in the pot, the conclusion is that what is lost is lost in the collimation from the pot into the oven. Although the apparatus is designed so that the geometrical shadow of the collimator is projected onto the bottom of the oven cavity (see Fig. 7c), a layer of silver was always deposited on the top of the oven around the cavity. It would be reasonable to say that when the silver leaves the oven, it leaves as a cloud rather than as a beam. As a result, the simple collimation considerations may not be valid. In any case, the yield of the method could be increased considerably by an improvement in the collimation of the beam. Figure 8 shows the gain in beam stability after physical separation of the active silver from the rhodium target.

2. Palladium Target

The 12-Mev proton beam of the 60-inch cyclotron is sufficiently energetic to produce only the (p, n) reactions. When a palladium target is exposed to this proton beam, many silver isotopes of widely differing half lives are produced. Table IV lists the abundances of each of the stable isotopes of palladium. Next to each abundance figure are noted the half lives of the silver isotopes having the same mass number A.

Certainly the most important of these reactions will be those on the three most abundant isotopes, A = 105, 106, 108. Appreciable quantities of the isotopes having A = 104, 110 may also be produced. The 16-min activity which results from the (p, n) reaction on the 1% Pd^{102} can probably be neglected because of the low relative abundance of Pd^{102}.

The half lives of Ag^{108} (2.3-min) and Ag^{110} (24 sec) are certainly too short to be of interest in these experiments. Of the remaining half lives, there is a "short group" including both isomers of Ag^{104} (27-min and 1.2-hr) and one isomer of Ag^{106} (25-min), and there is a "long group" including 40-day Ag^{105} 8.3-day Ag^{106}, and 253-day Ag^{110m}.

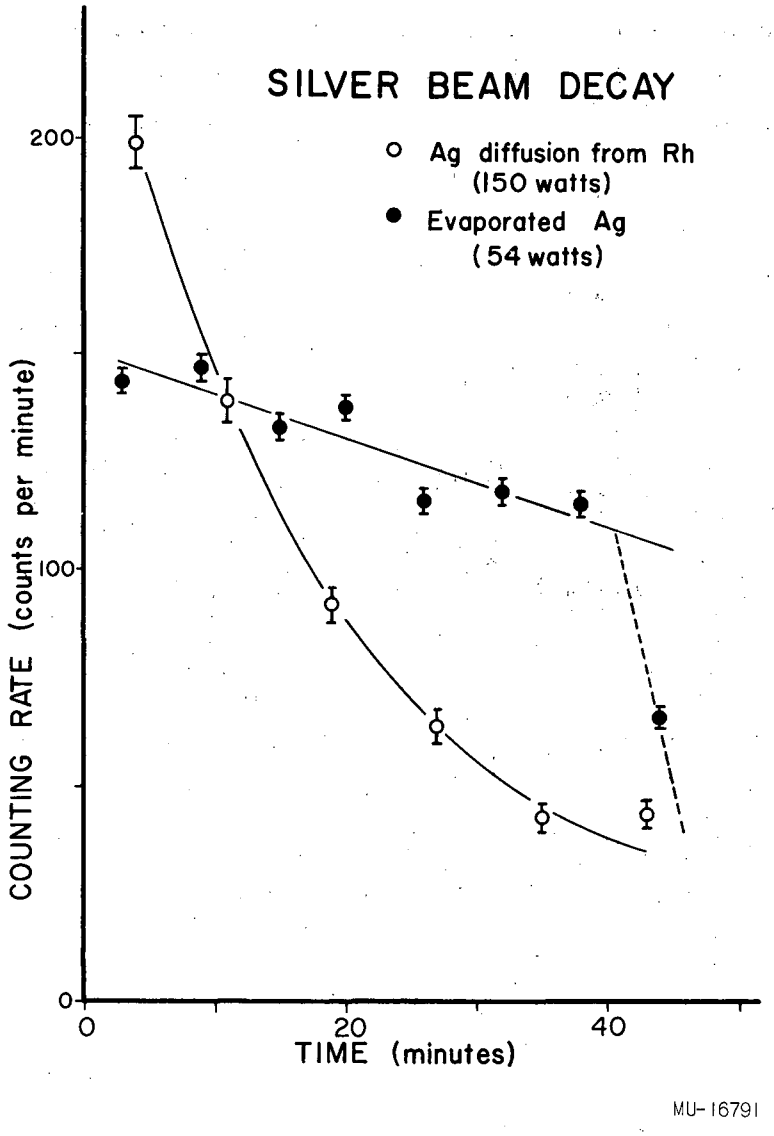

Fig. 8. Improvement in beam stability by the use of an evaporator to separate radioactive silver from the rhodium target.

Table IV

Silver isotopes produced by Pd(p, n) reactions		
A	Palladium abundances	Half lives of silver isotopes
102	1.0%	16 min
104	11.0	27 min; 1.2 hr
105	22.2	40 d
106	27.3	24 min; 8.3 d
108	26.7	2.3 min
110	11.8	24 sec; 253 d

If a short bombardment is used, the activity caused by the "long group" should be much smaller than that caused by the "short group." A short bombardment could then be followed by an experiment on any isotope in the "short group." In order to produce appreciable quantities of isotopes in the "long group", long bombardments must be used. The activity due to the members of the short group can be eliminated by merely waiting a day or so before performing the desired experiment on a member of the long group.

In practice, this method has been used almost exclusively to produce 40-day Ag^{105} and 8.3-day Ag^{106}. The shorter-lived isotopes can be identified less ambiguously if they are produced from rhodium, while the very long-lived Ag^{110m} can be conveniently produced in a reactor by neutron irradiation of natural silver.

It is most convenient to bombard the palladium on the internal probe if only the long-lived isotopes are desired. The high bombardment-particle density produces larger quantities of the desired isotopes than is possible using the external target assembly.

The separation of silver from a palladium target is straightforward. Both physical and chemical methods of separation have been used. In the physical method, the irradiated Pd was packed directly into the atomic-

beam oven. The oven was then heated to drive the silver out of the palladium target foil, much the same as in the rhodium targets. Although some acceptable results were obtained in this way, the much lower melting temperature of palladium (1549°C, compared with 1966°C for rhodium) made the process much more difficult to control. In most cases, therefore, chemical separation techniques were used to separate silver from a palladium target.

Since palladium is easily dissolved in aqua regia, the actual separation is trivial. At the same time that palladium is going into solution, silver chloride is precipitating out. This precipitate can be washed, dissolved in NH_4OH [with the formation of the complex ion $Ag(NH_3)_4^+$], and reprecipitated by boiling off the NH_3. Further washing and purifying can be continued until the AgCl is white with no discoloration from the orange $PdCl_2$. Silver chloride is a very stable compound. The reduction of silver to its metallic form from the chloride is the only serious problem of the separation chemistry. Two methods of reduction have been used. The first employed a straightforward electroplating technique, plating metallic silver from a solution of AgCl in NH_4OH. A platinum electrode proved quite satisfactory; the silver plated loosely onto the wire. The electrodes were then held over the oven and the silver was removed.

In the later runs, a different method of reduction was used with considerable success. This method made use of the fact that silver iodide decomposes at intermediate temperatures (~550°C) into metallic silver and iodine. (The process resembles the photoreduction of silver bromide in photographic processes. In fact, silver bromide could be used instead of silver iodide, with similar results.) After the silver chloride had been purified as described above, it was dissolved in ammonium hydroxide. Addition of ammonium iodide now caused the precipitation of silver iodide, which is insoluble in NH_4OH. This precipitate is much more bulky than silver chloride and is yellowish rather than white. After several washings, the silver iodide was carefully dried and loaded directly into the oven. Gradual heating of the oven in the apparatus reduced the compound to silver with the evolution of iodine. Further heating then produced the beam of radioactive silver which was used for the experiment.

E. The Gold Isotopes

1. Iridium Target

There are two stable isotopes in natural iridium, which have mass numbers 191 (38.5%) and 193 (61.5%). Because of this fact, the alpha bombardment of natural iridium does not yield gold isotopes in quite so clean a fashion as did the alpha bombardment of rhodium yield silver isotopes. For each value of k, the (α, kn) reaction on iridium will produce two isotopes of gold, as shown in Table V.

Table V

Gold isotopes from Ir(α, kn) reactions

k	Mass numbers of gold isotopes
1	194, 196
2	193, 195
3	192, 194
4	191, 193

The iridium used as targets in these experiments was in the form of a sintered foil about 0.005 inch thick. The mean range of a 48-Mev alpha particle in iridium is about three-fourths as far as for the same particle in rhodium.[60] Since the beam energy was degraded below the (α, n) threshold by a 0.007-inch thickness of rhodium, the 0.005-inch iridium foil would be expected to include products of all the reactions in Table V. Fortunately, the half lives of the gold isotopes are sufficiently different that unambiguous isotope assignments can be made to the resonances obtained from runs with irradiated iridium. In practice, bombardment of iridium targets has been used only for the isotopes $A \leq 194$. The longer-lived Au^{195} and Au^{196} can be produced more easily from platinum targets.

Because of the procedure found necessary for running gold isotopes as produced from iridium, bombardments were made using the external target assembly described before. The iridium foil was very brittle, and pieces could be broken off to use in the standard target assembly. The foil was mounted behind a thin aluminum cover foil.

As in the case of rhodium, the standard methods of chemical analysis were practically useless for separating radioactive gold from the target iridium. Iridium is even more impervious to strong acids and bases than is rhodium. Furthermore, the melting point of iridium metal(2454°C) is high enough to make difficult an evaporator separation such as was used for the short-lived isotopes. Consequently, it has been necessary to diffuse the radioactive gold directly out of the iridium target placed in the atomic-beam oven. This procedure brings with it the inherent uncertainties of normalization which were mentioned above in connection with the Rh(α, kn) Ag reactions. There is, however, no danger of melting the iridium with the power available for heating the oven. Also, a lower beam intensity can be tolerated. The consequently smaller resonances can be counted for longer periods of time, owing to the longer half lives of the gold isotopes.

A curve of beam intensity as a function of time is shown later (Fig. 9), in connection with the normalization example of Section IV-A.

2. Platinum Target

If a platinum target is exposed to the proton beam of the 60-inch cyclotron, there are several reactions that may be of importance. Of these isotopes, Au^{192} is produced in very small quantities and the 30-second Au^{195} has a short half life. Both may be ignored, therefore, in the analysis. Furthermore, although several attempts have been made to produce 14-hr Au^{196}, that isotope has not been observed. The only published reports of this isotope,[52, 57] attribute its production to an (n, 2n) reaction on stable gold. Au^{198} can be produced in a reactor and is of only passing interest here. It has been investigated by atomic-beam techniques.[15] The isotope Au^{198} decays by β^- emission to Hg^{198}. Since counting of the gold activities was done in crystal x-ray counters,

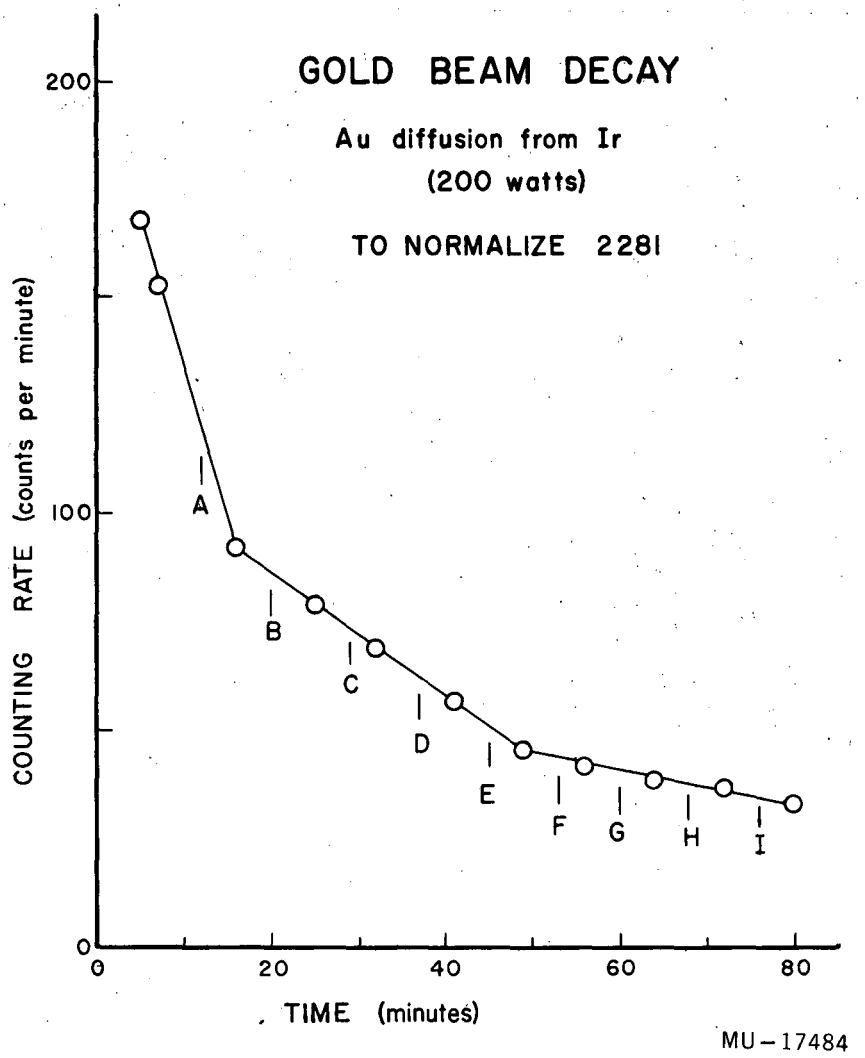

Fig. 9. Decrease in half-beam intensity as radioactive gold is diffused out of an iridium target.

Table VI

Gold isotopes produced by Pt(p, n) reactions

A	Platinum abundances	Half lives of gold isotopes
192	0.8%	4.8 hr
194	32.9	39 hr
195	33.8	30 sec; 180 d
196	25.2	14 hr; 5.6 d
198	7.2	2.7 d

the counting should discriminate against Au^{198}. Only the three longer-lived, neutron-deficient isotopes Au^{194}, Au^{195}, Au^{196} have been studied by using platinum targets.

The deuteron beam of the cyclotron was also used to produce these isotopes. The larger cross sections for deuteron-induced reactions provide larger quantities of the long-lived isotopes, where detection may indeed be marginal. The qualitative differences of (d, kn) results from (p, n) results will be the introduction of trace amounts of Au^{193} and possibly measurable amounts of Au^{199}. These have not been observed.

The platinum was bombarded on the internal probe target of the Crocker cyclotron. Ion currents of 100 microamperes or more have been used for long periods of time. Integrated beams of more than a thousand microampere-hours have been accumulated on single targets.

Qualitatively, the separation of gold from a platinum target is similar to the separation of silver from a palladium target. Here, too, a physical separation is possible and has been used successfully. As in palladium, however, the melting temperature of platinum ($1774^{o}C$) is so low as to make such a separation difficult. Consequently, chemical means have been found more satisfactory.

It is only with some difficulty that platinum may be dissolved. In practice, several hours in hot concentrated aqua regia were required to dissolve a target of 20-mil foil. The temperature of the acid seems to be a very important factor in determining the length of time necessary to dissolve a given foil. If the acid is allowed to boil freely, the HNO_3 is quickly exhausted and the reaction stops. If the acid is heated just strongly enough to cause the reaction to proceed (as evidenced by the formation of bubbles of Cl_2 and NO_2), then a minimum time will be required to dissolve the platinum target.

After the target has been dissolved along with some stable gold as a carrier, the solution is evaporated just to dryness. If the heating is continued too long, some of the gold chloride will be reduced to gold, which will not follow the next step in the chemistry. The residue from this evaporation should contain gold chloride and chloroplatinic acid

("platinum chloride"). Both are taken up in 6 N HCl and rinsed into a separatory funnel. If a similar quantity of ethyl acetate is mixed into the gold-platinum-chloride solution, and then is allowed to stand, there will be a separation into two layers. The lower HCl layer will be found to contain the platinum ions, while the upper organic layer has taken up the gold. The platinum-bearing lower phase can be drained off, leaving the gold chloride in the acetate phase. A washing of the acetate layer with 6 N HCl will remove any platinum that carried over. A further extraction into ethyl acetate from the HCl phase will remove any gold that was not separated the first time. In practice, it was not found necessary to perform the extraction more than once, since the separation seemed to be very efficient.

Evaporation of the ethyl acetate left gold chloride which could be dissolved in water. Sulphur dioxide gas was used to reduce the gold to its metallic form. Bubbling of the SO_2 through the solution containing gold ions was found to be undesirable. The gold crystals thus formed were very tiny, and were difficult to handle without large losses from sticking to the glass containers, etc. If the gas was blown across the surface of the gold solution, however, the crystals were somewhat larger, and handling losses were smaller.

The ethyl acetate extraction of gold from the platinum solution is a standard separation method,[61] and is probably the most satisfactory such method that is available. An alternative method has been used with variable results. This alternate method uses the thermal decomposition of gold chloride, as mentioned above. If the gold-platinum-chloride solution is evaporated to dryness and then further heated, some of the gold chloride is reduced to gold. Some also sublimes to recondense on the walls of the container. This can be washed down with water and evaporated again. After a few such evaporations, most of the gold has been reduced, and the platinum chloride may be washed off with water. This leaves crystalline gold, to be further processed as desired.

IV. RESULTS

A. Data Processing

1. Normalization

In a normal atomic-beam experiment, the rate at which atoms reach the detector of the apparatus is studied as a function of the frequency that is being used in the rf hairpin. When radioactive detection is used, such a study consists of comparing the radioactivity of samples that have been exposed in the apparatus for equal times, but while different radiofrequencies were available in the C field to induce transitions. Obviously, if the rate at which the material effuses from the source oven is not constant, then such a comparison of observed counting rates is meaningless. The fact that a button that was exposed during an excursion in the effusion rate exhibits a higher absolute counting rate than some other button does not necessarily indicate the existence of a resonance on the first button. Unfortunately, the effusion rate for most of the materials used in these experiments is observed to vary with time (Figs. 8 and 9). Consequently, some normalization procedure is needed which can correct the observed counting rates on resonance samples, according to the amount of material that left the oven during the time the samples were being exposed to the beam.

An ideal method of normalization would involve a measurement of the number of radioactive atoms that left the oven during a resonance button exposure and were deflected sufficiently that a transition could have been observed, had the proper rf frequency been present in the transition field. But such a method, involving the collection of all measurable radioactive atoms, precludes the measurement itself. A more practical procedure might be to monitor a fixed fraction of the deflectable radioactive beam or some other quantity that is proportional to it during each resonance exposure. On this apparatus, however, provision is made for taking radioactive samples at only one place—the detector end of the apparatus. Since this is in use during resonance exposures, an interpolation is made necessary. The beam can be measured before and after the exposure has been made. Counting rates on buttons exposed

at different frequencies can be compared if they are first expressed as a fraction of the average beam intensity to which they were exposed.

The atomic-beam apparatus used in these experiments was designed to operate most efficiently with a beam of alkali atoms. Its dimensions and field gradients are such that only a fraction of a percent of an alkali beam is able to reach the detector if both A and B fields are on and there is no rf in the transition field. (The rate at which atoms reach the detector under such conditions is called the "half-beam" rate—a traditional misnomer—as contrasted with the "full-beam" rate at which atoms reach the detector when there are no intervening magnetic fields.) A small part of this "half-beam" rate is no doubt due to Majorana transitions[62] induced in the atoms as they cross from one field region to the next. But the larger part of the half-beam rate consists of atoms and molecules that did not receive sufficient deflection in the inhomogeneous fields of the apparatus. A molecule is not expected to be deflected appreciably in this apparatus, since its magnetic moment is likely to be much smaller than the magnetic moment of an atom with a $^2S_{1/2}$ electron. The reason for the atomic component in the half beam derives from the existence of a velocity distribution of the atoms in the beam. Those atoms with high velocities do not remain in the deflecting fields long enough to attain an appreciable transverse component of velocity, hence they travel virtually undeflected through the magnet system. As the temperature of the source oven is raised, the mean velocity increases for atoms in the beam, and the fraction of undeflected atoms also increases. Since the oven temperatures required to maintain a beam of silver or gold atoms are much higher than those for an alkali beam, the half-beam rate is also expected to be a larger fraction of the full beam than the few percent mentioned above for alkali beams. The undeflected portion of the beam has been observed to be as much as 50% of the total beam for silver or gold.

The fact that a large part of the beam of radioactive silver or gold is not deflected in the apparatus gives rise to special problems. In the first place, it is necessary to obtain higher beam intensities than for the alkalis. Since only half the beam is being used for measurements,

twice as many radioactive atoms are required in order to obtain a given amount of information. The presence of the stop wire now becomes essential. If the undeflected part of the beam were not blocked from reaching the detector, it could mask any resonance signal that might appear.

The advantage of having such a large fraction of the beam undeflectable is that it provides a satisfactory way of monitoring the radioactive beam. At a given temperature, the undeflectable fraction of a beam should remain the same throughout a run. If the half-beam intensity is sampled periodically, e. g., before and after each resonance exposure, then the average half-beam intensity during the resonance exposure can be interpolated easily. Furthermore, since the half-beam intensity is proportional to the full-beam intensity, which is in turn proportional to the deflectable-beam intensity, a normalization referred to the average half beam during an exposure will be accurate except for a constant factor. This factor can be determined, if desired, but it is usually more convenient to express normalized counting rates in arbitrary units.

Experimentally, the half-beam normalization has proved quite adequate, in spite of a number of uncertain features about it. The fact that the procedure gives consistently good results indicates that there are no large erratic changes in beam intensity. The beam intensity often exhibits a slow decrease with time, but this seems to be predictable. The temperature dependence of the undeflected fraction of the beam does not seem to be too important. Experimental checks on the "throw-out" of a silver or gold beam (i. e., the percentage of the radioactive beam that is deflected away from the detector by the inhomogeneous fields when there is no resonance) indicate that from 50 to 60% of the beam is thrown out in most cases. A significant exception has been observed in thermal decomposition of AgI to obtain a beam of silver. Here, the throwout has been measured consistently higher—about 80 to 85%.

When several isotopes are present in the beam, a resonance of one of them should actually be normalized to the amount of that isotope that is in the beam. However, if all isotopes are well mixed in the oven,

then the amount of any one in the beam should be proportional to the amount of any other. In some cases, resonances of short-lived isotopes have actually been normalized to the amount of long-lived activity in the beam. This is more convenient, since the counting of the normalization buttons can then be done at leisure some time after the resonance exposures have been finished.

If radioactive isotopes of elements other than that being measured are also present in the oven, then special problems may arise. Such isotopes may be produced by competing cyclotron reactions--e. g., (α, p)--or may be due to impurities in the target materials. The rhodium and iridium used in these experiments were pure enough that the latter problems were not of importance. Competing reactions no doubt produced some palladium and platinum activities in the respective alpha bombardments, but the boiling temperatures of palladium and platinum are sufficiently higher than those of silver and gold that probably none of the activity from (α;p, kn) reactions was able to appear in the beam.

One problem did arise as the result of a presumably impure target material. The reactor-produced Ag^{110m} (half life = 253 days) was observed to be contaminated with a shorter-lived (~40-day) activity. A chemical separation of silver from a solution of the target material left a residual activity which was identified by its characteristic gamma ray as probably Hg^{203} (47-day). The heating of the irradiated silver in the oven was such that bursts of radioactive mercury were released from the silver at unpredictable times. Fortunately, it was possible to distinguish between buttons with high counting rates of silver or of mercury by using the crystal x-ray counters. Buttons with mercury contamination could then be eliminated from consideration.

2. OMNIBUS Program for Data Analysis

In order to minimize the work required to obtain significant information from a series of measurements, a number of different programs have been written whereby the data are analyzed by high-speed computing machines. Of these, the OMNIBUS program of H. B. Silsbee (formerly of this group, presently at the University of Washington) has been most useful in this work. A complete description of the computations done by OMNIBUS will not be given here, but a brief outline may be useful in evaluating the experimental conclusions.

The OMNIBUS program includes three distinct parts, each of which performs a calculations often used in processing the data from atomic-beam measurements. In the first part, the decay curve of any sample of radioactivity is analyzed into its component parts. In the second part, a bell-shaped curve is fitted to the points of a radioactive resonance as a function of frequency. The third part calculates the hfs $\Delta\nu$ of an isotope from a knowledge of its resonant frequency and of that of a calibration isotope in the same transition field. Curve fitting is done by OMNIBUS, using a least-squares procedure. The difference of each point from the fitted curve is weighted by the reciprocal square of the uncertainty of the experimental point. The weighted sum of these differences is then minimized by adjusting the parameters which describe the curve.

The decay-fit part of the OMNIBUS program actually synthesizes a complex decay curve including as many as five different isotopes with known half lives. The initial activity due to each isotope is adjusted to provide a least-squares fit between the synthesized curve and the counting rates observed at various times. As a result of this procedure, the relative amount of each isotope on each sample exposed to the radioactive beam can be determined.

The bell-fit part of the OMNIBUS program attempts to describe the dependence of counting rate upon frequency in the neighborhood of a resonance. A bell-shaped curve is fitted by least-squares techniques to the observed initial counting rates of exposures made at several frequencies around the resonance. The experimental points are also

weighted by the squares of their counting rates, so that the bell-shaped curve fits best those points near the peak of the resonance, rather than the somewhat less important points on the wings of the resonance. The bell-shaped curve is described by three parameters: a maximum height, a frequency at which the maximum occurs, and a half width at half maximum. The half width is considered in later calculations of the hfs $\Delta\nu$ from the resonance-fit parameters.

The $\Delta\nu$ program uses the frequency at which a known calibration isotope has a resonance. From this it calculates the magnetic field in the transition region. This field value is then used in a calculation of the unknown hfs $\Delta\nu$ from its resonance frequency according to Eq. (22). Since there is an ambiguity in the sign of g_I, the calculation of $\Delta\nu$ is made by first assuming $g_I > 0$, then assuming $g_I < 0$. (A preliminary value for $|g_I|$ is obtained from the Fermi-Segrè formula and the $\Delta\nu$ calculated from Eq. (22) assuming $g_I = 0$). The two values of $\Delta\nu$, $\Delta\nu_+$ and $\Delta\nu_-$, may differ appreciably if the moment is large in absolute value. However, for all the isotopes considered here, the nuclear moments are so small that the two calculations give substantially the same result for $\Delta\nu_+$ and $\Delta\nu_-$.

The uncertainty in a value of $\Delta\nu$ calculated by the OMNIBUS program is obtained by combining by standard methods the uncertainty in the field (due to uncertainty in the frequency of the calibration resonance), the statistical uncertainty in the frequency at which the radioactive resonance occurs, and a certain fraction of the width of the resonace. How large a fraction of the resonance width it is necessary to include depends on the quality of the resonance and its symmetry. Usually, the fraction chosen was about a sixth of the line width, measured at half maximum. The half width at half maximum is obtained from the bell-fit program, and is included in the $\Delta\nu$ calculations.

3. Sample Analysis

As an illustration of the procedure used to obtain reliable values of $\Delta\nu$ from raw data, consider the nonnormalized resonance No. 2281 shown in Fig. 10. (The first three digits of the resonance number indicate the run during which the resonance sweep was made. The last digit indicates the sweep number, if more than one resonance was attempted). In this graph, the ordinate represents the observed initial counting rate on each of the several resonance exposures made at the frequencies noted on the abcissa. Since the intensity of the radioactive beam was observed to decrease with time (Fig. 9), it was necessary to make a normalization as described above. Each of the observed counting rates in Fig. 10 was divided by the corresponding half-beam intensity as shown in Fig. 9. The result of this normalization is to change the relative counting rates of each exposure to the "normalized" rates of Fig. 10. It is clear that the resonance sweep has covered two resonances.

The identification of the two resonances was obtained from analysis of the decay curves corresponding to each of the resonance exposures. Since the resonance was obtained at a frequency near that of the Zeeman frequency for $I = 3/2$, only the two isotopes Au^{191} and Au^{193} (both of which have spin 3/2) were considered. The two overlapping resonances are shown in Fig. 11 as they appear after a decay-fit analysis by the OMNIBUS program. The smooth curve through each set of resonance points is the least-squares-fitted bell-shaped curve obtained from the OMNIBUS program. Both resonances appear to be somewhat asymmetric, so that the bell-shaped curve does not fit the points exactly. However, the limits of uncertainty on the frequency of each resonance (shown by the bracket over each resonance) are large enough to include the peak of an asymmetric line, if it were drawn through the same set of points.

The calculation of the hyperfine-structure separation for each of the iosotopes Au^{191} and Au^{193} was performed by the OMNIBUS program, and the results are included with those from other resonances of the same isotopes in Tables XXIV and XXIII, respectively.

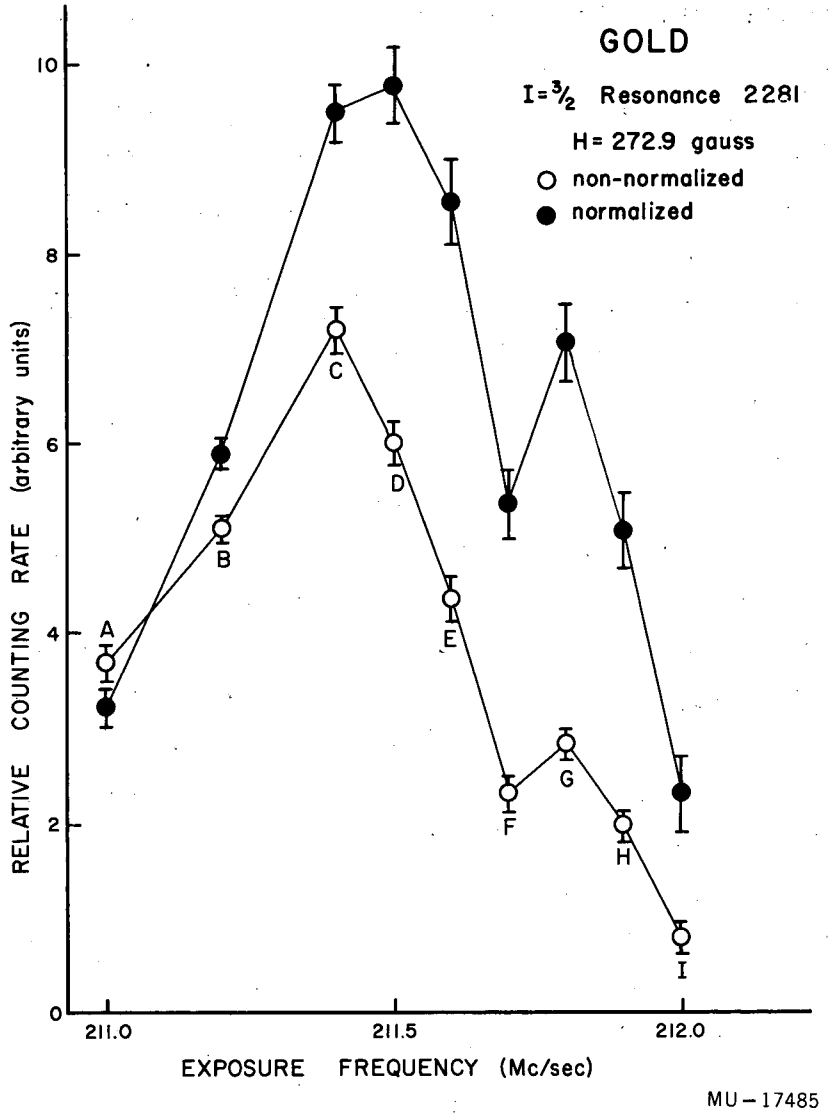

Fig. 10. Normalization of gold resonance sweep obtained with gold diffused from iridium.

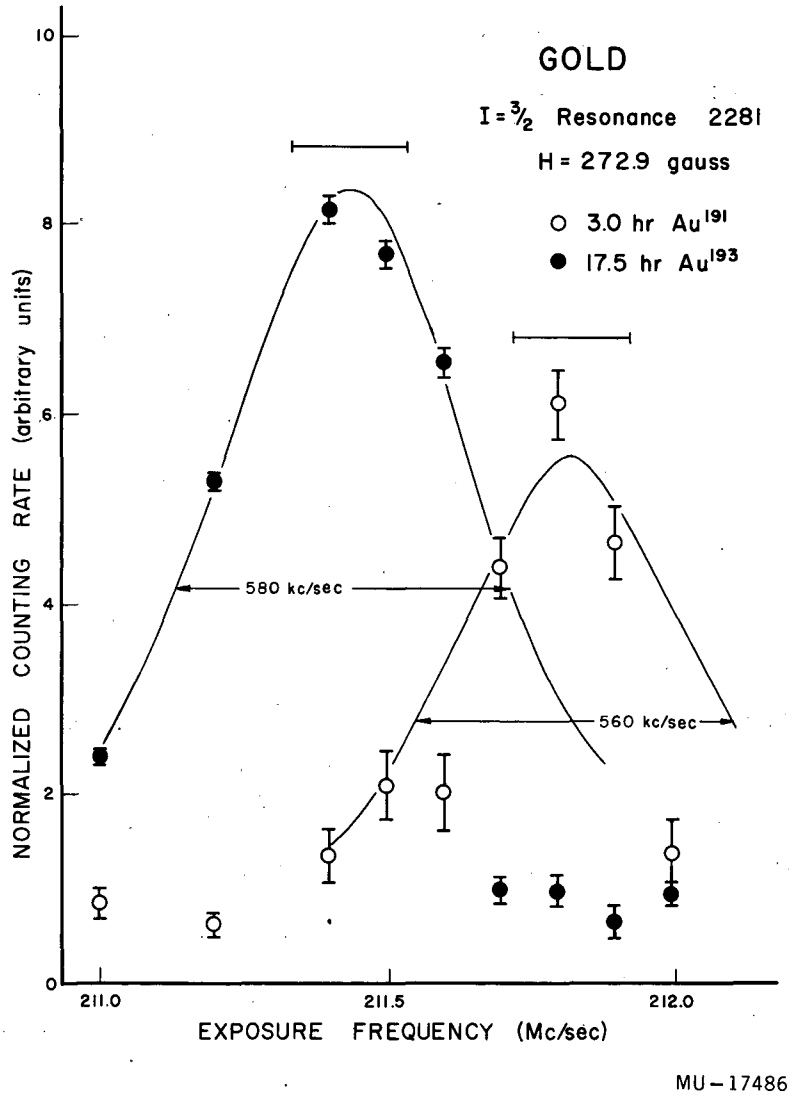

Fig. 11. Resolution of two resonances by decay-curve analysis.

B. Silver Results

1. Nuclear Spins

Often, when a series of experiments is initiated on the radioactive isotopes of some element, it is best to start with those isotopes which have reasonable half lives (several hours to several days). The refinements of running procedure which are necessary for isotopes of very short or very long half lives can often be worked out in the first runs when they are not really necessary. Such was the case here for the several neutron-deficient isotopes of silver. The first few bombardments of rhodium and of palladium were used to find spin resonance of 40-day Ag^{105} and 8.3-day Ag^{106}.

Since very little was known about the beam decay, which was observed later, no attempt was made to normalize the exposures of the first few runs. Exposures on I = 1/2 and I = 6, however, were observed to be high and to decay with ~40-day and ~8-day half-lives, respectively. The first reliable normalized results on these two isotopes were obtained with a beam being diffused out of the palladium target. A decay curve of the monitored half-beam intensity was plotted, as described in the example of Section IV-A, and the average half-beam intensity during each resonance exposure was obtained. The normalized counting rates obtained on the four spin resonance exposures are listed in Table VII.

Table VII

$Pd(p,n)Ag^{105,106}$ Normalized counting rates

I =	1/2	5	6	7
Normalized rates (arbitrary units)	15.1(3)	0.38(10)	3.26(11)	0.50(8)

The decay curves of Fig. 12 illustrate the method of isotope identification used here. The three curves represent the decays of the two high-resonance samples (I = 1/2 and I =6) and a full-beam exposure for comparison. From the markedly different half life of the spin-6 exposure, the assignment of I = 6 to 8.3-day Ag^{106} is unambiguous.

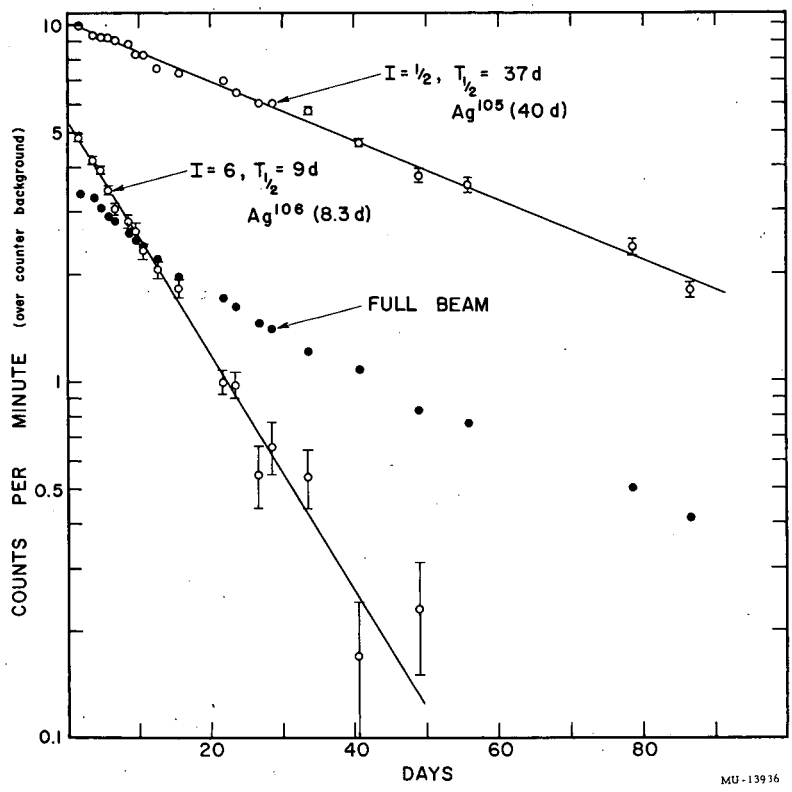

Fig. 12. Identification of silver spin resonances by decay analysis.

The virtual absence of 8-day activity on the I = 1/2 exposure, as compared with the decay of the full-beam button, established I = 1/2 for Ag^{105}. The OMNIBUS decay-fit routine described in Section IV-A was used to analyze each button to find the original percentages of Ag^{105} and Ag^{106} that would be required to give the observed decay curve. The results of such analyses are listed in Table VIII.

Table VIII

Decay-fit analysis of Pd(p, n)Ag spin exposures

	Full-beam exposure(FB)	I = 1/2	I = 5	I = 6	I = 7
40-d Ag^{105}	19.7(2)cpm	14.1(1)units	0.2(2)units	0.10(3) units	0.4(2) units
8.3-d Ag^{106}	16.7(3)	1.4(3)	0.2(3)	3.35(7)	0.1(2)

A similar analysis has been performed on the full-beam exposure so that a comparison of relative amounts can be made. (The normalized counting rates for the resonance exposures are expressed in arbitrary units. Usually the normalization is adjusted so that the normalized rates are similar in magnitude to the actual counting rates.) The composition of the beam as obtained from the full-beam decay shows almost equal parts of activity due to Ag^{105} and Ag^{106}. The resonance exposures for both I = 5 and I = 7 agree with this, within the accuracy of their measurement. The exposure for I = 6 shows a resonance of 8.3-day Ag^{106}, as seen in Fig. 12. The exposure for I = 1/2 shows that the Ag^{105} activity is higher by a factor of ten than Ag^{106} activity. The large amount of Ag^{106} on the I = 1/2 exposure is not explainable in any obvious way.

The positive assignment of a nuclear spin to a certain radioactive isotope is the result of several observations of the spin resonance of the isotope at different fields. A final check may be made by sweeping

through a resonance of the isotope at low fields. Both confirmations have been made for these two silver isotopes. The frequencies at which the spin resonances have been observed are listed in Table IX.

Table IX

Spin resonances of Ag^{105}, Ag^{106}	
40-day Ag^{105}	8.3-day Ag^{106}
I = 1/2	I = 6
(Mc)	(Mc)
7.4	1.3
8.0	2.4
8.4	3.1
12.2	8.6
15.4	15.7

An entire series of resonances has been obtained for Ag^{105}. These resonances are discussed later in connection with the consequent measurement of the hyperfine-structure $\Delta\nu$ of Ag^{105}. Three low-field resonances have been obtained for Ag^{106}, but the resonance is not shifted enough away from the Zeeman frequency to afford a reliable calculations of $\Delta\nu$ for this isotope. The resonance at 72.8 gauss is shown in Fig. 13. Evidently, this field is not sufficient to decouple the electronic and nuclear magnetic moments. The resonance in Fig. 13 does confirm the spin assignment of I = 6 to 8.3-day Ag^{106}.

Since 253-day Ag^{110m} was produced in a reactor by neutron irradiation of stable silver, no chemical separation was necessary. A beam was easily produced by merely heating the irradiated silver in an oven. Detection of the beam could not be done so efficiently as for the K-capture isotopes, but counting rates were sufficient to establish the

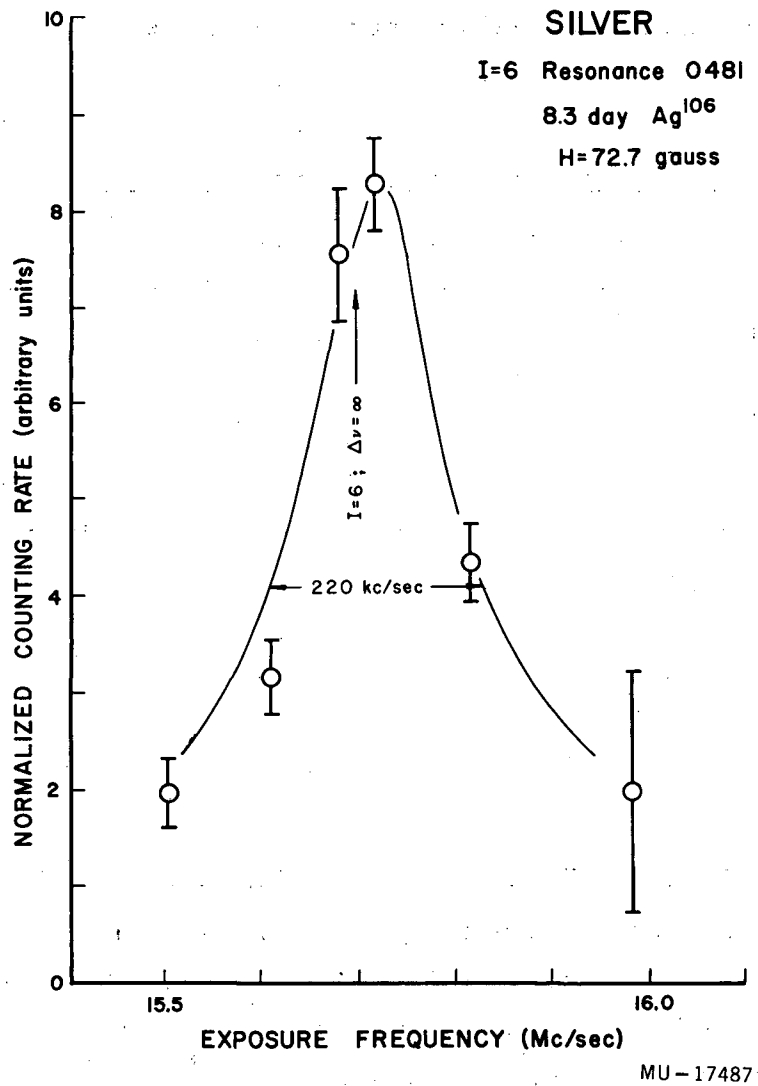

Fig. 13. Resonance sweep confirming spin assignment of 8.3-day Ag^{106}.

nuclear spin of $I = 6$ for Ag^{110m}. The results of a complete spin search, using a beam of radioactive Ag^{110m}, are shown graphically in Fig. 14. No spin resonance other than that corresponding to $I = 6$ has an appreciable counting rate. As is indicated, the exposure on $I = 6$ was made twice, and the resonance is observed to be repeated.

The spin resonance of Ag^{110m} has been observed several times at five different fields. The resonance has been detected at frequencies of 2.4, 3.9, 7.9, 12.7, and 15.7 Mc. As with Ag^{106}, there is no appreciable shift from the Zeeman frequency at fields up to about 70 gauss. The magnetic moment is thus indicated to be large. The best $I = 6$ resonance that has been obtained for Ag^{110m} is shown in Fig. 15.

The resonance lines of the $I = 6$ resonances of both Ag^{106} and Ag^{110m} were observed to be narrower by a factor of three or four than the resonances of other isotopes at comparable frequencies. This phenomenon has been tentatively explained by the hypothesis of very large nuclear moments for these two isotopes. If the nuclear magnetic moment is so large that the lines on the Breit-Rabi diagram (see Section II-B) curve only slightly, even in fields as strong as the A and B fields of the apparatus, then it may be necessary to induce multiple quantum transitions ($\Delta m \geqslant 2$) in order to produce an observable resonance. Multiple quantum transition lines were expected to be narrower[63] than the usual transition lines, and have actually been found to be so.[15] Further measurements on the high-spin silver isotopes are required before any sound conclusions can be drawn.

It is convenient to treat the four short-lived silver isotopes together, since they are all part of the same problem in identification.

The first results on the short-lived silver isotopes were obtained after a short proton bombardment of palladium. After chemical separation and electroplating, a satisfactory beam was obtained which was observed to include large amounts of a $\sim$30-min activity. Spin-resonance exposures were made on integral spin values up to $I = 6$. The exposure corresponding to $I = 1$ was observed to have a high counting rate which decreased with a half life of less than an hour. After an OMNIBUS decay-fit analysis, the composition of the resonance was clear. Table X lists

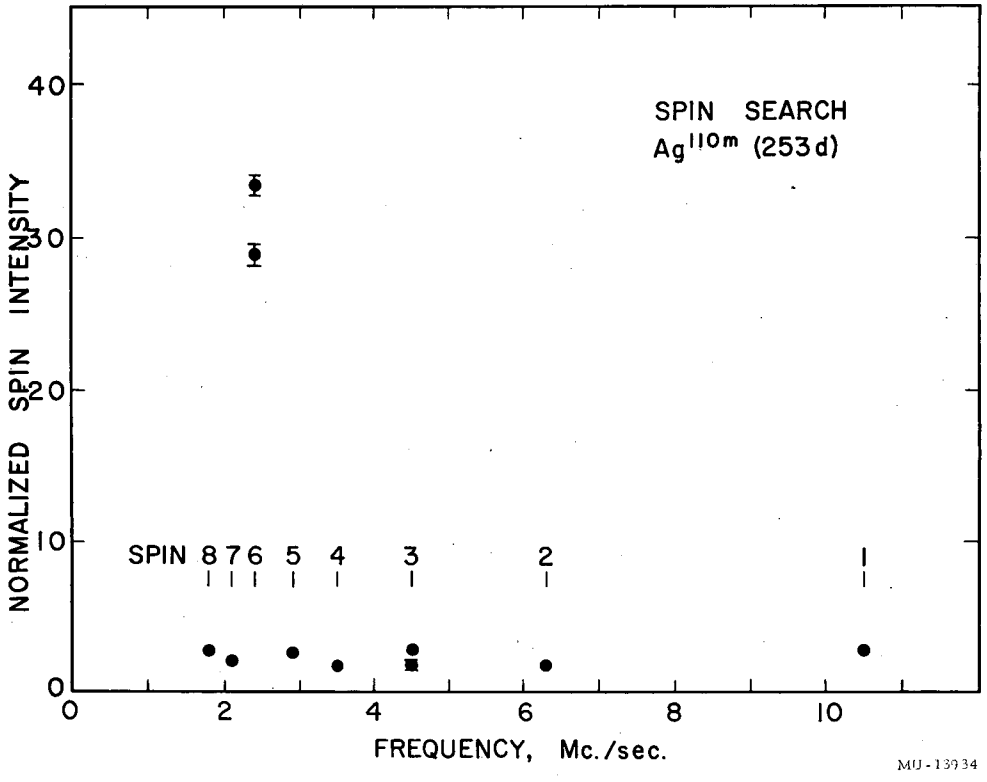

Fig. 14. Results of a search for the spin resonance of 253-day Ag^{110m}.

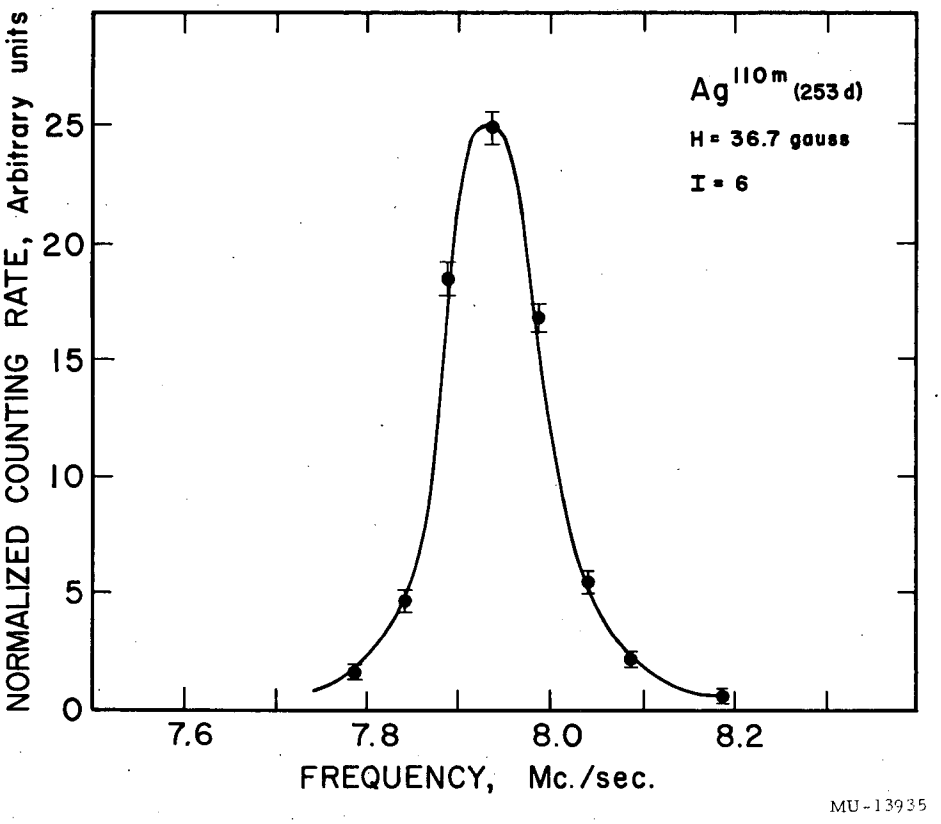

Fig. 15. Resonance sweep confirming spin assignment of 253-day Ag^{110m}.

only the amount of ~30-min activity on the several spin exposures. Evidently, one of the short-lived isotopes of silver has I = 1. Since more 24-min Ag^{106} than 27-min Ag^{104} was made in a proton bombardment of palladium (Section III-D), it seemed reasonable to assign the I = 1 to Ag^{106}. However, there was considerable ambiguity in such an assignment.

Table X

Spin search for ~30-min silver from Pd(p, n)Ag

Spin	Normalized counting rate
1	32(4) units
2	8(5)
4	1(1)
5	3(2)
6	2(4)

The uncertainty of the spin assignment was removed by an experiment on Ag^{106} produced by the (α, n) reaction on rhodium. As described in Section III-D, Ag^{106} can be produced uncontaminated by Ag^{104} if a rhodium target is covered with ~21 mils of aluminum foil before alpha bombardment in the cyclotron. Such a bombardment was made, and spin resonances were attempted on I = 1, 2, 3, and 4. The results of this experiment are summarized by Fig. 16. When the first exposure at I = 1 seemed to be higher than the others, it was repeated during the same run with the same result. No resonance sweeps have been made of the I = 1 resonance of Ag^{106}, but the spin assignment has been confirmed by spin resonances at 5.3, 8.3, and 9.9 Mc.

Spin assignments for the two isomers of Ag^{104} were made possible by use of only a 5-mil aluminum cover foil on the rhodium target

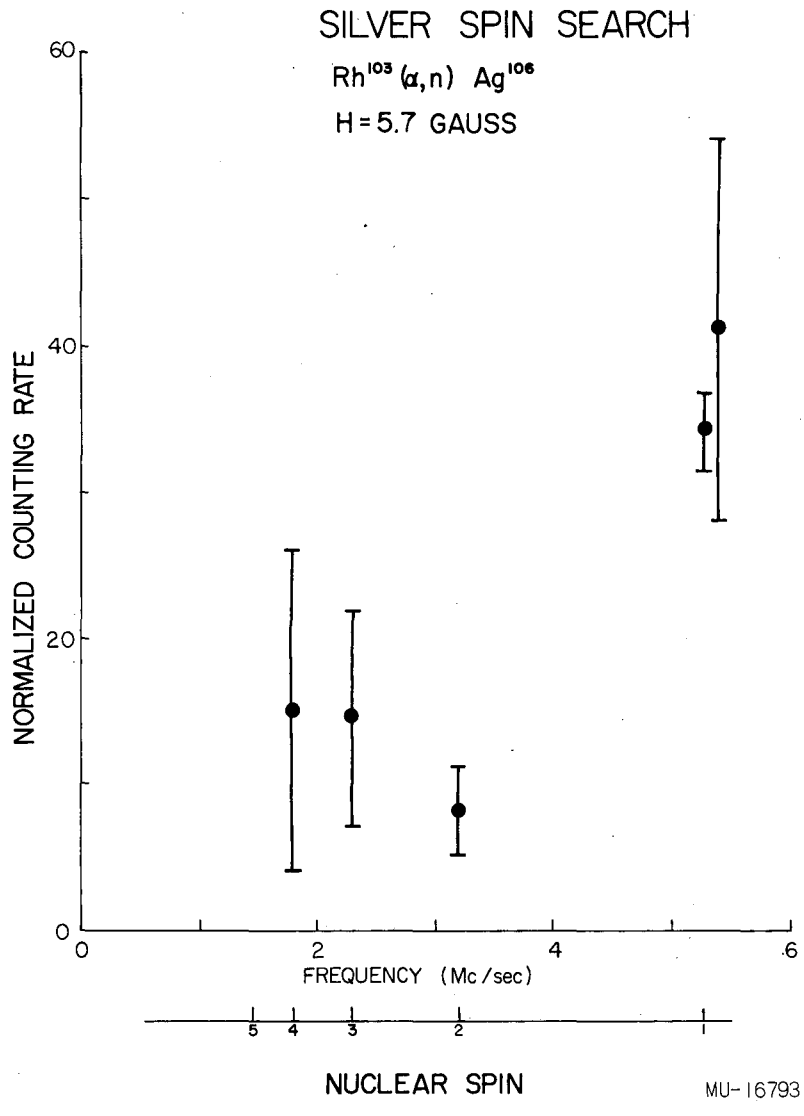

Fig. 16. Results of a search for the spin resonance of 24-minute Ag^{106}.

This cover foil served to prevent the production of Ag^{103}, which has a half life almost identical to that of one of the Ag^{104} isomers. The results of a search for Ag^{104} spins are shown in Fig. 17. Two spin resonances were observed, corresponding to I = 5 and I = 2. The decay curves were consistent with the assignment of I = 5 to 1.2-hr Ag^{104} and I = 2 to 27-min Ag^{104}. The possible small signal on the exposure for I = 1 was shown to be spurious by a confirmation run using thinner rhodium foil. The results of a decay analysis of exposures made corresponding to I = 1, 2, 3 are summarized in Table XI.

Table XI

Ag^{104} Analysis of spin-search exposures

I	Ag^{104}(27-min)	Ag^{104}(1.2-hr)
1	0(3) cpm	33(2) cpm
2	30(4)	35(2)
3	6(3)	34(2)
Half beam	210(20)	1110(10)

On the resonance button corresponding to spin 2, the counting rates of the two isotopes are comparable. On spin 1 and spin 3, however, as on the half-beam exposure, the 1.2-hr activity is dominant by a large factor. The low-field spin resonance corresponding to I = 2 for 27-min Ag^{104} has been observed at frequencies of 3.8, 4.4, 4.5, 5.5, and 6.4 Mc.

The assignment of I = 5 to 1.2-hr Ag^{104} is based on observations of low-field spin resonances at frequencies of 1.4, 1.7, 3.0, 3.4, 3.6, 3.7 and 8.1 Mc.

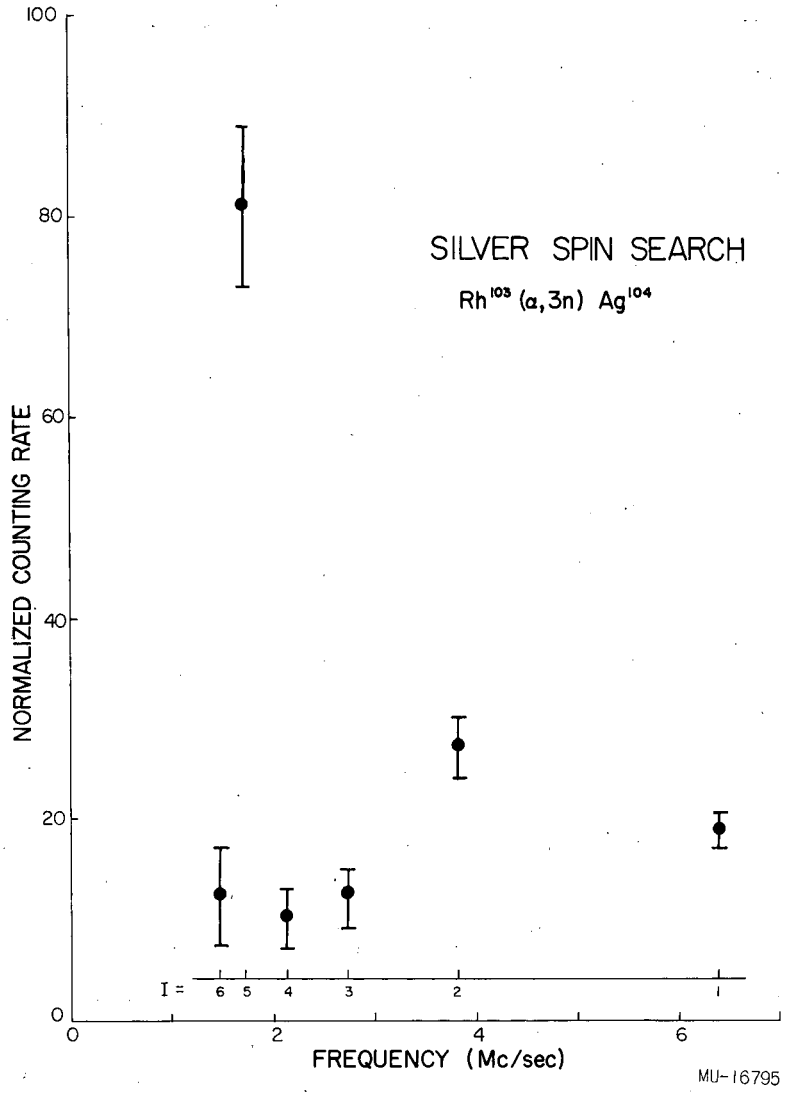

Fig. 17. Results of a search for the spin resonances of 27-minute Ag^{104} (I=2) and 1.2-hr Ag^{104}(I=5).

In experiments on the two isotopes with half lives of about an hour (Ag^{103} and Ag^{104}), it was possible to discriminate against the contamination of 27-min Ag^{104}. The short-lived Ag^{104} appears to decay principally by β^+ emission, while for the longer-lived pair, the main decay process is electron capture (see Fig. 6). If only silver x-rays are counted, then an effective discrimination against 27-min Ag^{104} is achieved. The results of a spin search in which counting was done of x-rays only are shown in Fig. 18. (The exposure at $I = 7/2$ represents a confirmation of the Ag^{103} spin assignment.)

The high spin of Ag^{103} was not expected from comparisons with the other odd-A isotopes of silver (four silver isotopes have $I = 1/2$). When a signal of 1-hour activity was obtained at the low-field resonance frequency corresponding to $I = 7/2$, it was believed to be a part of a wide resonance of the 1.2-hr Ag^{104}. Such effects have been observed at low fields, where the resonant frequencies of nearly equal spins become close together. However, after observations at higher fields, where the two resonances corresponding to $I = 5$ and $I = 7/2$ were well resolved (Fig. 18), there could be no doubt of the separate resonance on $I = 7/2$. The spin resonance of $I = 7/2$, Ag^{103}, has been observed at 2.0, 4.7, 4.9, 9.1, and 9.4 Mc.

Measurements have been described in the preceding paragraphs that led to the assignment of nuclear spins to seven isotopes of silver. The data there presented are summarized in Table XII.

Reynolds et al.[64] have reported identical results for 27-min Ag^{104} and for 24-min Ag^{106}, using deuteron-irradiated palladium targets. Publications of these results by the Berkeley atomic-beams group include Refs. 65 (Ag^{103}), 66 (8.3d Ag^{106}, Ag^{110m}), 67 (Ag^{105}), 68 (Ag^{105}, 8.3d Ag^{106}, Ag^{110m}), and 69 (Ag^{104}, Ag^{106}).

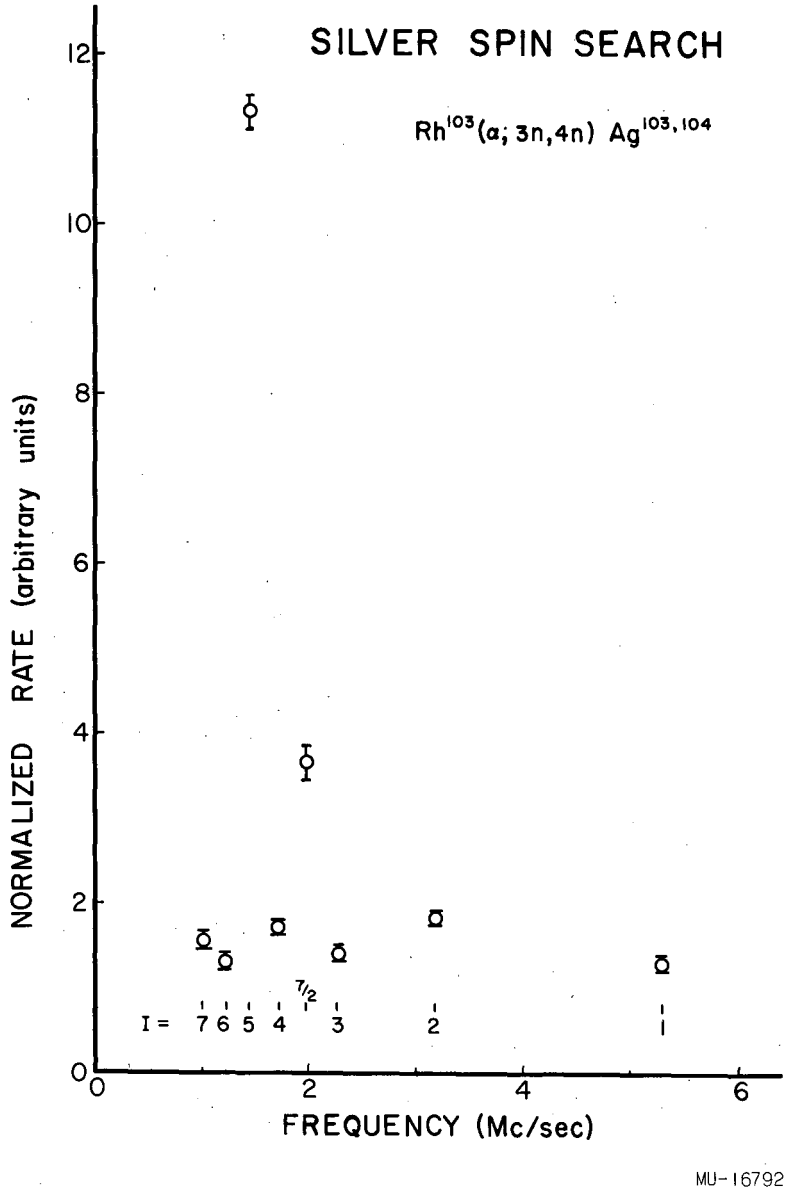

Fig. 18. Separation of spin resonances corresponding to 1.1-hr Ag^{103}(I=7/2) and 1.2-hr Ag^{104}(I=5).

Table XII

Summary of spin data for silver

Isotope	Half life	Nuclear spin	Observation frequencies (Mc)
Ag^{103}	1.1 hr	7/2	2.0, 4.7, 4.9, 9.1, 9.4
Ag^{104}	27 min	2	3.8, 4.4, 4.5, 5.5, 6.4
Ag^{104}	1.2 hr	5	[a] 1.4, 1.7, 3.0, 3.4, 3.6, 3.7, 8.1, 20.5
Ag^{105}	40 d	1/2	[b] 7.4, 8.0, 8.4, 12.2, 15.4
Ag^{106}	24 min	1	[a] 5.3, 8.3, 9.9
Ag^{106}	8.3 d	6	1.3, 2.4, 3.1, 8.6, 15.7
Ag^{110m}	253 d	6	[a] 2.4, 3.9, 7.9, 12.7, 15.7

[a] Includes one or more low-field resonance sweeps.

[b] Additional observations on Ag^{105} are described in the next paragraph.

2. Hyperfine-Structure Separation of Ag^{105}

As yet, the hyperfine-structure separation has been measured for only one neutron-deficient isotope of silver. The low spin (1/2) and convenient half life (40 days) of Ag^{105} made comparatively simple the observation of enough resonances to obtain the hfs $\Delta\nu$ quite accurately. In fact, this $\Delta\nu$ was found to be small enough that a direct ($\Delta F = \pm 1$) transition could be observed at a low transition field.

The principal $\Delta F = 0$ resonances that led to the direct measurement are shown in Fig. 19. No normalization procedure was deemed necessary, since the beam was chemically pure silver. (Periodic monitoring of the half-beam intensity supported this conclusion in a general way.) The solid curve through each set of resonance points is the bell-shaped curve, which was given by the OMNIBUS analysis as the best such curve that could be drawn through the points. The bell-shaped curve appears not always to be the best smooth curve that can be drawn through the data points. For example, the resonance at 203.5 Mc in Fig. 19 seems to be slightly asymmetric and somewhat flatter on top than the bell-shaped curve is able to describe. However, the peak of this resonance is still within the uncertainty limits set for the peak of the bell-shaped curve.

After the resonance at 708 Mc was obtained, a search for the direct transition was instituted in the region of 1520-1530 Mc. Since the width of a resonance, because of inhomogeneities in the C field, is greater for field-dependent lines than for field-independent lines, the resonance search was made for the transition $(F, m) = (1,1) \leftrightarrow (0, 0)$. The field dependence of this line is comparable to that of the standard transition, so the line width (at half-maximum intensity) should also be a few hundred kc/sec at low fields. The resonance that was observed at $\sim$ 1529 Mc was less than 100 kc wide (Fig. 20). When the fields were raised slightly, the resonance position shifted only about 30 kc, compared with an expected shift of the strongly field-dependent line $(1,1) \leftrightarrow (0,0)$ of nearly 3 Mc. The observed resonance was thus identified as corresponding to the nearly field-independent transition $(1,0) \leftrightarrow (0,0)$. Calculations of the hfs $\Delta\nu$ from the observed resonance frequencies are listed in Table XIII, assuming that the observed resonance

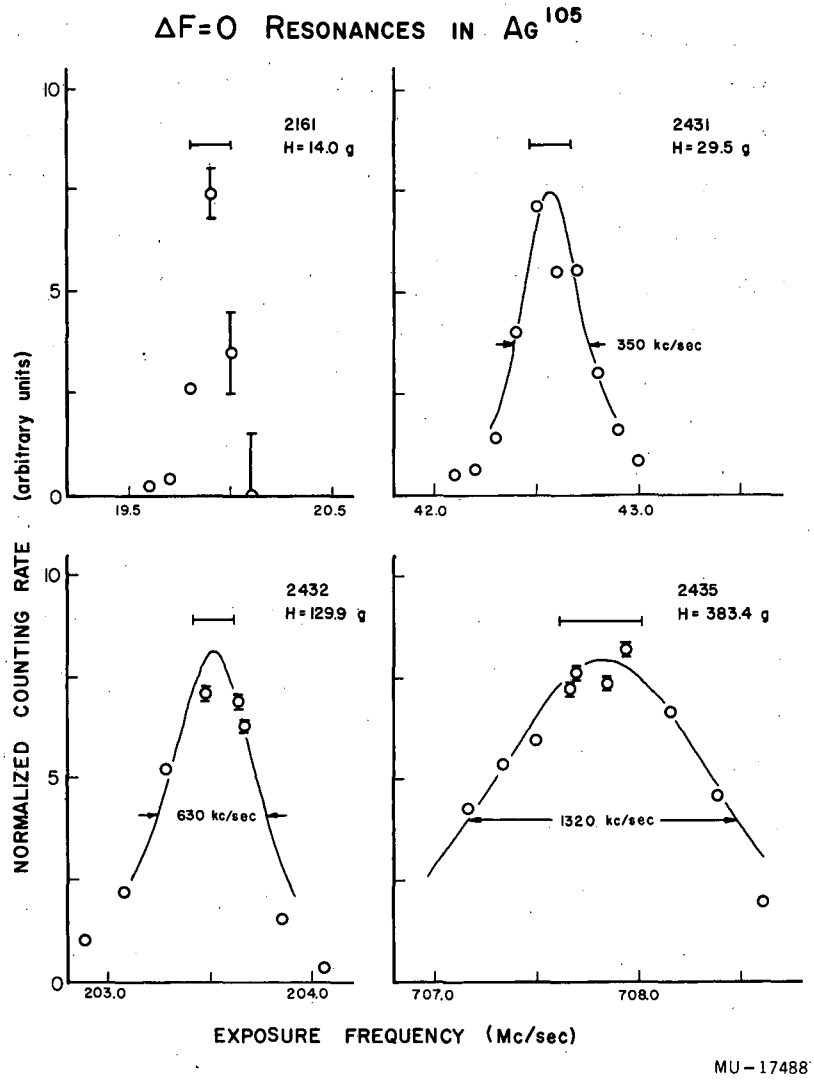

Fig. 19. Progressive $\Delta F = 0$ resonances in 40-day Ag^{105}.

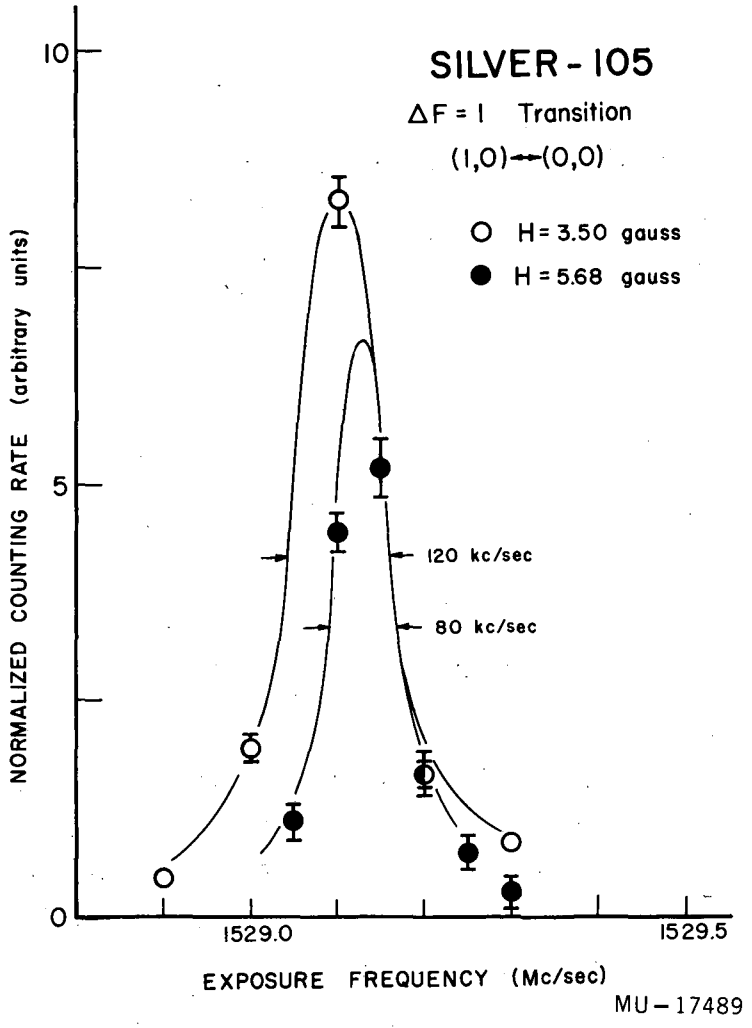

Fig. 20. Direct transition resonances in 40-day Ag^{105}.

is due first to one transition, then to the other. (These are the only two direct transitions that satisfy the focusing condition of the apparatus.)

Table XIII

Ag^{105} Confirmation of direct transition assignment

Resonance	Transition field(gauss)	Calculated $\Delta\nu_{\pm}$, assuming $(1,1)\longleftrightarrow(0,0)$ (Mc)	$(1,0)\longleftrightarrow(0,0)$ (Mc)
2436	3.50	1524.18(4)	1529.07(5)
2437	5.85	1520.89(4)	1529.04(2)
2438	5.68	1521.13(4)	1529.05(2)

The consistency of the calculated hfs $\Delta\nu$ values gives assurance that the observed transition was indeed $(1,0)\longleftrightarrow(0,0)$.

In Table XIV are summarized the calculations of $\Delta\nu$ from each of the observed resonances of Ag^{105}. The calculations were performed on the IBM-650 computer by the OMNIBUS program (Section IV-A). The uncertainty associated with each computed value of $\Delta\nu$ was found by combining (using standard methods of propagation of error[70]) the uncertainties in the field calibration and in the assignments of the resonance frequencies. The weighted average of the several calculated values of $\Delta\nu$ was obtained by weighting each individual $\Delta\nu$ calculation by the square of the reciprocal of its stated uncertainty. This procedure assures the greatest weight to the most precise measurements. In the over-all average, the very small uncertainties in the directly measured values of $\Delta\nu$ cause them to be weighted so heavily that the measurements of $\Delta F = 0$ transitions might as well be ignored.

It is unfortunate that the values of $\Delta\nu$ as calculated from measurements of the standard transition converge so well to a number so different from the directly measured $\Delta\nu$. Such behavior of the calculated $\Delta\nu$ values suggests that possibly a systematic error is introduced in the procedure or by the apparatus. If the measurement of the direct transition had not been undertaken, then the hfs $\Delta\nu$ would have been quoted at 1521(5) Mc, which does not include the directly measured value. In order to ensure the inclusion of the actual value within the quoted experimental uncertainties, it may be wise to increase the uncertainties in the final average values by a factor of two until this situation has been further investigated. This has been done for each of the weighted averages for $\Delta\nu$ of the gold isotopes as well as of Ag^{105}.

The apparent change of the calculated $\Delta\nu_{\pm}$ (which represents an average of two calculations, first assuming $g_I > 0$, then $g_I < 0$) with field is not attributable to a greater inconsistency of the calculations for $\Delta\nu_+$ or $\Delta\nu_-$. In each case, the difference $|\Delta\nu_+ - \Delta\nu_-|$ was less than the uncertainty associated with $\Delta\nu_{\pm}$. For example, at the highest field used (383.4 gauss), the difference was only $\Delta\nu_- - \Delta\nu_+ = 0.3$ Mc, while the uncertainty of the calculation was 3 Mc. This is another way of saying that the nuclear magnetic moment of Ag^{105} is too small for its sign to be determined with the precision of the present apparatus.

Until such time as the field deviations of the calculated values of $\Delta\nu$ can be investigated more closely, the hyperfine-structure separation of Ag^{105} can be given as

$$\text{40-day } Ag^{105}: \ \Delta\nu_{\pm} = 1529.05(10) \text{ Mc} .$$

Table XIV

Ag^{105} $\Delta\nu$ summary

Resonance	Frequency (Mc)	Calibration Isotope	Calibration Frequency (Mc)	Transition field (gauss)	$\Delta\nu_{\pm}$ (Mc)
		$Ag^{105}[(1,0) \longleftrightarrow (1,-1)]$			
2161	19.9(1)	Rb^{87}	9.85(2)	14.01(2)	1500(900)
2431	42.57(10)	Rb^{87}	20.84(1)	29.52(1)	1410(130)
2432	203.51(10)	Rb^{87}	94.65(2)	129.94(3)	1525(8)
2433	203.61(10)	Rb^{87}	94.67(2)	129.97(3)	1521(8)
2434	203.48(10)	Rb^{87}	94.60(1)	129.88(1)	1519(7)
2435	707.82(20)	Rb^{87}	302.46(5)	383.39(6)	1521(3)
			Weighted average $\Delta\nu_{\pm}$ =		1521(5)
		$Ag^{105}[(1,0) \longleftrightarrow (0,0)]$			
2436	1529.10(5)	Rb^{87}	2.45(2)	3.50(3)	1529.07(5)
2437	1529.13(2)	Rb^{87}	4.10(2)	5.85(3)	1529.04(2)
2438	1529.13(2)	Rb^{87}	3.98(2)	5.68(3)	1529.05(2)
			Weighted average $\Delta\nu_{\pm}$ =		1529.05(2)
			Over-all weighted average $\Delta\nu_{\pm}$ =		1529.05(2)

3. Calculated Magnetic Moments of Ag^{105}

The magnetic-dipole moment of silver-105 can be obtained most easily from the Fermi-Segrè formula (Eq. (46), Section II) and the measured moments and hfs $\Delta\nu$ of the stable silver isotopes, both of which also have $I = 1/2$. Since the spins are the same, the ratio of the magnetic moments should be equal to the ratio of hfs $\Delta\nu$ (except for the small hfs anomaly), that is,

$$\left|\mu_{105}\right| = \left|\mu_{ref}\right| \frac{\Delta\nu_{105}}{\Delta\nu_{ref}} ,$$

where the subscript "ref" indicates either 107 or 109, the masses of the two stable isotopes of silver. The hfs $\Delta\nu$ of each of the stable silver isotopes has been measured by atomic-beams methods.[32] Wessel and Lew obtained $\Delta\nu_{107} = 1712.56(4)$Mc and $\Delta\nu_{109} = 1976.94(4)$Mc. Nuclear-resonance methods have been used by two groups[71] to obtain direct measurements of the nuclear magnetic-dipole moments; $\mu_{107} = -0.1130$ nuclear magneton (nm) and $\mu_{109} = -0.1299$ nm. Combining these with the measured $\Delta\nu_{105} = 1529.05(10)$Mc gives the magnetic moment of Ag^{105}:

$$\left|\mu_{105}\right| = 0.1009 \text{ nm (referred to } Ag^{107}) \\ = 0.1005 \text{ nm (referred to } Ag^{109}) .$$

The sign of the magnetic moment is probably negative, in accord with the measured moments of the stable isotopes, although the present measurements are not precise enough to warrant a definite statement. The hfs anomaly for the two stable silver isotopes is 0.41%.[71] It does not seem reasonable, then, to report an accuracy better than about 1% for the magnetic moment of Ag^{105}. Therefore (using the subscript "FS" to indicate a moment calculated using the Fermi-Segrè relation)

$$\left|\mu_{105}\right|_{FS} = 0.101(1) \text{ nm} .$$

It will be of interest to calculate the magnetic moment of Ag^{105} directly from a measurement of its hfs $\Delta\nu$, using the longer formalism developed in Section II-E. A comparison of the magnetic moment so calculated with that obtained above from the Fermi-Segrè relation should give some information about the reliability of such calculations when they are later applied to the gold isotopes, for which no magnetic moments have been measured directly.

The calculation of μ from $\Delta\nu$ is made possible from Eq. (43) (Section II) by the evaluation of all the correction terms there described. Wessel and Lew[32] have obtained the electronic g factor as $g_J = -2.00224(20)$ Bohr magnetons. For neutral silver atoms, $Z = 47$, $Z_0 = 1$.

The Fermi-Segrè factor $(1 - \frac{d\sigma}{dn})$ has been evaluated from spectroscopic measurements by Shenstone[72] as re-interpreted by Brix et al.[73] The effective quantum number for the 5s electron of silver is $n_0 = 1.34009$. Replacing $\frac{d\sigma}{dT}$ by $\Delta\sigma/\Delta T$, with differences between the 5s and 6s energy levels of the valence electron of silver, Eq. (31) gives

$$\left(1 - \frac{d\sigma}{dn}\right)_{Ag} = 1.25 ,$$

which is in agreement with Brix et al.

The Racah correction for relativistic effects (Eq. (33a)) is evaluated directly, using the value of α in the Appendix,

$$F_r\left(\frac{1}{2}, 47\right) = 1.2626.$$

The Breit-Rosenthal correction for the finite extent of nuclear charge (Eq. (36a)) gives, for silver, $\delta = 1.088\,(y_1)^{0.8787}$. Assuming, with Crawford and Schawlow, a uniform nuclear charge distribution, then $y_1 \approx y_0 = 0.1006$ for Ag^{105}, for $r_0 = 1.20 \times 10^{-13}$ cm. Then $\delta_{Ag} = 0.019$, in agreement with Crawford et al.[74], and

$$(1 - \delta)_{Ag} = 0.981 .$$

The Bohr-Weisskopf correction, ϵ, which includes the effects of a finite distribution of nuclear magnetism, has been evaluated with the help of the graphs and tables included in Ref. 27. Since a_s and a_ℓ involve g_I for the nucleus, it is necessary to iterate from the final, calculated moment to get a consistent value for ϵ. After two such iterations, the calculation of ϵ yields

$$\epsilon_{105} = -2.31\%$$

$$(1+\epsilon)_{105} = 0.9769 .$$

The assumption of a sign for the magnetic moment of Ag^{105} is implicit in this calculation. The sign has been chosen negative, in accord with the stable isotopes.

Combining all the factors listed above, as in Eq. (45), gives

$$(\mu_{105})_{calc.} = -0.108 \text{ nm} .$$

The agreement between the magnetic moment as calculated in this way and that obtained from the Fermi-Segrè formula is not as good as it might be. However, the indication is that magnetic moments calculated directly from the measured hfs $\Delta\nu$ may be expected to be good to about 10%.

C. Gold Results

1. Nuclear Spins

As with silver, the first experiments on gold were performed on the isotopes with conveniently long half lives. Small pieces of platinum foil were bombarded with 12-Mev protons in the cyclotron and then loaded directly into the oven. When the oven was heated, a beam was obtained which was sufficient to obtain resonance exposures corresponding to I = 1 through 6, although an adequate normalization was not possible. The counting rates on most exposures were not sufficient to warrant counting them more than once, although both I = 1 and I = 2 exposures were somewhat higher. A comparison of the decay curves for the buttons corresponding to I = 1, I = 2 with the decay curve of a full-beam exposure is shown in Fig. 21. The decay curve of the I = 1 exposure very clearly indicates a resonance of ~40-hr activity. This corresponds to an assignment of I = 1 to 39-hr Au^{194}. The decay curve of the I = 2 button is definitely different from that of the half-beam exposure, but its exact composition is questionable. An OMNIBUS decay-fit analysis of all three curves gave the normalized results listed in Table XV.

Table XV

Au^{194} and Au^{196} comparison of resonance samples

Sample	39-hr Au^{194}	5.6-day Au^{196}
I = 1	45(2) units	0(2) units
I = 2	5.8(7)	4.7(7)
half-beam	52.9(9)	8.1(4)

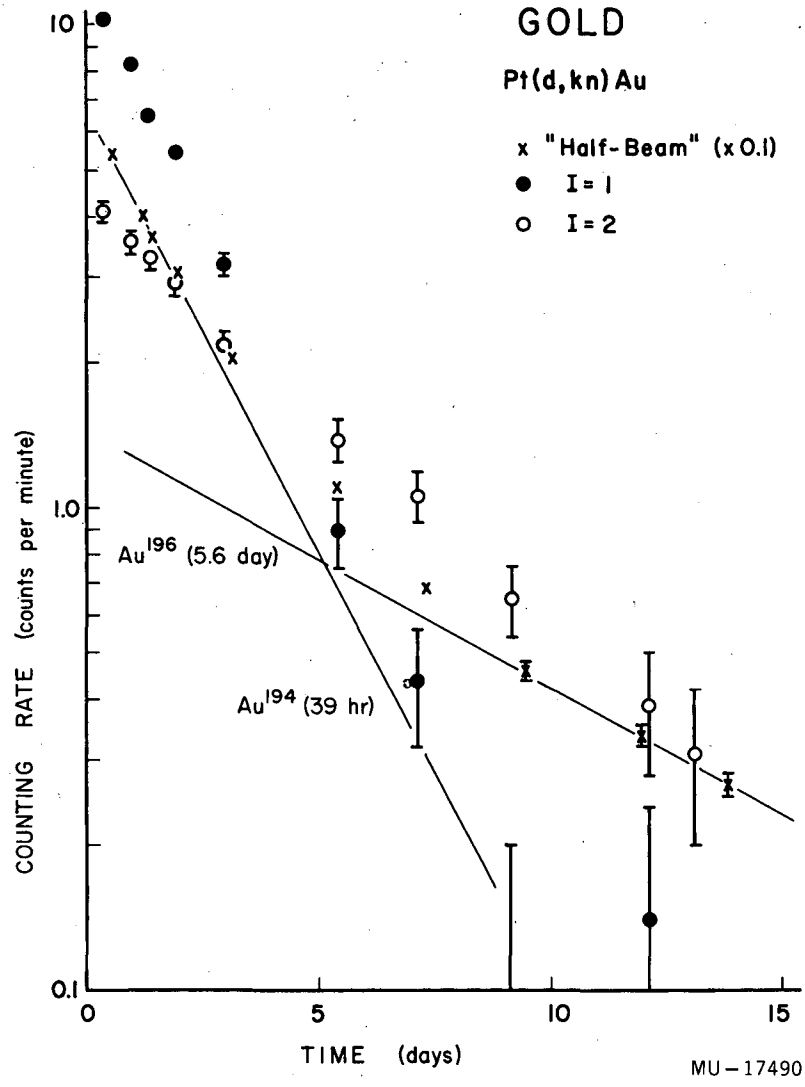

Fig. 21. Identification of gold spin resonances by decay analysis.

The enrichment of Au^{196} on the resonance button establishes its spin as I = 2. Spin resonances of 5.6-day Au^{196} have been observed at transition frequencies of 4.1, 4.5, 5.6, 5.8, 6.0, and 9.9 Mc. A low-field resonance sweep of Au^{196} has been obtained at 19.5 Mc (Fig. 22). The measurable shift of this resonance at such a low field precludes the possibility of confusion with Au^{198}, which has a measured[15] hfs $\Delta\nu_{+}$ = 21,800(150) Mc. Counting of the resonance samples with x-ray counters also discriminates against any Au^{198} that might be present.

Spin resonances of Au^{194}(I = 1) have been obtained at twelve different frequencies below 17 Mc. In addition, the standard transition resonance has been observed at several higher fields up to 640 gauss, as will be discussed later.

The long half life and consequent low counting rates make Au^{195} a difficult isotope to observe. When attempts were made to study it, platinum targets were exposed to proton or deuteron beams for periods of several hours. The target was then set aside for several days or even weeks while the shorter activities decayed away. The platinum was then dissolved and the gold separated chemically (Section III-D). After chemical purification, the gold was loaded into a tantalum oven and a beam was obtained. In Table XVI, are compared the actual counting rates of several different exposures at I = 1/2, 3/2, and 5/2.

Table XVI

Au^{195} spin search

	I = 3/2	I = 5/2	I = 1/2	I = 1/2	I = 3/2
Counting rate	3.0(1)	1.8(2)	1.1(3)	1.2(1)	3.0(2)

Both times the rate is seen to be higher for I = 3/2. Since the target was allowed to wait for such a long time after the bombardment, any competing activities were expected to be negligible. The spin resonance was thus presumed to be due to Au^{195}. Confirmation of the assignment

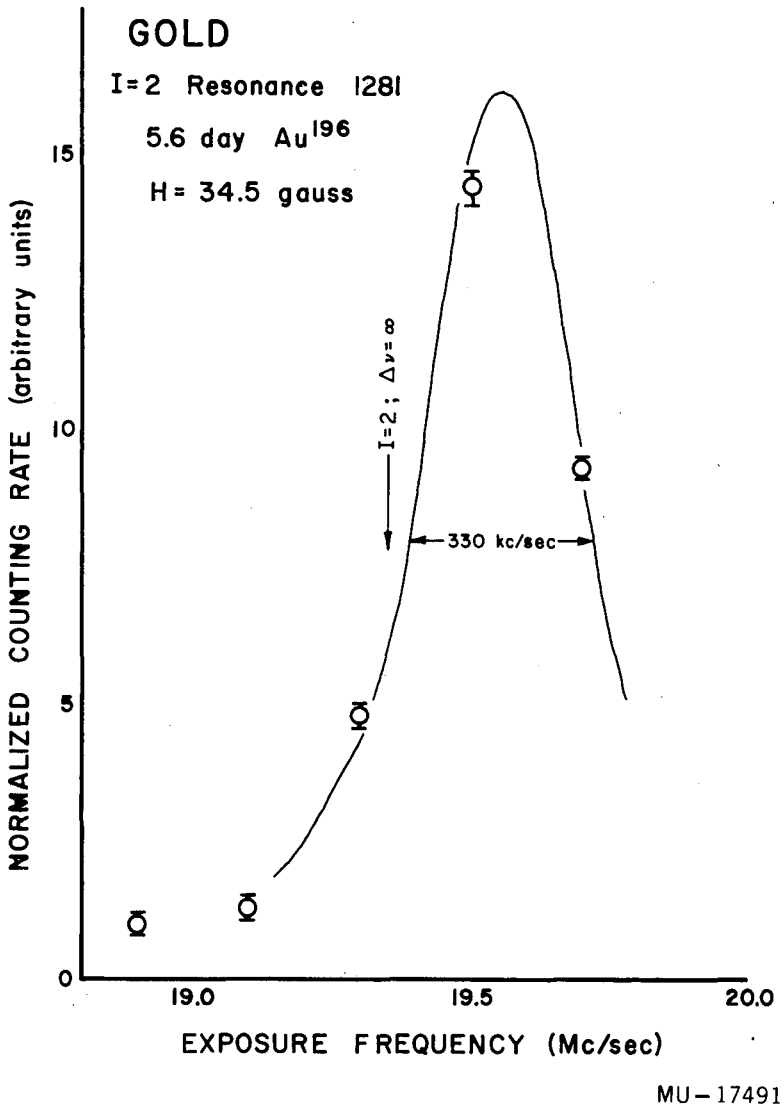

Fig. 22. Resonance sweep confirming spin assignment of 5.6-day Au^{196}.

of I = 3/2 to Au^{195} has been obtained at frequencies of 5.0, 5.7, 6.3, and 6.6 Mc. Because of the low specific activity, no resonance sweeps of Au^{195} have been observed.

The 5-mil iridium foil which was available for cyclotron bombardments to produce gold was broken into pieces before irradiation. After the bombardment, the gold-containing foil was placed in a tantalum oven and heated strongly to produce a beam of radioactive gold. The dominant activities here were the shorter-lived ones: Au^{191}(3.0-hr), Au^{192}(4.8-hr), Au^{193}(17.5-hr), and Au^{194}(39-hr). The fact that Au^{194} was produced from alpha bombardment of iridium provided an independent check of the spin (I = 1) obtained for that isotope from proton bombardment of platinum.

Normalized counting rates obtained for the first spin search using alpha-irradiated iridium are listed in Table XVII.

Table XVII

Ir(α,kn)Au spin search

	I = 0	I = 1/2	I = 1	I = 3/2	I = 2	I = 5/2
Normalized counting rate	2.2(6)	2.4(4)	33.5(13)	29.7(13)	1.7(5)	1.9(6)

The only apparent resonances are at frequencies corresponding to I = 1 and I = 3/2. The normalized compositions of these two spin resonances as obtained by OMNIBUS are compared in Table XVIII.

Table XVIII

Composition of Au spin-resonance exposures

	Au^{191}	Au^{192}	Au^{193}	Au^{194}
I = 1	0(11)	32(10)	3(2)	4.3(6)
I = 3/2	16(6)	1(6)	16(2)	0.6(5)
half-beam	48(14)	119(13)	60(3)	25.2(9)

It is apparent from Table XVIII that four spin resonances have been observed: I = 3/2 for Au^{191}, I = 1 for Au^{192}, I = 3/2 for Au^{193}, and I = 1 for Au^{194}. This conclusion is affirmed by a comparison of the decay curves for the three samples (Fig. 23). Each of the spin-resonance exposures corresponding to I = 1 and I = 3/2 has a short-lived component, with a half life of a few hours. The two decay curves then change slope quite differently, with I = 1 going into a 39-hr decay and I = 3/2 going into a 17-hr decay. High-field resonances of all four of these isotopes have been observed and will be described later.

The measurements described in the preceding paragraphs made possible the assignments of nuclear-spin values to six isotopes of gold. The results are summarized in Table XIX.

Table XIX

Summary of spin data for gold

Isotope	Half life	Nuclear spin	Observation frequencies (Mc)
Au^{191}	3.0 hr	3/2	[a]6.2, 6,3, 8.2, 8.9, 13.9
Au^{192}	4.8 hr	1	[a]8.2, 8.4, 12.9
Au^{193}	17.5 hr	3/2	[a]6.2, 6.3, 8.2, 8.9, 13.9
Au^{194}	39 hr	1	[a]5.4, 6.9, 7.6, 8.1, 8.2, 8.4, 9.3, 10.9, 11.9, 14.4, 20.0
Au^{195}	180 d	3/2	5.0, 5.7, 6.3, 6.6
Au^{196}	5.6d	2	[b]4.1, 4.5, 5.6, 5.8, 6.0, 9.9, 19.5

[a]Further resonances (in high fields) are discussed in Section IV-C-2, below.

[b]Includes a resonance sweep at 19.5 Mc.

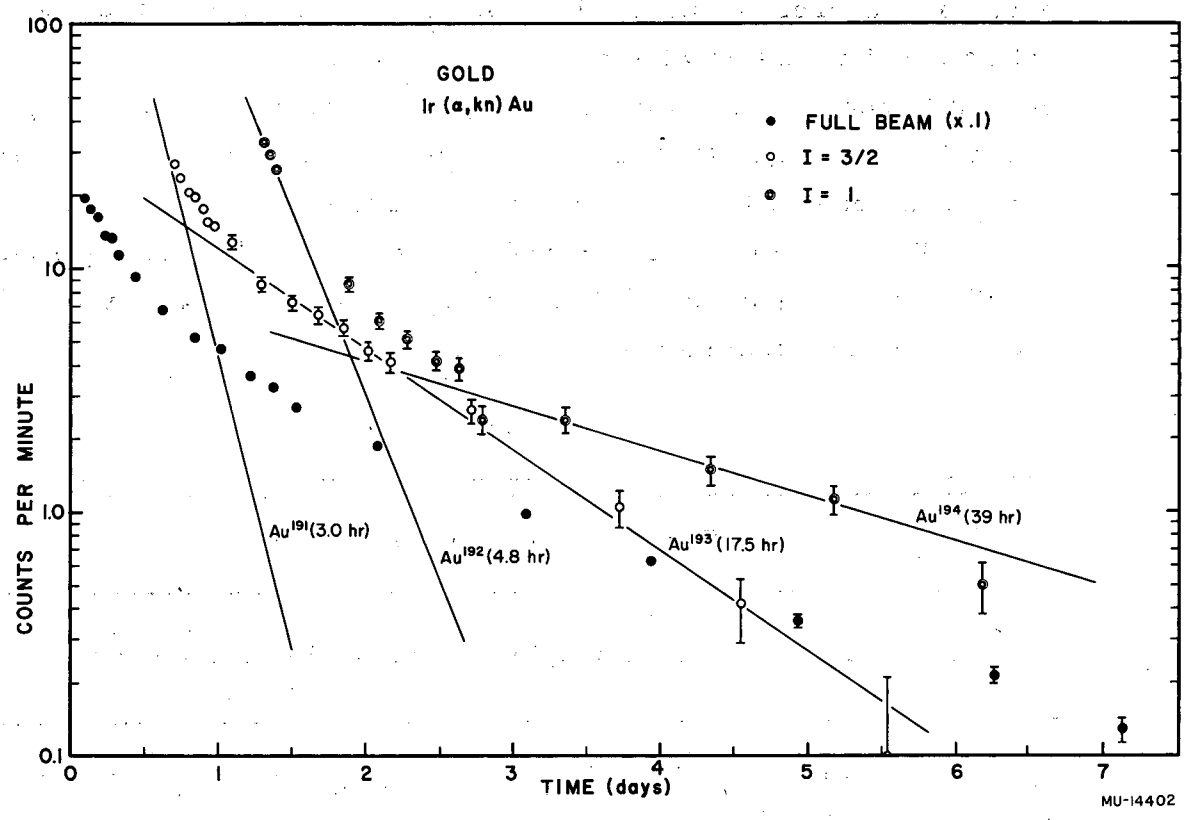

Fig. 23. Identification of gold spin resonances by decay analysis. The time scale has been shifted for the spin-resonance samples in order to provide a clear separation of the decay curves.

The results of some of these spin measurements have been published in Refs. 75 (Au^{191}, Au^{192}, Au^{193}) and 76 (Au^{194}). The measurement for Au^{194} was done simultaneously by the Berkeley and the Princeton atomic-beams groups and was reported jointly by the two groups.[76]

2. Hyperfine-Structure Separations of the Gold Isotopes

The hyperfine-structure separation $\Delta\nu$ has been measured for the four lightest isotopes of gold, Au^{191}, Au^{192}, Au^{193} and Au^{194}. All four can be produced by alpha bombardment of iridium, and most of the successful resonances have been obtained from gold isotopes produced in this way. Resonances of Au^{194} produced from platinum have also been observed.

In the data for the gold isotopes, not all observed radioactive resonances will be presented. Only a few will be used to illustrate particular points. A summary of all reliable resonances for each isotope, together with the hfs $\Delta\nu$ calculated from the resonance data, will be included as for Ag^{105}. It is to be understood that each gold resonance has been analyzed in the same manner that was described in Section IV-B-2. In addition, a normalization of each of the resonances has usually been necessary. The nuclear magnetic moments of these four gold isotopes are so small that it has not been possible to establish the signs of the moments. OMNIBUS calculations of $\Delta\nu_+$ and $\Delta\nu_-$, assuming positive or negative moment respectively, have not differed by so much as the uncertainties in the calculations. As it was for Ag^{105} (Section IV-B-2), the quantity $\Delta\nu_\pm$ is an average of $\Delta\nu_+$ and $\Delta\nu_-$ from the OMNIBUS delta-nu calculation.

For Au^{192}, the first indication of the magnitude of $\Delta\nu$ was obtained when an I = 1 spin resonance at 12 Mc was observed to be composed of almost pure Au^{194}, even though Au^{192} was present in the beam. Further investigation revealed that even at this low field the Au^{192} resonance was already shifted away from the Zeeman frequency by almost 1 Mc. This is illustrated by the resonance sweep shown in Fig. 24. Whereas the resonance of Au^{194} has no appreciable shift,

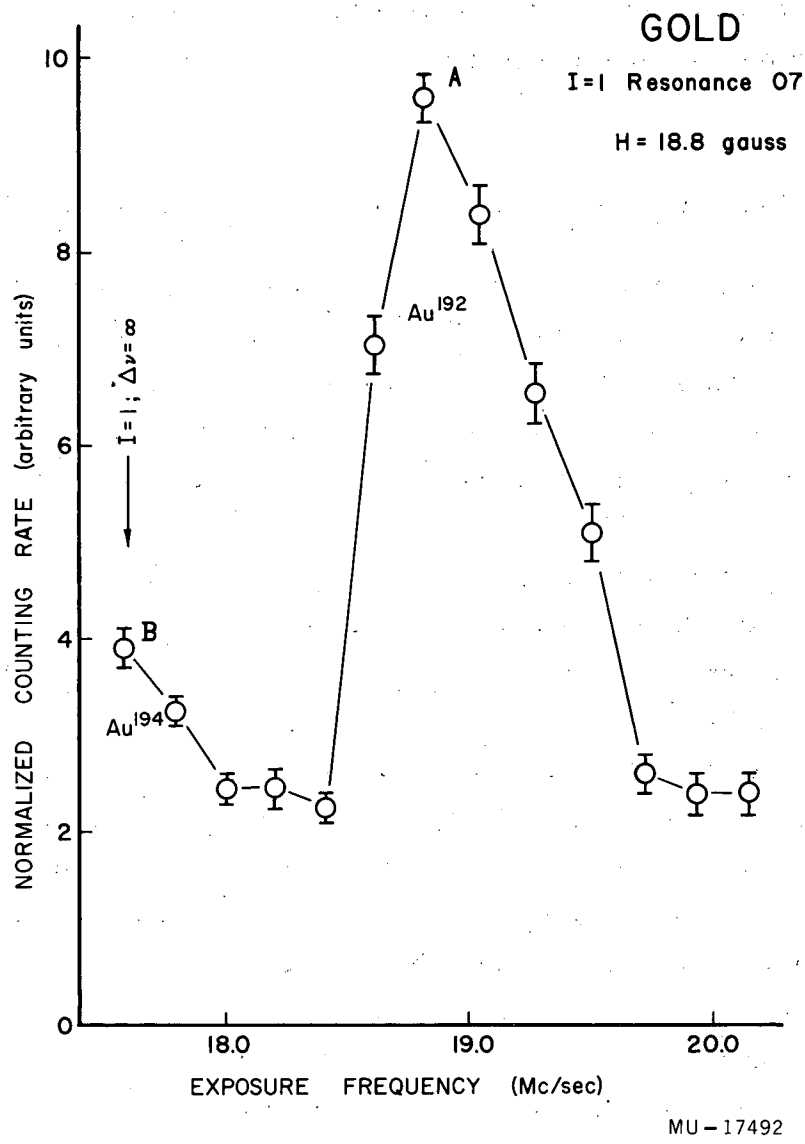

Fig. 24. Resonance sweep illustrating the resolution of resonances corresponding to 4.8-hr Au^{192}(A) and 39-hr Au^{194}(B).

the Au^{192} resonance is shifted far enough that the two resonances are well resolved. The two resonances were identified by the difference in the observed decay of the radioactivity on the two exposures marked A and B (see Fig. 25). Subsequent resonances (Table XX) at transition fields up to $\sim$75 gauss indicated that the $\Delta\nu$ for Au^{192} was only about 375 Mc, so that an attempt to see the direct transitions at low fields was feasible. A direct transition was observed at two values of transition field. The resonances obtained are shown in Fig. 26. Identification of the transition involved in the resonance is based (as for Ag^{105}) on the consistency of the hfs $\Delta\nu$ as calculated from the resonance frequencies at the two separate fields. The observable direct transitions in Au^{192} are shown in Fig. 27. Of the five possible transitions, the doublet $\left[(3/2,\ 1/2) \longleftrightarrow (1/2,\ -1/2)\right] + \left[(3/2,\ -1/2) \longleftrightarrow (1/2,\ 1/2)\right]$ (which would not be resolved at these low fields) has the smallest field dependence. The hfs $\Delta\nu$ was calculated from each of the observed resonances in Fig. 26, assuming in turn that the resonances were caused by each of the focusing transitions shown in Fig. 27. The results, listed in Table XXI, clearly show that the observed transition was indeed the unresolved doublet $\left[(3/2,\ 1/2) \longleftrightarrow (1/2, -1/2)\right] + \left[(3/2, -1/2) \longleftrightarrow (1/2, 1/2)\right]$.

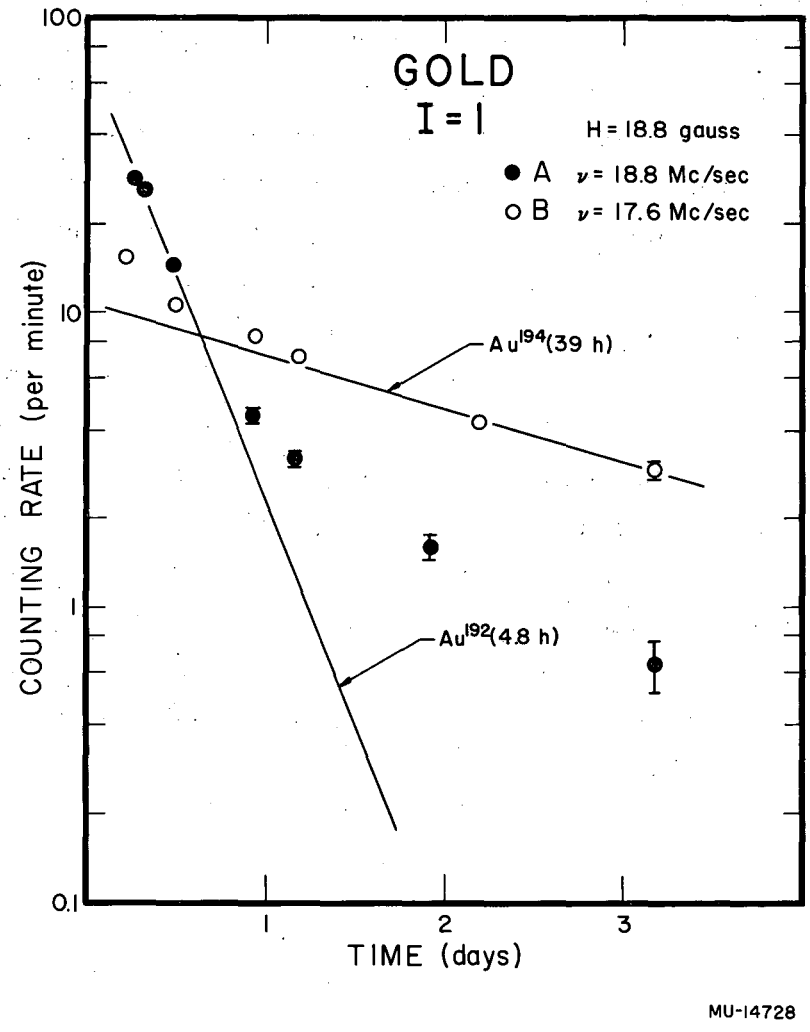

Fig. 25. Identification of resonances in Fig. 24.

Table XX

Au^{192} $\Delta\nu$ summary

$Au^{192}\left[(3/2,-1/2)\leftrightarrow(3/2,-3/2)\right]$

Resonance	Frequency (Mc)	Calibration Isotope	Calibration Frequency (Mc)	Transition field(gauss)	$\Delta\nu_{\pm}$ (Mc)
0691	12.84(15)	Rb^{87}	9.20(5)	13.10(7)	520(180)
0781	18.92(20)	Rb^{87}	13.23(5)	18.80(7)	480(80)
0821	30.25(15)	Rb^{87}	20.06(3)	28.41(4)	407(17)
0841	56.38(10)	Rb^{87}	33.96(1)	47.83(1)	376(3)
1161	100.38(15)	Rb^{87}	54.07(2)	75.50(3)	375(2)
1162	100.31(20)	Rb^{87}	54.05(3)	75.47(3)	376(3)
			Weighted average $\Delta\nu_{\pm}$ =		376(3)

$Au^{192}\left[(3/2,1/2)\leftrightarrow(1/2,-1/2)+(3/2,-1/2)\leftrightarrow(1/2,1/2)\right]$

1191	374.94(5)	Rb^{85}	3.95(5)	8.41(11)	374.28(5)
		Rb^{87}	5.90(3)	8.41(4)	374.28(5)
1192	375.15(5)	Rb^{85}	4.40(5)	9.36(11)	374.33(5)
		Rb^{87}	6.63(5)	9.45(7)	374.32(5)
			Weighted average $\Delta\nu_{\pm}$ =		374.30(5)
			Weighted average of all measurements $\Delta\nu_{\pm}$ =		374.30(5)

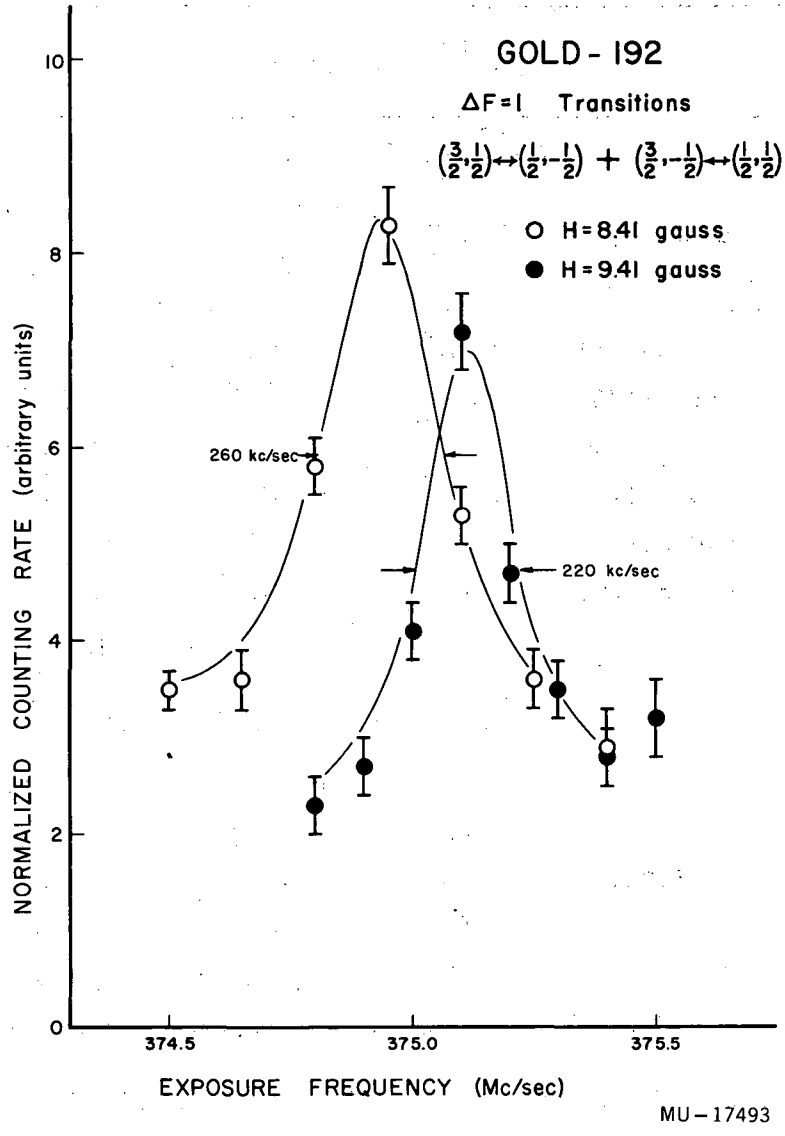

Fig. 26. Direct transition resonances in 4.8-hr Au^{192}.

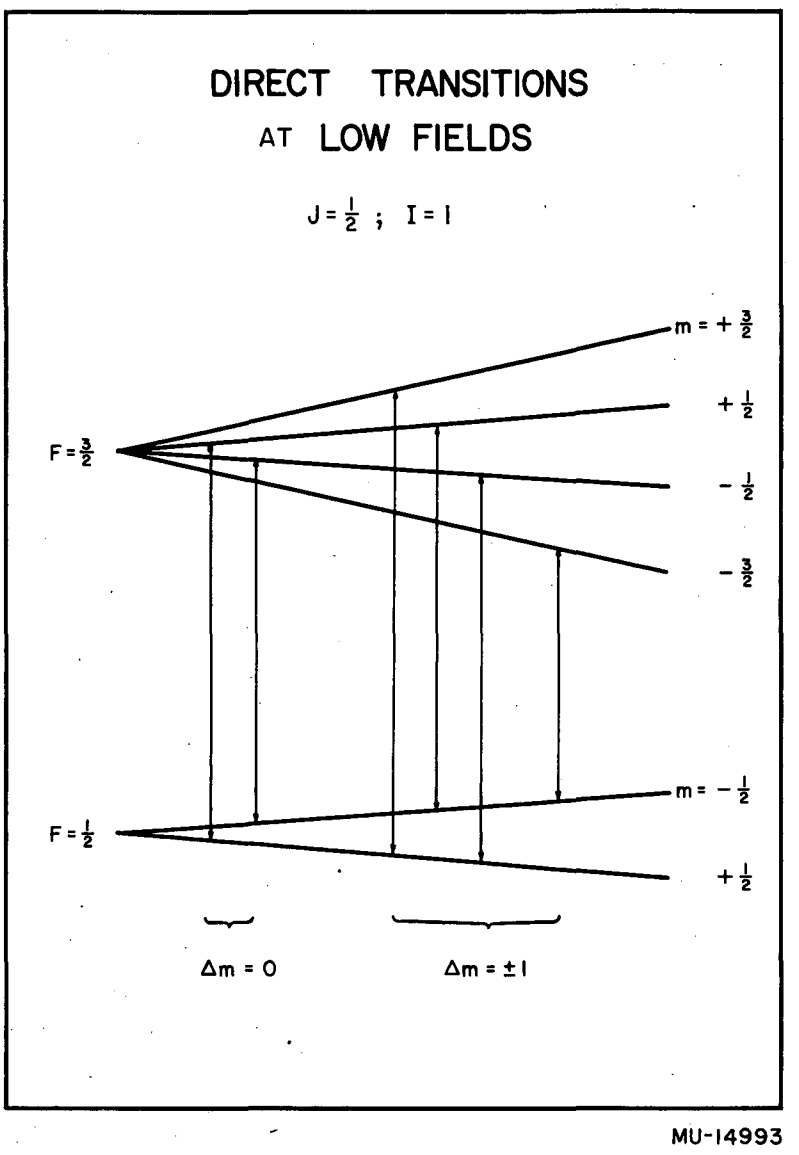

Fig. 27. Possible direct ($\Delta F = \pm 1$) transitions in 4.8-hr Au^{192}.

Table XXI

Au^{192} assignment of the direct transition

Assumed transition	$\Delta\nu_{\pm}$ from ν_{192} = 374.94(5)Mc, H = 8.41(10)gauss (Mc)	$\Delta\nu_{\pm}$ from ν_{192} = 375.15(5)Mc, H = 9.40(10)gauss (Mc)
(3/2, 1/2) ⟷ (1/2, 1/2)	366.42(13)	365.58(13)
(3/2, -1/2) ⟷ (1/2, -1/2)	382.14(10)	383.08(9)
(3/2, 3/2) ⟷ (1/2, 1/2)	358.88(21)	357.23(21)
(3/2, 1/2) ⟷ (1/2), -1/2) + (3/2, -1/2) ⟷ (1/2, 1/2)	374.28(5)	374.32(5)

As in the case of Ag^{105} (Section IV-B-2), the calculated values of $\Delta\nu$ for Au^{192} show a systematic variation, which depends on the field at which the resonance data were taken. The weighted average of all $\Delta\nu$ values calculated from $\Delta F = 0$ transitions is, however, still uncertain enough to include the value calculated from measurements of the direct transition. Again, the weighted average of all $\Delta\nu$ calculations is the same as the weighted average of those calculated from the direct transitions alone. The high precision of these measurements is sufficient to provide a $\Delta\nu$ value within 0.1 Mc. The best value for the hfs $\Delta\nu$ of Au^{192} has been found to be

$$\text{4.8-hr } Au^{192}: \ \Delta\nu_{\pm} = 374.30(10) \text{ Mc} .$$

Because of the very low $\Delta\nu$ of Au^{192}, its standard transition resonance was shifted considerably even at relatively low values of the transition field. At only 12 Mc, the Au^{192} resonance was observed to be shifted almost a full Mc away from the unshifted Zeeman resonance

frequency for $I = 1$. On the other hand, the resonance of Au^{194}, which has the same spin, occurred at almost exactly the Zeeman frequency at such low fields. Because preliminary work[77] had been done on the measurement of $\Delta\nu$ for Au^{194}, it was not necessary to make resonance sweeps below 100 Mc. The first observed resonance of Au^{194} was exposed at a transition field of 112 gauss, and the standard transition resonance was followed out in field to 640 gauss. The results of the measurements on Au^{194} are summarized in Table XXII.

Except for one (starred) determination, the $\Delta\nu$ values calculated from the observed Au^{194} resonances are in agreement with the weighted average. In Run 162, as in several others, the magnetic fields were calibrated by using both Rb^{87} and Rb^{85}. Usually, the intensity of the transition field was consistent as calculated from independent resonances of the two isotopes. Here, although both resonances were observed three separate times, in each case the field intensity was different by about a gauss, depending on which isotope was used for the calibration. Evidently, one of the calibration resonances was observed incorrectly. The inconsistency of the $\Delta\nu$ calculated from the Rb^{87} calibration for Resonance 1621 would indicate that it is this measurement which is in error. However, neither calibration is a priori more suspect than the other. If the inconsistent calculation is not included in the averaging, then the second weighted average is obtained. It seems reasonable, since the two weighted average values of $\Delta\nu$ are not far different, to accept the second as the more probable value, but to increase the limits of uncertainty to include the first weighted average. With these considerations, the hfs $\Delta\nu$ can be given for Au^{194}:

$$39\text{-hr } Au^{194}: \ \Delta\nu_{\pm} = 3503(10) \text{ Mc} .$$

Both Au^{191} and Au^{193} have $I = 3/2$. At the low frequencies at which spin resonances were observed, there seemed to be no difference between the field behavior of the two isotopes. The half life of Au^{193} is 17.5 hours, while that of Au^{191} is only 3.0 hours. Consequently, radioactive samples of Au^{193} (along with Au^{194}) could be prepared free of Au^{191} contamination by the simple precedure of waiting for several hours before performing the experiment. Ordinarily, the cyclotron bombardment was performed at night and the radioactive beam was not run until the next day.

Table XXII

Au^{194} $\Delta\nu$ summary

Au^{194} $\left[(3/2, -1/2) \leftrightarrow (3/2, -3/2)\right]$

Resonance	Frequency (Mc)	Calibration Isotope	Calibration Frequency (Mc)	Transition field(gauss)	$\Delta\nu_+$ (Mc)
1201	111.09(20)	Rb^{85}	57.08(3)	111.94(5)	3510(110)
		Rb^{87}	81.17(1)	112.05(1)	3580(110)
1402	231.12(20)	Rb^{85}	122.64(4)	219.97(6)	3500(30)
		Rb^{87}	164.85(5)	220.02(6)	3510(30)
1621	657.15(30)	Rb^{85}	391.92(5)	533.95(5)	3499(6)
		Rb^{87}	442.89(5)	535.01(5)	3533(7)*
197-8	827.48(30)	Rb^{85}	516.36(5)	640.26(4)	3502(5)
		Rb^{87}	548.14(5)	640.35(5)	3505(5)
			Weighted average $\Delta\nu_\pm$ =		3508(10)
			Weighted average (omitting*) $\Delta\nu_\pm$ =		3503(5)

The results of thirteen resonance measurements of the hfs $\Delta\nu$ of Au^{193} are listed in Table XXIII. Resonances were observed in transition fields as high as 640 gauss. The last three calculations were made from resonances obtained in connection with simultaneous measurements on Au^{191} described below. The unexplained systematic decrease in $\Delta\nu$ calculated from measurements on the standard transition resonance is observed again for Au^{193}. The best value for $\Delta\nu$ of Au^{193} is therefore

$$17.5\text{-hr } Au^{193}: \ \Delta\nu_{\pm} = 5890(20)\ \text{Mc} .$$

After this value of $\Delta\nu$ was obtained for Au^{193}, a tentative value was assigned to Au^{191} on the basis of a comparison of the $\Delta\nu$ of Au^{197} with that of Au^{193}. It was not found necessary to go to very low fields, but the first separation of resonances of Au^{191} from those of Au^{193} was accomplished at 272.9 gauss. At this field, the two resonances actually overlapped, but the OMNIBUS decay-fit program clearly separated a resonance for each isotope (Fig. 11). Further measurements on the standard transition at higher transition fields gave the other results listed in Table XXIV. These high-field measurements are consistent with a weighted average value of $\Delta\nu$ for Au^{191} of

$$3.0\text{-hr } Au^{191}: \ \Delta\nu_{\pm} = 5780(20)\ \text{Mc} .$$

A summary of all $\Delta\nu$ values measured for these four neutron-deficient gold isotopes is given in Table XXV.

Table XXIII

Au^{193} $\Delta\nu$ Summary

Au^{193} $\left[(2,-1)\longleftrightarrow(2,-2)\right]$

Resonance	Frequency (Mc)	Calibration Isotope	Calibration Frequency (Mc)	Transition field(gauss)	$\Delta\nu_{\pm}$ (Mc)
0692	13.93(10)	Rb^{87}	14.00(2)	19.89(3)	
0693	34.37(15)	Rb^{87}	34.31(1)	48.31(1)	7000(3000)
0694	60.07(10)	Rb^{87}	59.85(2)	83.37(3)	6500(400)
0822	105.70(20)	Rb^{87}	104.90(8)	143.41(10)	6100(260)
0842	172.10(20)	Rb^{87}	169.98(2)	226.41(2)	5980(90)
1511	208.10(40)	Rb^{87}	204.81(2)	269.16(2)	5880(120)
1512	207.93(20)	Rb^{87}	204.77(2)	269.11(2)	5920(60)
1601	451.6(5)	Rb^{87}	437.33(10)	529.26(10)	5800(30)
1911	446.44(20)	Rb^{87}	433.90(3)	525.70(5)	5901(14)
1961	562.95(20)	Rb^{85}	511.44(5)	636.34(4)	5894(9)
		Rb^{87}	543.84(5)	636.16(5)	5886(9)
2241	203.59(20)	Rb^{87}	200.46(3)	263.88(4)	5890(60)
2281	211.43(10)	Rb^{87}	207.90(5)	272.90(6)	5840(30)
2311	569.5(5)	Rb^{87}	549.98(3)	642.13(1)	5880(20)
			Weighted average $\Delta\nu_{\pm}$=		5888(10)

Table XXIV

Au^{191} $\Delta\nu$ summary

$Au^{191}\left[(2,-1)\longleftrightarrow(2,-2)\right]$

Resonance	Frequency (Mc)	Calibration Isotope	Calibration Frequency (Mc)	Transition field(gauss)	$\Delta\nu_{\pm}$ (Mc)
2281	211.82(10)	Rb^{87}	207.90(5)	272.90(6)	5738(30)
2311	571.44(20)	Rb^{87}	549.29(3)	641.46(3)	5770(9)
2421	571.96(10)	Rb^{87}	549.94(5)	642.09(5)	5777(5)
2422	571.88(15)	Rb^{87}	550.00(5)	542.15(5)	5784(7)
			Weighted average $\Delta\nu_{\pm}$=		5777(10)

Table XXV

Hyperfine-structure separations of some gold isotopes

Isotope	Half life (hr)	Spin	$\Delta\nu_{\pm}$ weighted average (Mc)
191	3.0	3/2	5780(20)
192	4.8	1	374.30(10)
193	17.5	3/2	5890(20)
194	39	1	3503(10)

3. Calculated Magnetic Moments for Gold

Unfortunately, the magnetic moment of stable Au^{197} has not been measured directly. Consequently, there is no solid foundation from which the magnetic moments of these four isotopes of gold can be calculated. As an alternate procedure, the magnetic moment of Au^{197} has been calculated from its measured hfs $\Delta\nu$. The result of this calculation has then been used as a basis for the evaluation of the magnetic moments of the other gold isotopes. The sample calculation carried out for Ag^{105} indicated that an accuracy of about 10% may reasonably be expected from such calculations.

The hfs $\Delta\nu$ and electronic g factor have been measured by Wessel and Lew,[32] who obtained $\Delta\nu_{197} = 6107.1(10)$Mc, $(g_J)_{Au} = -2.00412(12)$ Bohr magnetons. For neutral atoms of gold, $Z = 79$, $Z_0 = 1$.

The term values of the valence electron in gold have been studied by Platt and Sawyer,[78] using standard methods of optical spectroscopy. For the effective quantum number of the 6s electron in gold, they obtain $n_0 = 1.215$. The derivative $\frac{d\sigma}{dT}$ was again replaced by $\frac{\Delta\sigma}{\Delta T}$ with differences between the ground state 6s and the 7s levels. When the 6s term value of Platt and Sawyer, is introduced into Eq. (31), the Fermi-Segrè factor is obtained:

$$\left(1-\frac{d\sigma}{dn}\right)_{Au} = 1.424.$$

This is in agreement with Kelly.[79] However, von Siemens[89] has pointed out that if σ is expressed as a quadratic function of T [Eq. (29)], then the calculated value of $(1-\frac{d\sigma}{dn})$ is increased by about 4 %. Evaluation of the constants A, B, and C in Eq. (29) from the term values and effective quantum numbers measured by Platt and Sawyer for the 6s, 7s, and 8s energy levels leads--through the use of Eq. (32)--to a value for $(1-\frac{d\sigma}{dn})$ of 1.482. In order to maintain the calculation parallel to that carried out for Ag^{105}, the value of the Fermi-Segrè factor will be taken to be that obtained by assuming no perturbation[18] between the energy levels, i.e., $(1-\frac{d\sigma}{dn}) = 1.424$. The added uncertainty from this factor must be considered in the final figures, however.

The relativistic correction of Racah [Eq. (33a)] is straightforward:

$$F_r\left(\frac{1}{2}, 79\right) = 2.1976.$$

The Breit-Rosenthal correction is made, assuming a uniform distribution of nuclear charge,

$$\delta_{Au} = 10.4\% ,$$

$$(1-\delta_6)_{Au} = 0.896 ,$$

which is in approximate agreement with Kelly.[79]

For the purpose of evaluating the Bohr-Weisskopf correction, the nuclear spin (I = 3/2) and magnetic moment are assumed to be due to a single proton in a $d_{3/2}$ orbit. The sign of the moment is assumed to be positive, as has been concluded from spectroscopic evidence.[79] With the use of the graphs and tables of Ref. 27, a value of ϵ consistent with the calculated moment is obtained:

$$\epsilon_{Au^{197}} = 14.8\% ,$$

$$(1+\epsilon)_{Au^{197}} = 1.148 .$$

When all the above factors are combined according to Eq. (44), the nuclear magnetic moment of Au^{197} is calculated to be

$$\mu_{197} = +\ 0.127 \text{ nm}.$$

This number may be expected to be at least 10% uncertain, according to the results of the similar calculation for Ag^{105} (Section IV-B-3). In addition, there is another uncertainty in the calculation of the Fermi-Segrè factor. If the value calculated by von Siemens[80] is used instead of that of Kelly[79] then the calculated nuclear moment is about 4% lower. As a basis for calculation of the magnetic moments of the gold isotopes, an average has been taken of these two values, i.e.,

$$\mu_{197} = +0.125(15) \text{ nm}.$$

In Table XXVI are summarized the nuclear magnetic moments of the four gold isotopes calculated from this basis by the Fermi-Segrè formula.

Table XXVI

Nuclear moments of some gold isotopes

Isotope	Spin	hfs $\Delta\nu$ (Mc)	$\lvert\mu_I\rvert$[a] (nm)
191	3/2	5780(20)	0.118(15)
192	1	357.30(10)	0.0068(10)
193	3/2	5890(20)	0.121(15)
194	1	3503(10)	0.064(10)

[a]Calculated from the Fermi-Segrè formula on the basis of a moment + 0.125(15) nm for Au^{197}.

V. DISCUSSION

A. Silver Results

Since the atomic number of silver (Z = 47) is so near the closed shell at Z = 50, the shell model[22] is expected to provide a good approximation to the nuclear configurations for the odd-A isotopes. In fact, the ground-state nuclear spins of all the silver isotopes discussed here can be justified (though not necessarily predicted) by the shell model. Table XXVII lists the probable single-particle orbits for both neutrons and protons of the silver isotopes. In the body of the table, these single-particle states have been combined by Nordheim's rules[81] to give a list of the possible integral spins for the even-even isotopes of silver.

Table XXVII

Single-particle orbits for silver

neutron →	$2d_{5/2}$	$1g_{7/2}$
proton ↓		
$2p_{1/2}$	2	4
$1g_{9/2}$	3, 4, 5, 6, 7	1

The underscore indicates an integral spin that is predicted by Nordheim's "strong rule," while all other integral spins are obtained from application of the "weak rule."

The observed spin 7/2 for Ag^{103} is to be contrasted with the value 1/2, measured for the other odd-A isotopes of silver. It is easier to justify I = 1/2 on the basis of the shell model. There is a $p_{1/2}$ proton level, first appearing at Z = 39, which might be expected to contain an odd proton if the pairing energy of the competing $g_{9/2}$ level were sufficiently high. From a first look at the levels, however, the only other possible spin should be 9/2. The nearest level with spin 7/2 is above the magic number 50, and would be expected to have an energy considerably higher[82] than the $g_{9/2}$ level. The fact that the spin I = 7/2 has been tentatively assigned to several states of isotopes with odd Z between 43 and 47 indicates that the spin-7/2 state has a low energy. It has been suggested[82] that seven $g_{9/2}$ protons may couple to a total spin of 7/2, and this is the configuration that must be assumed here. The first excited states in both Ag^{107} and Ag^{109} have been observed to have I = 7/2, and are presumed to have the same configuration.

Configurations of the even-A isotopes of silver can be assigned uniquely if the "group approach" of Way et al.[83] is adopted. It is this approach that has led to the construction of Table XXVII. The ground-state spins are expected to be the states of lowest energy among those formed from the competing neutron and proton orbits. Although there is no a priori evidence for making orbit assignments, the measurements of the nuclear spins provide unique assignments if the group approach is valid.

The high-spin low-spin isomerism observed in the silver isotopes is not unexpected before the closed shell at 50 protons. The results for Ag^{106} have been anticipated by Bendel et al.,[34,41] who, from decay-scheme systematics, assigned a spin of 1 to the 24-min isomer and a spin $\geqslant 4$ to the 8.3-day isomer. The short-lived isomer of Ag^{104} has been studied by Johnson,[36] who correctly predicted the spin of 2. The 1.2-hr isomer of Ag^{104} has not been previously studied in a manner that would distinguish it from 1.1-hr Ag^{103}. The work reported here confirms the existence of two light isotopes of silver, each with half life of about 1 hour.

The magnetic moment calculated from present measurements for Ag^{105} is in good agreement with those measured for the other silver isotopes.[71] However, all these are in only approximate agreement with the moment expected from the simple shell model, for which the Schmidt limit[84] is $\mu = -0.265$ nm. The deviation from the Schmidt limit is customarily attributed to "quenching" of the meson fields around the free particle when it is placed in a nucleus. A second correction to the Schmidt-limit magnetic moment may be expected to arise from configuration-mixing interactions.[85, 86] Arima and Horie[85] have calculated a first-order correction to the magnetic moments obtained from the simple model. These first-order interactions vanish for a $p_{1/2}$ particle, however. More recently, Sano[87] has used a higher-order mixing to explain the observed transition rates between the $p_{1/2}$ and $(g_{9/2})^n_{7/2}$ levels in the neighborhood of silver. Such a configuration interaction has not yet been applied to a calculation of magnetic moments.

B. Gold Results

The result[33] $I = 3/2$ for all measured odd-A isotopes of gold requires that the 79th proton be assigned to the $d_{3/2}$ shell. The Schmidt limit for a $d_{3/2}$ proton predicts that the magnetic moments, then, should be $+0.126$ nm. Except for the fact that the measured moment decreases with the mass of the isotope (and hence all $d_{3/2}$ protons do not have the same magnetic moment), the results may be said to agree very well with the expected shell-model value. The uncertainties that must be attached to the values obtained here, although not affecting the agreement, must raise some question about a possible fortuity of the agreement.

A coupling of the $d_{3/2}$ proton to a $p_{1/2}$ neutron has been postulated[15] to explain the observed spin ($I = 2$) and magnetic moment of Au^{198}. The same coupling could be expected to cause the observed $I = 2$ of Au^{196}. However, $I = 1$ for Au^{192} and Au^{194} suggests the necessity for some unusual coupling to explain the spins and magnetic moments of these iosotopes. The competing proton and neutron levels are listed in Table XXVIII, together with the possible nuclear spins, assuming strict adherence to Nordheim's rules.

Table XXVIII

Shell-model levels for gold

neutron → / proton ↓	$p_{1/2}$	$f_{5/2}$	$i_{13/2}$
$d_{3/2}$	2	2, 3, 4	5
$s_{1/2}$	0	2	7
$h_{11/2}$	5	4	$\geqslant 2$

Gallagher and Moskowski[88] have recently suggested an adaptation of Nordheim's rules to explain the ground-state spins of a wide variety of even-even isotopes. The rules are applied to the component of I along the nuclear symmetry axis and are able to provide justification for I = 1, observed for Au^{192} and Au^{194}.

A collective-model calculation of the magnetic moments of odd-odd isotopes has been applied to Au^{194} by Hooke.[89] His calculations provide small moments, $\mu \sim 0$, but the uncertainties in the calculation preclude any concrete comparison with experiment.

APPENDIX

The physical constants used for the calculation of the magnetic moments of Ag^{105} and Au^{197} from their measured hyperfine-structure separations have been taken from E. R. Cohen, K. M. Crowe, and J. W. M. DuMond, The Fundamental Constants of Physics (Interscience Publishers, New York, 1957):

$$a_H = 5.29172(2) \times 10^{-9} \text{cm}$$

$$M_p/m_e = 1836.12(2)$$

$$\alpha = 7.29729(3) \times 10^{-3}$$

$$h = 6.62517(23) \times 10^{-27} \text{ erg-sec}$$

$$\mu_0 = 0.92731(2) \times 10^{-20} \text{ erg/gauss}$$

$$\mu_N = \mu_0(M_p/m_e) = 0.505038(18) \times 10^{-23} \text{ erg/gauss.}$$

In order to calibrate the transition field of the apparatus, the constants of Rb^{85} and Rb^{87} have been taken from N. F. Ramsey, Molecular Beams (Oxford University Press, Oxford , 1956):

Rb^{85}: $I = 5/2$: $\Delta\nu = 3035.730(5)$ Mc: $\mu_I = +1.34818(11)$ nm

Rb^{87}: $I = 3/2$: $\Delta\nu = 6834.681(10)$ Mc: $\mu_I = +2.74138(4)$ nm

$g_J(Rb) = -2.00238(4)$ Bohr magnetons.

ACKNOWLEDGMENTS

It is a pleasure to acknowledge the material assistance and moral support that have been received from the Atomic Beams Group at the Lawrence Radiation Laboratory during the performance of this research. In particular, I would like to express my deep appreciation to Professor William A. Nierenberg, whose ebullient enthusiasm has often dulled the disappointment of an unsuccessful run and led to renewed effort, to Professor Henry B. Silsbee, whose attention to detail has prevented the untimely failure of too-hastily planned experiments, to Doctor Howard A. Shugart, whose constant presence at each run, as teacher or as associate, has been a most valued personal and professional experience, to my fellow graduate assistants, Lawrence L. Marino, and, later, Vernon J. Ehlers and F. Russell Petersen, with whom many profitable hours have been spent in discussion and in cooperative laboratory work.

I would like to thank the crew of the Crocker 60" cyclotron and the Health Chemistry division of the Lawrence Radiation Laboratory for their patient assistance throughout the radioactive parts of these experiments.

For her acceptance of the unsocial part of the life of a physicist, I am grateful to my wife, Happy, for still being my wife--and happy.

REFERENCES

1. L. Dunoyer, Compt. rend. 152, 594 (1911).
2. W. Gerlach and O. Stern, Ann. Phys. 74, 673(1924); 76, 163 (1925). For a complete bibliography of publications on molecular beams, see N. F. Ramsey, Molecular Beams (Oxford University Press, Oxford, 1956).
3. R. O. Frisch and O. Stern, Z. Physik 85, 4 (1933).
4. I. I. Rabi and V. W. Cohen, Phys. Rev. 43, 582 (1933).
5. I. I. Rabi, J. R. Zacharias, S. Millman, and P. Kusch, Phys. Rev. 53, 318 (1938).
6. J. P. Hobson, J. C. Hubbs, W. A. Nierenberg, H. B. Silsbee and R. J. Sunderland, Phys. Rev. 104, 101 (1956).
7. J. R. Zacharias, Phys. Rev. 61, 270 (1942).
8. K. F. Smith, Nature 167, 942 (1951).
9. J. M. Blatt and V. F. Weisskopf, Theoretical Nuclear Physics (Wiley, New York, 1952), p. 23.
10. E. Fermi, Z. Physik 60, 320 (1930).
11. L. I. Schiff, Quantum Mechanics (McGraw-Hill, New York, 1949), p. 151.
12. A. R. Edmonds, Angular Momentum in Quantum Mechanics (Princeton University Press, Princeton, 1957), p. 36.
13. Ramsey, op. cit., Appendix C, p. 424.
14. G. Breit and I. I. Rabi, Phys. Rev. 38, 2082 (1931).
15. R. L. Christensen, D. R. Hamilton, A. Lemonick, F. M. Pipkin, J. B. Reynolds and H. H. Stroke, Phys. Rev. 101, 1389 (1956).
16. For a useful summary of such calculations, see H. Kopfermann, Nuclear Moments, E. E. Schneider, Trans. (Academic Press, New York, 1958).
17. E. Fermi and E. Segrè, Z. Physik, 82, 729 (1933).
18. A. G. Shenstone and H. N. Russell, Phys. Rev. 39, 415 (1932).
19. G. Racah, Nuovo cimento 8, 178 (1931).
20. J. E. Rosenthal and G. Breit, Phys. Rev. 41, 459 (1932).
21. M. F. Crawford and A. L. Schawlow, Phys. Rev. 76, 1310 (1949).

22. M. G. Mayer and J. H. D. Jensen, Elementary Theory of Nuclear Shell Structure (Wiley, New York, 1955).
23. A. Bohr, Phys. Rev. 81, 133 (1951); A. Bohr and B. R. Mottelson, Kgl. Danske Videnskab. Selskab, Mat.-fys. Medd. 27, 16 (1953).
24. A. Bohr and V. F. Weisskopf, Phys. Rev. 77, 94 (1950).
25. A. Bohr, Phys. Rev. 81, 331 (1951).
26. K. W. Ford and D. L. Hill, Ann. Rev. Nuclear Sci. 5, 25 (1955).
27. J. Eisinger and V. Jaccarino, Revs. Modern Phys. 30, 528 (1958).
28. Ramsey, op. cit. Chapter VI.
29. R. J. Sunderland, Ph. D. Thesis, University of California (1956).
30. H. A. Shugart, Ph. D. Thesis, University of California (1957).
31. Ramsey, op. cit., p. 379.
32. G. Wessel and H. Lew, Phys. Rev. 92, 641 (1953).
33. D. Strominger, J. M. Hollander and G. T. Seaborg, Revs. Modern Phys. 30, 585 (1958); Nuclear Data Cards, C. L. McGinnis Ed. (National Research Council, Washington, D. C., 1957).
34. W. L. Bendel, F. J. Shore, H. N. Brown, and R. A. Becker, Phys. Rev. 90, 888 (1953).
35. B. C. Haldar and E. O. Wiig, Phys. Rev. 94, 1713 (1954).
36. F. A. Johnson, Can. J. Physics 33, 841 (1955).
37. T. Enns, Phys. Rev. 56, 872 (1939).
38. M. Lindner and I. Perlman Phys. Rev. 78, 499 (1950).
39. J. R. Gum and M. L. Pool, Phys. Rev. 80, 315 (1950).
40. W. Bothe and W. Gentner, Naturwiss. 25, 90, 126, 191 (1937).
41. W. L. Bendel, F. J. Shore, R. A. Becker, Phys. Rev. 83, 677 (1951).
42. M. L. Pool, Phys. Rev. 53, 116 (1938).
43. J. D. Kraus and J. M. Cork, Phys. Rev. 52, 763 (1937).
44. L. K. Hurst and M. L. Pool, Phys. Rev. 65, 60A (1944).
45. J. R. Gum, L. E. Thompson, and M. L. Pool, Phys. Rev. 76, 184A (1949).
46. H. Reddemann and F. Strassmann, Naturwiss. 26, 187 (1938).
47. J. J. Livingood and G. T. Seaborg, Phys. Rev. 54, 88, 3 (1938).
48. J. M. Cork, W. C. Rutledge, C. E. Branyan, A. E. Stoddard, W. J. Childs, and J. M. LeBlanc, Phys. Rev. 80, 286 (1950).

49. K. W. Geiger, Phys. Rev. 105, 1539 (1957).
50. J. Miskel, Phys. Rev. 79, 403 (1950).
51. W. G. Smith and J. M. Hollander, Phys. Rev. 98, 1258 (1955).
52. G. Wilkinson, Phys. Rev. 75, 1019 (1949).
53. T. C. Engelder, Phys. Rev. 90, 259 (1953).
54. L. P. Gillon, K. Gopalakrishnan, A. de-Shalit, and J. W. Mihelich, Phys. Rev. 93, 124 (1954).
55. R. M. Steffen, O. Huber, and F. Humbel, Helv. Phys. Acta 22, 167 (1949).
56. J. M. Cork, and O. Halpern, Phys. Rev. 58, 201A (1940).
57. E. M. McMillan, M. Kamen, and S. Ruben, Phys. Rev. 52, 375 (1937).
58. M. T. Thieme and E. Bleuler, Phys. Rev. 101, 1031 (1956).
59. Ramsey, op. cit., p. 11.
60. Aron, Hoffman, and Williams, UCRL-121 (1949).
61. W. W. Meinke, UCRL-432 (1949).
62. E. Majorana, Nuovo cimento 9, 43 (1932).
63. H. Salwen, Phys. Rev. 99, 1274 (1955); P. Kusch, Phys. Rev. 101, 627 (1956).
64. J. B. Reynolds, R. L. Christensen, D. R. Hamilton, W. M. Hooke, and H. H. Stroke, Phys. Rev. 109, 465 (1958).
65. W. B. Ewbank, L. L. Marino, W. A. Nierenberg, H. A. Shugart, and H. B. Silsbee, Bull. Am. Phys. Soc. Ser. II, 3, 370 (1958).
66. W. B. Ewbank, W. A. Nierenberg, H. A. Shugart, and H. B. Silsbee, Bull. Am. Phys. Soc. Ser. II 2, 317 (1957).
67. H. B. Silsbee, W. A. Nierenberg, H. A. Shugart, and P. O. Strom Bull. Am. Phys. Soc. Ser. II 1, 389 (1956).
68. W. B. Ewbank, W. A. Nierenberg, H. A. Shugart, and H. B. Silsbee, Phys. Rev. 110, 595 (1958).
69. W. B. Ewbank, L. L. Marino, W. A. Nierenberg, H. A. Shugart, and H. B. Silsbee, UCRL-8663 (1959); Phys. Rev. (to be published).
70. R. D. Evans, The Atomic Nucleus (McGraw-Hill, New York, 1955), p. 768.
71. P. Sogo and C. D. Jeffries, Phys. Rev. 93, 174 (1954); E. Brun, J. Oeser, H. H. Staub, and C. G. Telschow, Phys. Rev. 93, 172 (1954).

72. A. G. Shenstone, Phys. Rev. 57, 894 (1940).

73. P. Brix, H. Kopfermann, R. Martin, and W. Walcher, Z. Physik 130, 88 (1951).

74. M. F. Crawford, A. L. Schawlow, W. M. Gray, and F. M. Kelly, Phys. Rev. 75, 1112 (1949).

75. W. B. Ewbank, L. L. Marino, H. A. Shugart, and H. B. Silsbee, Bull. Am. Phys. Soc. Ser. II, 2, 383 (1957).

76. Reynolds, Christensen, Hooke, Hamilton, Stroke, Ewbank, Nierenberg, Shugart, and Silsbee, Bull. Am. Phys. Soc. Ser. II, 2, 317 (1957).

77. W. M. Hooke, R. L. Christensen, D. R. Hamilton, J. B. Reynolds, and H. H. Stroke, Bull. Am. Phys. Soc. Ser. II, 2, 344, (1957).

78. J. R. Platt and R. A. Sawyer, Phys. Rev. 60, 866 (1941).

79. F. M. Kelly, Proc. Phys. Soc. (London) A65, 250 (1952).

80. W. von Siemens, Dissertation, Göttingen, (1952) - as quoted in Ref. 32.

81. L. W. Nordheim, Phys. Rev. 78, 294 (1950); Revs. Modern Phys. 23, 322 (1951).

82. J. W. Mihelich, M. Goldhaber, E. Wilson, Phys. Rev. 82, 972 (1951).

83. K. Way, D. N. Kundu, C. L. McGinnis, and R. van Lieshout, Ann. Rev. Nuclear Sci. 6, 129 (1956).

84. T. Schmidt, Z. Physik 106, 358 (1937).

85. A. Arima and H. Horie, Prog. Theoret. Phys. 12, 623 (1954).

86. R. J. Blin-Stoyle and M. A. Perks, Proc. Phys. Soc. (London) 67A, 885 (1954); 66A, 1158 (1953).

87. M. Sano, Prog. Theoret. Phys. 18, 223 (1957).

88. C. J. Gallagher and S. A. Moskowski, Phys. Rev. 111, 1282 (1958).

89. W. M. Hooke, Bull. Am. Phys. Soc. Ser. II. 3, 186 (1958).

This report was prepared as an account of Government sponsored work. Neither the United States, nor the Commission, nor any person acting on behalf of the Commission:

A. Makes any warranty or representation, expressed or implied, with respect to the accuracy, completeness, or usefulness of the information contained in this report, or that the use of any information, apparatus, method, or process disclosed in this report may not infringe privately owned rights; or

B. Assumes any liabilities with respect to the use of, or for damages resulting from the use of any information, apparatus, method, or process disclosed in this report.

As used in the above, "person acting on behalf of the Commission" includes any employee or contractor of the Commission, or employee of such contractor, to the extent that such employee or contractor of the Commission, or employee of such contractor prepares, disseminates, or provides access to, any information pursuant to his employment or contract with the Commission, or his employment with such contractor.